1972

Air-water turbulent mixing in simulated rod bundle geometries.

Kuldip. Singh

University of Windsor

AIR-WATER TURBULENT MIXING IN SIMULATED ROD BUNDLE GEOMETRIES

A Dissertation
Submitted to the Faculty of Graduate Studies through the
Department of Chemical Engineering in Partial Fulfilment
of the Requirements for the Degree of
Doctor of Philosophy at the
University of Windsor

by

Kuldip Singh

Windsor, Ontario
1972

to Bhole
for love and patience

ABSTRACT

In recent years, there has been increased interest generated in the fundamentals of nuclear reactor coolant mixing which affect the thermal and hydraulic characteristics of the subchannel flow in order to improve reactor performance. Single-phase air, single-phase water and two-phase air-water mixing experiments have been carried out in simulated square-square and square-triangular rod bundle geometries at 50 psia, using methane and potassium nitrate as the air and water tracers respectively. The variation of turbulent mixing rates with mass flux and quality (for two-phase flow) was investigated over a gap spacing range of 15-80 mils.

For single-phase air and water runs, turbulent mixing rates were found to be a function of Reynolds number, gap spacing and subchannel geometry. Secondary flows are believed to exert considerable influence on the mixing rates.

For two-phase air-water runs, turbulent mixing rates were quality dependent, exhibiting a maximum in the slug-flow regime. The mixing results for the square-square and triangular-triangular geometries were correlated over a limited parameter range using a Stanton number type mixing parameter. The air and water fractional mixing rates increased with gap spacing but not in the same proportion. Enhanced liquid interchange occurred in the bubble and annular flow regimes while enhanced gas interchange occurred in the slug and slug-annular flow regimes. The results obtained here are in qualitative agreement with the high pressure steam-water mixing experiments in similar geometries.

ACKNOWLEDGEMENTS

The author is indebted to Dr. Carl C. St. Pierre for his guidance and personal considerations throughout this work.

A number of persons have rendered valuable assistance in completing this assignment. Particular mention must be made of O. Brudy and R. Dickinson of the Central Research Shop; G. Ryan of the Chemical Engineering Department and my friends Ken Petrunik, Kaz Rudzinski, Om Chandna, Surath Rao and Sharad Kumar. The author is also thankful to the Department of Engineering Science, University of Oxford, England for providing research facilities during part of this study.

The financial assistance for this program was provided by Atomic Energy of Canada Ltd under a cooperative research agreement with the University of Windsor and by National Research Council of Canada.

CONTENTS

CONTENTS (Contd.)

CONTENTS (Contd.)

FIGURES

FIGURES (Contd.)

TABLES

I. INTRODUCTION

Many nuclear reactors have fuel elements which constitute a cluster of parallel fuel rods forming subchannels interconnected by the gaps between the rods. The reactor coolant absorbs the heat of fission as it flows along the subchannels. Two typical fuel rod bundle arrays are shown in Figure 1.1. In recent years, there has been an increased interest generated in the fundamentals of coolant mixing, which affect the thermal and hydraulic characteristics of the subchannel flow, in order to improve reactor performance. For parallel flow in rod bundle coolant assemblies with an open matrix, similar to those encountered in the Canadian designed CANDU Pressurized Heavy Water Reactor (CANDU-PHW), a knowledge of the local flows and enthalpies is of importance in predicting the onset of boiling and the critical heat flux. When operating conditions of the reactor result in appreciable boiling heat transfer, as in the CANDU Boiling Light Water Reactor, then mixing rates must be predicted for two-phase flowing mixtures.

Since detailed information on the structure of two-phase flows is not available, most current analyses use a "subchannel approach". Boundaries of subchannels are defined by appropriate fuel element and pressure tube surfaces and by imaginary lines drawn between rod element centres as

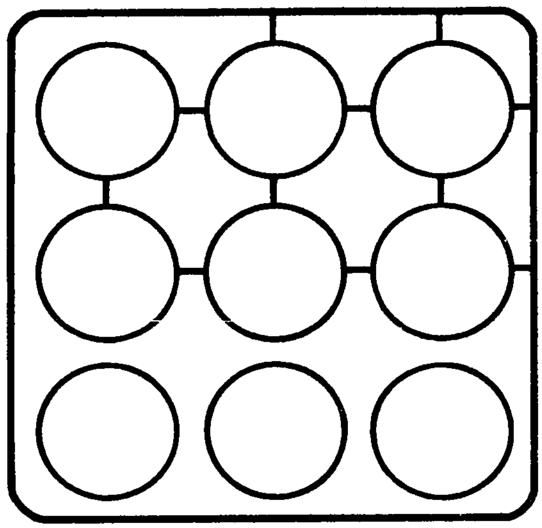

NS = 16
NDS = 3

9-ELEMENT BUNDLE

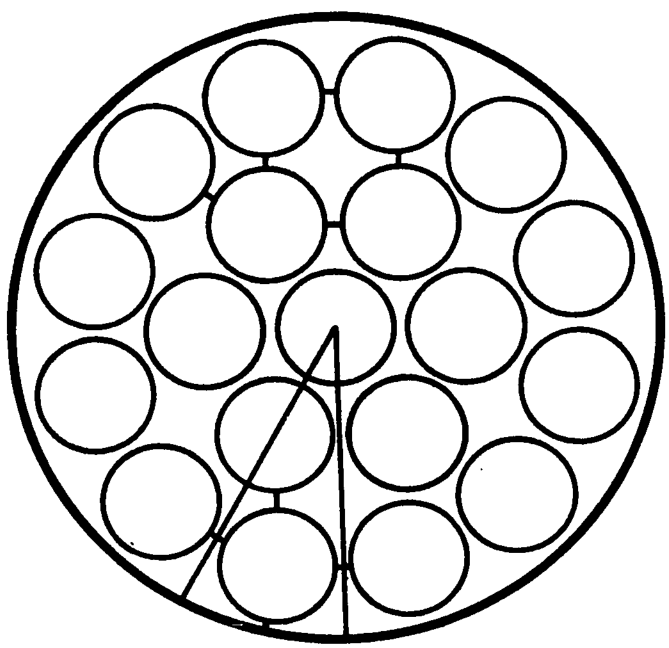

NS = 30
NDS = 5

19-ELEMENT BUNDLE

NS ≡ NUMBER OF SUBCHANNELS

NDS ≡ NUMBER OF DISTINCT SUBCHANNELS

FIGURE 1.1 Subchannel Arrangements for Typical Fuel Rod Bundles illustrated in Figure 1.1.

In the subchannel analysis approach, radial and circumferential variations of pressure, coolant velocity, quality and physical properties within a subchannel are neglected. Each subchannel is divided into axial nodes. Then finite difference forms of the macroscopic conservation equations are solved stepwise over the whole axial length using computer codes (1-4) which account for mass, energy and momentum transport between interconnected subchannels. This analysis, which allows simple geometry Critical Heat Flux (CHF) correlations to be applied, also provides useful information for reactor designers to account for local phenomena related to rod bowing, rod spacer effects and heat flux peaking - even though detailed differential flow information is not obtained. Thus, subchannel analysis of this type will help provide codes that could be used for basic reactor design purposes.

It is of interest to consider the form of the energy equation used in the available steady-state computer codes. For any two interconnected subchannels "i" and "j", the energy balance over an axial length Δz for subchannel "j" is written as:

$$\frac{\Delta}{\Delta z}(W_j H_j) = q_j P_j + W_{ij} H_{ij} + W'_{ij}(H_j - H_i)$$

Here W_{ij} is defined as the mass crossflow rate transported from subchannel "i" to "j" with an effective enthalpy H_{ij}, while the final term is the energy exchange contribution due to turbulent mixing. Diversion crossflows are the net rates of mass transfer between subchannels in order to satisfy the conservation equations. Crossflows are directed by radial pressure gradients which may result from large differences in subchannel heat flux distributions, rod bowing, changes in flow area etc. Turbulent mixing is a semi-fictitious fluctuating mass flow and is used only to express the turbulent energy transport between subchannels due to pressure and flow fluctuations. Turbulent mixing is normally assumed to be independent of crossflow, although one code makes provision for mixing suppression (1), and does not involve a net mass transfer between subchannels.

In practice, turbulent mixing rates are determined from measurements of subchannel enthalpy or tracer distribution, as the amount of lateral flow which, according to some model, would have caused the observed conditions. This semi-fictitious fluctuating mass flow, termed the turbulent interchange rate, can be related to the classical mixing length theory for single phase flows. However, for two-phase flowing systems at saturated conditions it becomes more difficult to link mixing rates obtained with tracer data to an energy exchange mechanism.

The present project was formulated to conduct a fundamental study of mixing rates in simulated reactor rod bundle geometries. This study was designed to obtain qualitative and quantitative data on the parameters that influence mixing between adjacent subchannels. Data of this kind are very difficult and expensive to obtain for a steam-water system on prototype coolant assemblies operating at elevated pressures (400-2000 psia). Therefore, a two-component, two-phase air-water system operating at low pressure was used to model a steam-water system with mixing rates being obtained from tracer analysis. This common practice of modelling steam-water systems with air and water yields valuable qualitative information and in some instances, useful quantitative data when proper scaling factors are employed.

This work is divided into two parts. In the first part, turbulent interchange rates between adjacent flow channels have been measured for air-water systems at 50 psia in the absence of diversion crossflow and any forced mixing effects. The test section was designed to simulate two identical square array subchannels in a typical BLW fuel bundle with three different gap spacings: 80, 35 and 15 mils. Single phase air, single phase water and two-phase air-water turbulent mixing rates were obtained. Under two-phase flow conditions, mixing rates of each component were determined simultaneously from tracer analysis. Void fraction data were also obtained for the geometry with a 35-mil gap spacing.

In the second part of this study, the test section was designed to simulate the subchannel arrangement formed by rods in a square pitch array located next to rods in a triangular pitch array. Mixing rates were obtained for single phase air, single phase water and two-phase air-water mixtures under conditions of negligible radial pressure difference between the two subchannels having a gap spacing of 35 mils.

II. LITERATURE REVIEW

In recent years there has been an increasing interest in an evaluation of mixing rates in rod bundle geometries. Figure 2.1, reproduced from Reference (5), vividly demonstrates the increasing interest in this subject. This interest

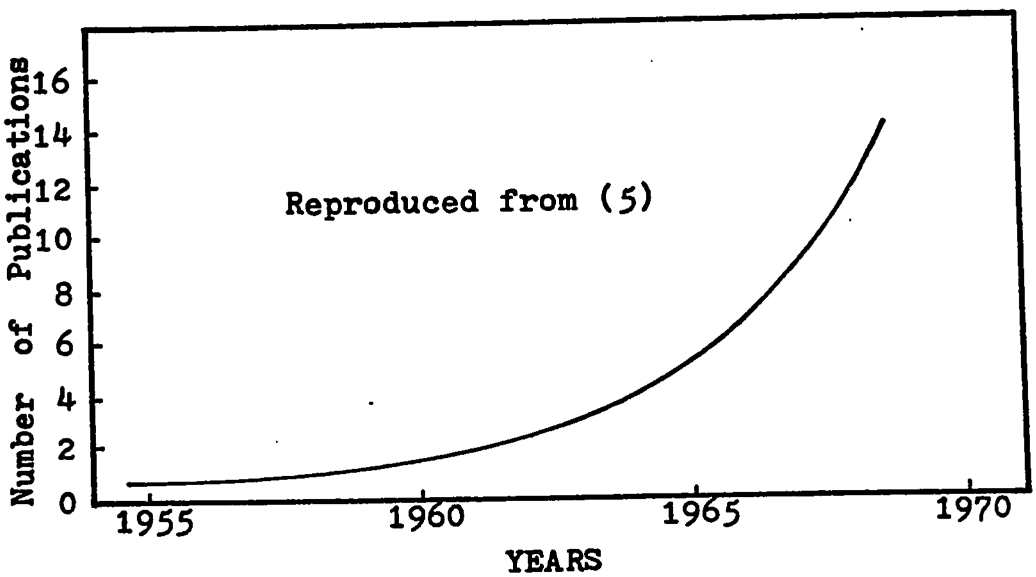

FIGURE 2.1 Single Phase Mixing Publications

is largely motivated by the need in reactor design to predict, as closely as possible, enthalpy and flow conditions in the various subchannels of a fuel rod bundle. The mixing experiments have been performed either in two subchannel geometries or in rod clusters with essentially two experimental techniques: by injection of tracers (salts, dyes, radioactive fluids etc.) in one of the subchannels at the inlet of the test section or by heating one or more of the channels with electrically heated elements. The mixing rates are calculated from tracer concentration or temperature measurement at the exit of the subchannels.

A. Single Phase Mixing

A comprehensive review of single phase mixing experiments and predictive correlations has been given by Rogers and Todreas (6). Turbulent energy transport between adjacent subchannels "i" and "j" expressed in terms of a hypothetical turbulent mass interchange rate per unit length, W'_{ij}, is related to the heat transfer by transverse eddy diffusivity as:

$$W'_{ij} \, (H_i - H_j) = \rho \, b \, \epsilon_{Hij} \left(\frac{dH}{dY} \right)_{ij} \qquad (2.1)$$

This equation is, in fact, the defining equation for the turbulent mixing rate, W'_{ij}.

As an approximation,

$$\left(\frac{dH}{dY} \right)_{ij} \approx \frac{H_i - H_j}{Y_{ij}} \qquad (2.2)$$

where Y_{ij} is the "effective mixing distance". From equations (2.1) and (2.2) is obtained:

$$W'_{ij} = \frac{\rho \, b \, \epsilon_{Hij}}{Y_{ij}} \qquad (2.3)$$

Then equation (2.3) is divided by ($G_i b$) to yield:

$$\frac{W'_{ij}}{G_i\, b} = \frac{\rho\, \epsilon_{H_{ij}}}{G_i\, Y_{ij}} \qquad (2.4)$$

The dimensionless parameter $W'_{ij}/(G_i\, b)$ is the ratio of the mixing mass flux to the axial mass flux in one of the subchannels and by analogy with turbulent convective heat transfer is called the mixing Stanton number.

1. Predictive Mixing Correlations

Several correlations (1,2,7-11) have been proposed for the prediction of single phase turbulent mixing rates between adjacent subchannels of a fuel rod bundle. A majority of the correlations use the now conventional approach that mixing is governed by the mechanism of eddy diffusion alone and then use equation (2.3) or (2.4) in the development of the correlation. Eddy diffusivity data for the core of a duct is assumed to apply for various shaped subchannels; and some interchannel "effective mixing distance" is defined. In order to account for imperfections in this formulation, some of the correlations use a corrective mixing factor. A summary of available predictive correlations is given in Table 2.1. The detailed descriptions are available in Reference (6).

2. Turbulent Mixing Experiments

A summary of the experimental programs (11-19) concerned with single phase natural turbulent mixing is given in Table 2.2. Those experiments in which some forced

TABLE 2.1

Turbulent Mixing Correlations

Investigator and Reference	Assumption for $\epsilon_{H_{ij}}$	Assumption for Y_{ij}
Bowring (1)	$\frac{\epsilon}{\nu} = \frac{Re}{20}\sqrt{\frac{f}{2}}$	$Y_{ij} = S_m d$ where S_m is a geometrically defined subchannel shape factor
St. Pierre (2)	Correlation from available single channel data in the form of Peclet number-Reynolds number plot	One-half the average equivalent diameter of the subchannels
Moyer (7)	Eddy diffusivity in the central region of a circular pipe $\frac{\epsilon}{\nu} = \frac{Re}{20}\sqrt{\frac{f}{2}}$	Centroidal distance between subchannel axes
Ingesson (8)	$\frac{\epsilon}{\nu} = \frac{Re}{20}\sqrt{\frac{f}{2}}$ corrected by introducing a mixing factor	Centroidal distance between subchannel axes
Rapier (9)	$\frac{\epsilon}{\nu} = \frac{Re}{20}\sqrt{\frac{f}{2}}$	Centroidal distance Effective clearance gap, larger than actual, is used
Rosehart and Rogers (10)	$\frac{\epsilon}{\nu} = K\ (Re^m)$	$\frac{Y_{ij}}{d} = K_g\ (b/d)^{\frac{1}{\alpha_{ij}}}$
Rowe and Angle (11)	$\frac{\epsilon}{\nu} \propto Re\sqrt{\frac{f}{2}}$	Equal to clearance gap

TABLE 2.2

Summary of Single Phase Mixing Experiments

Reference	Number of Rods and/or Geometry Description	Rod Diameter (in)	Gap Spacing (in)	Inter-connection length (in)	Fluid	Range of Experimental Parameters: Temperature °F	Pressure psia	Mass Flux lb/(hr·sq ft)x10^{-4}	Re x10^{-4}	Technique
Rowe and Angle (11)	Two subchannel S-T	0.564	0.020 0.084 0.028	60 60 60	Water Water Water	70	900 900 Low	100-300 100-300	17-40 17-40 0.7-2.5	Heat Input (subchannel. ΔT) Lithium tracer
Hetsroni (12)	6 S-S	0.4	0.1	48	Water	Hot 85-156 Cold 64-71		153-222	1.9-4.2	Hot water injection enthalpy balance
Rowe and Angle (13)	Two subchannel S-S	0.563	0.020 0.085	60 60	Water Water		400, 750 400, 750	100-300 100-300	7-30 7-30	Lithium tracer Lithium tracer
Petrunik (14)	Rectangular-rectangular (No fillers)		0.040, 0.10	2-14	Air	Room	50.0	1.0-10.0	1.5-15	Methane tracer
			0.040-0.10	4-14	Water	Room	14.7	20-200	0.5-3.0	Potassium tracer
Walton (15)	Two subchannel T-T	0.78 0.78	0.040 0.040	9,18 9,18	Air Water	Room Room	50.0 14.7	1.6-27 38-107	0.5-8.0 0.2-0.57	Methane tracer Potassium tracer
Skinner et. al. (16)	7	1.35	0.4	156	Air				2-8	Nitrous oxide tracer
Galbraith and Knudsen (17)	6 S-S	1.0	0.011 to 0.0228	16	Water	60			0.8-3.0	Dye tracer (Rhodamine B)
Van der Ros (18)	Square cross-section (No fillers)		0.04 0.08	74	Water	Inlet 68 to 122			5-30	Heat Input
Singleton (10,19)	Round slot Square slot	1.2	0.248 0.48 0.272 0.504		Water Water Water Water				1.4-3.0 2.4-3.6 1.6-3.3 2.7-9.2	Dye tracer Dye tracer Dye tracer Dye tracer

S Square-pitch Subchannels
T Triangular-pitch Subchannels

mixing effects are present (due to grid spacers, wart type spacers, axial or circumferential fins etc.) are not considered here.

Hetsroni et. al. (12) determined an expression for the overall effective diffusivity for heat:

$$\epsilon_H = 0.0061 \ \nu \ Re^{0.98}$$

for mixing between two square-square array subchannels. This expression is similar to those suggested by Elder (20) and Nijsing (21).

Rowe and Angle (11) determined mixing rates between two adjacent subchannels formed by rods on a square pitch array located next to rods on a triangular pitch array. The turbulent mixing rate was determined by comparing the enthalpy values at the test section exit with the predictions from a computer code COBRA (22); thus mixing rate data depended upon the assumptions in the mathematical model. Mixing rates, W', were nearly independent of the gap spacing, (in fact, reducing the gap spacing from 0.084-in to 0.020-in seemed to increase W'/W by a small amount), and nearly proportional to the hydraulic diameter and mass velocity. The results were correlated in the form:

$$W' = 0.0062 \ \overline{G} \ D_e \ (Re)^{-0.1} \qquad (2.5)$$

In a subsequent report (13), Rowe and Angle directly calculated mixing rates in a square-square array from tracer analysis. Mixing rates were again found to be nearly independent of gap spacing and pressure and flow rates did not significantly affect the fractional mixing rate, W'/W. Fractional mixing rates between square-square subchannel arrays were significantly lower than those obtained in the square-triangular array so that an additional correlation parameter was required in equation (2.5) to account for the subchannel shape. Rowe and Angle also suggested that an additional phenomenon was responsible for the experimentally observed effect of gap spacing on mixing rates as eddy diffusion alone could not provide a satisfactory explanation.

Single phase air and water mixing experiments were carried out in two adjacent rectangular-rectangular subchannels by Petrunik (14) and in a triangular-triangular geometry by Walton (15) at the University of Windsor. Their results were correlated on a Stanton number versus Reynolds number plot as: $St \propto Re^{-0.13}$. Petrunik also demonstrated that entrance effects at the interconnection length were negligible after an entrance length of approximately 15 equivalent diameters.

Skinner <u>et</u>. <u>al</u>.(16), who employed a cluster of six rods and a central tie tube concluded that the air mixing rates through the gaps could not be explained by turbulent diffusion alone. The very high mixing rates were attributed to the existence of secondary flows in the gap region. For a smooth rod cluster, the mixing Stanton number decreased with Reynolds number while for the rough rod cluster, the converse was found in the range of Reynolds number investigated (20,000-80,000).

Galbraith and Knudsen (17) determined single phase (water) mixing rates between adjacent subchannels in a simulated rod bundle made by placing six 1-in diameter rods in a square-square array. Five different gap spacings were used. Empirical correlations of the type $W'/\mu = A\ Re^B$, where A and B are functions of the gap spacing, were proposed. They concluded that i. the turbulent mixing rate, W', increases with rod spacing and Reynolds number and ii. the flow conditions in the immediate vicinity of the rod spacing are important,especially for the small gap spacing.

No single turbulent mixing model predicts mixing rates accurately for the range of flow conditions and geometries normally encountered. Proof that the theoretical prediction of mixing rates is very complicated is presented by the failure of different investigators to agree even on the question of the effect of gap spacing on the single phase mixing rates. Mixing is a result of intensity and scale of turbulence and of the local temperature and velocity distribution, especially near the gap region. There is growing evidence now (16,23) to suggest that in addition to eddy diffusion, secondary flows have considerable influence on the mechanism of inter-subchannel mixing. Advanced turbulence models, such as those suggested by

Launder and Spalding (24) are needed to predict the occurence and effect of these secondary flows on convective transport.

B. Two-Phase Mixing

Rogers and Todreas (6), in their summary paper on single phase mixing, also reviewed some of the two-phase mixing data. In a following paper, Lahey and Schraub (25) examined and summarized available data on two-phase mixing, void fraction and flow regimes in rod bundle geometries. Two-phase mixing data have been obtained in two subchannel geometries using air-water flows (5,14,15,26,27) or boiling steam-water systems (11,13). Mixing rates have also been measured for steam-water (28,29), boiling freon (30) and air-water (31) flows in multirod bundles. Some of these investigations measured the diversion crossflow component of mixing only (5,27), others considered only turbulent mixing (13-15,26) while still others studied the combined effect of the two modes of mixing (11,28-30).

Rowe and Angle (11), from their mixing measurements with square-triangular array subchannels, concluded that mixing is a strong function of subchannel quality, peaking at qualities just before the slug-annular transition. Mixing during boiling improved by about a factor of two for the 0.084-in gap but there was no significant improvement for the 0.020-in spacing. However, the values of turbulent mixing parameter, β , were calculated using the computer code COBRA (22) and therefore, depended on the assumptions of the mathematical model. The dependence of turbulent mixing on the subchannel quality was confirmed by their tests on a square-square geometry (13). Mixing quality equalled subchannel quality and mixing increased noticeably with increased gap spacing.

The effect of flow regime on mixing was also observed by Spigt et. al. (27), Van der Ros (5), Petrunik (14) and Rudzinski (26) in two subchannel air-water tests.

Van der Ros (5) determined diversion crossflow rates in a two channel geometry using air-water at low pressure. The measurements covered the bubble flow regime only. Gas mixing occured through diffusion mechanism whereas the exchange of liquid resulted from the balancing of the axial pressure gradients in the two interacting channels. Liquid crossflow was superimposed on the gas diffusion without interference although the direction of exchange was often opposite. The gas diffusion rate between the two subchannels increased with gap spacing.

Casterline et. al. (28), who employed a sixteen rod square array, postulated a non-homogeneous diversion of flow and/or different rates of turbulent transport in the gas and liquid phases.

Bowring (30), who used a 7-rod cluster concluded that mixing rates for a boiling freon system were less than the single phase values when averaged over the entire channel length. Also the average interchannel mixing rates were independent of quality and the mixing parameter, G'/G, was inversely proportional to mass flux.

With the possible exception of Rowe and Angle's and Van der Ros's data, no systemetic investigation is available in literature to indicate the effect of gap spacing on the turbulent mixing rates over the whole range of system parameters. Lahey and Schraub (25) pointed out that in order to better understand the mixing phenomena, more work is needed in the following areas:

1. The correct effect of gap spacing on single and two-phase turbulent energy exchange,

2. The effect of subchannel geometry on turbulent mixing,

3. The extent of mass transfer associated with two-phase turbulent energy transfer and

4. The precise nature of the flow regime enhancement of turbulent mixing.

The purpose of the present investigation was to expand our knowledge of the fundamentals of mixing mechanism in single and two-phase flowing mixtures; especially the effect of gap spacing and geometry on turbulent mixing rates.

III. EXPERIMENTAL EQUIPMENT AND PROCEDURE

A. Air-Water Test Loop

The air-water test loop and associated equipment used in this study were located in the Chemical Engineering Research Laboratories of the University of Windsor. The test rig consisted essentially of a high pressure (95 psig) air source, a centrifugal pump for water supply, a bank of rotameters to cover the whole range of air and water flow rates, two small rotameters to measure tracer flow rates, two air-water separators and a number of pressure and temperature measuring devices. The loop is shown schematically in Figure 3.1.

Compressed air at 95 psig pressure was filtered, passed through a pressure regulating valve (PRV) and a 1/2-in flexible hose before being split into two parts. Each part was then fed to a matched pair of rotameters for flow measurement. Water was similarly supplied through a Goulds (Model 3775) centrifugal pump with a capacity of 125 IGPM at a head of 130 psia.

In order to achieve natural flow split conditions, two valves were installed in parallel in each of the exit lines from the test section to permit fine and coarse control of the downstream resistances in the two flow channels. The

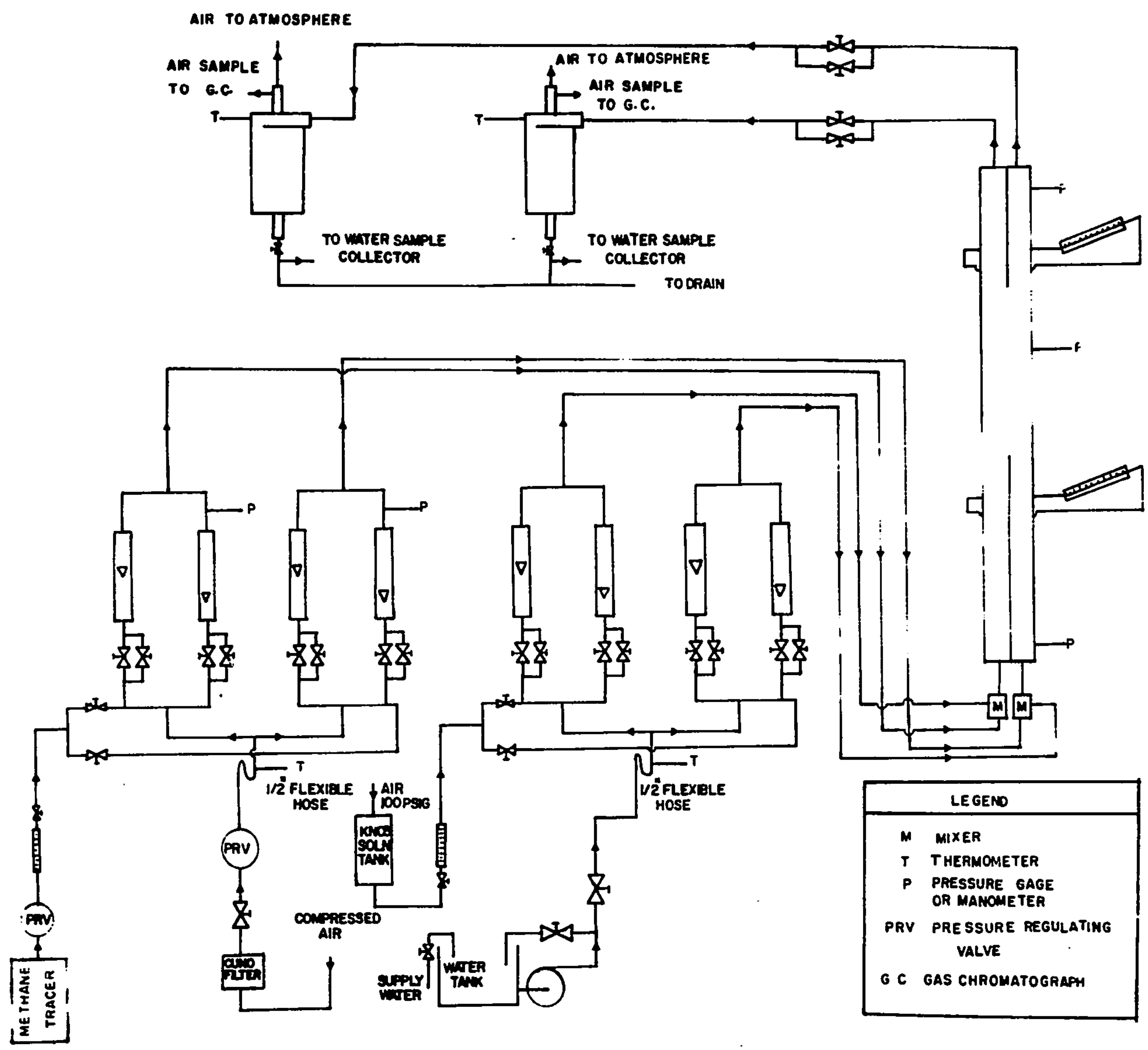

FIGURE 3.1 Schematic Flow Diagram of Test Loop

two-phase air-water mixture from the exit of the subchannels was passed through air-water separators made of plexiglas, each with a capacity of 125 lb/hr of air and 390 lb/hr of water. Air samples were fed directly from each separator to an on-line gas chromatograph for analysis and the remaining air was discharged to the atmosphere. A representative water sample was collected for later analysis. All effluent from the separators was dumped in order to avoid contamination.

For the square-triangular array test section, air from each of the separators was passed through a large oil drum (which acted as a capacitor to dampen fluctuations) before being fed to a rotameter of appropriate capacity for flow measurement. Flow rates of water from the cyclone-separators were determined by direct weighing technique.

The air and water tracers (methane and potassium nitrate solution respectively) were introduced in the flow streams as shown in Figure 3.1.

B. Test Section Assemblies

1. Material of Construction

In the previous mixing experiments of this series (14,15), acrylic was used as the material of construction of the test sections. While this allowed visual identification of the flow regimes, the test section often developed cracks and leaks during operation. It was decided, therefore, to machine this test section out of free cutting brass. The advantages of using this metal were its excellent machinability, good mechanical and corrosion resistant properties and its suitability for joining by soft soldering. The disadvantages were its weight and the consequent difficulty in handling. The whole test section assembly was flash plated with nickel to prevent corrosion by the potassium nitrate solution which was used as the water tracer.

2. Test Section Dimensions

a. Square-Square Array Subchannel Arrangement

A square channel, 0.86-in x 0.86-in in cross-section was milled out of a brass bar. Fillers (quarter rods) were machined out of brass bars of 1/2-in cross-section. The rods were mounted in the square channels to form a simulated square-square subchannel array of a typical fuel bundle. The milling machine in the Central Machine Shop at the University of Windsor could handle a maximum length of four feet only. Three such lengths formed the test section, giving a total length of approximately 12 feet. One entrance section, about 4-in long, provided a transition from the loop piping to the subchannel cross-sectional flow area. Another identical transitional piece was constructed as the exit section. Flow development was allowed over 150 equivalent diameters in the separated region. The three machined lengths and two transition sections were joined together using brass flanges. "LocTite Plastic Gasket" was used as the sealant between the flanges.

A 6-mil thick, 13-feet long stainless steel strip was used to physically separate the two subchannels, except in the mixing region. A 86-mil cut was made in the middle of the stainless steel strip for a total length of 5 feet. This formed the interconnection length where the mixing between the two subchannels was allowed to take place.

In order to allow variations in the gap width, rods of various diameters were used. Only the rods near the gap were changed. A cross-sectional view of the test section is given in Figure 3.2. The machine tolerances in the test section dimensions, rod diameters etc. were ± 0.003-in. A summary of the relevant test section parameters is given in Table 3.1. The average gap width reported along the interconnection length was always within ± 0.002-in of the actual measured values.

b. Square-Triangular Array Subchannel Arrangement

A procedure similar to the one described previously was followed for the construction of the square-triangular subchannel arrangement. One half of the square pitch array test section with 35-mil gap was used for this arrangement. For the triangular pitch array half, the flow area was machined from two solid brass bars as shown in Figure 3.2.

3. Pressure Taps

A total of 19 pressure taps were drilled along each of the two subchannels to measure the axial pressure drop and radial pressure differential between the two

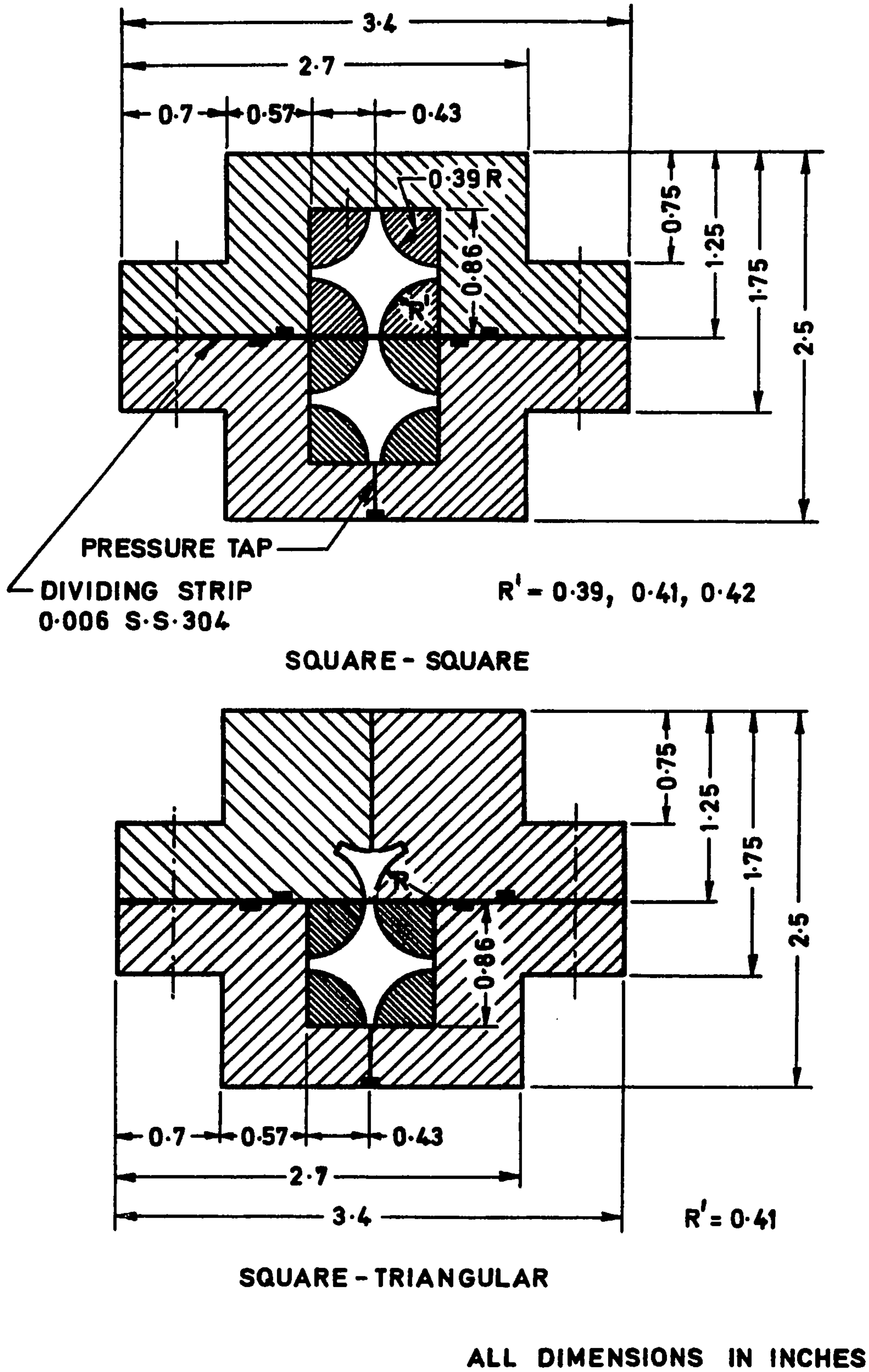

FIGURE 3.2 Detail of Flow Channels

TABLE 3.1

Details of Test Section Dimensions

Square-Square Array Geometry

Gap Width, in	0.015	0.035	0.080
Rod Diameter, in	0.84	0.82	0.78
Hydraulic Diameter, D_e, ft	0.0272	0.0287	0.0315
Cross-sectional Area, sq ft	0.00155	0.00164	0.00182
Wetted Perimeter, ft	0.231	0.229	0.228
Pitch/Diameter	1.0178	1.0426	1.102
Gap/Diameter	0.0178	0.0427	0.103
Interconnection Length, L, ft	5.0	5.0	5.0
Length/Hydraulic Diameter, L/D_e	184.	175.	159.

Square-Triangular Array Geometry

	Geometrical Array	
	Square	Triangular
Hydraulic Diameter, ft	0.0287	0.0134
Cross-sectional Area, sq ft	0.00164	0.00039
Gap Width, in	0.035	
Rod Diameter, in	0.82	
Pitch/Diameter	1.043	
Gap/Diameter	0.0427	
Interconnection Length, ft	5.0	

subchannels at the same axial position. The burrs from the inside of the 1/16-in diameter static pressure taps were carefully removed to avoid any errors in the pressure measurement. The location of the pressure taps is shown in Figure 3.3.

4. Observation Window

In order to facilitate viewing of the flows in the test section for identification of the flow regimes, an observation window (2-in x 0.080-in), made of plexiglass was installed near the exit of the test section. Two high intensity (300-ma, 2.5 volts) Welch Allyn No. 2 miniature bulbs were used for illumination of the test section.

C. Measurement of Experimental Variables

1. Operating Pressure

The pressure at the middle of the interconnection length was measured with a 0-125 psig Heise pressure gauge graduated in 0.5 psi increments. This pressure gauge and all those used for recording exit pressures at the air rotameters were calibrated against a standard dead weight tester and the corrections applied where necessary.

2. Differential Pressure

The differential pressure between subchannels was one of the more important experimental parameters of interest in this investigation. A precise measurement of radial pressure difference between the two subchannels at exactly the same axial position was essential to insure natural flow split conditions and to minimize any diversion cross flow

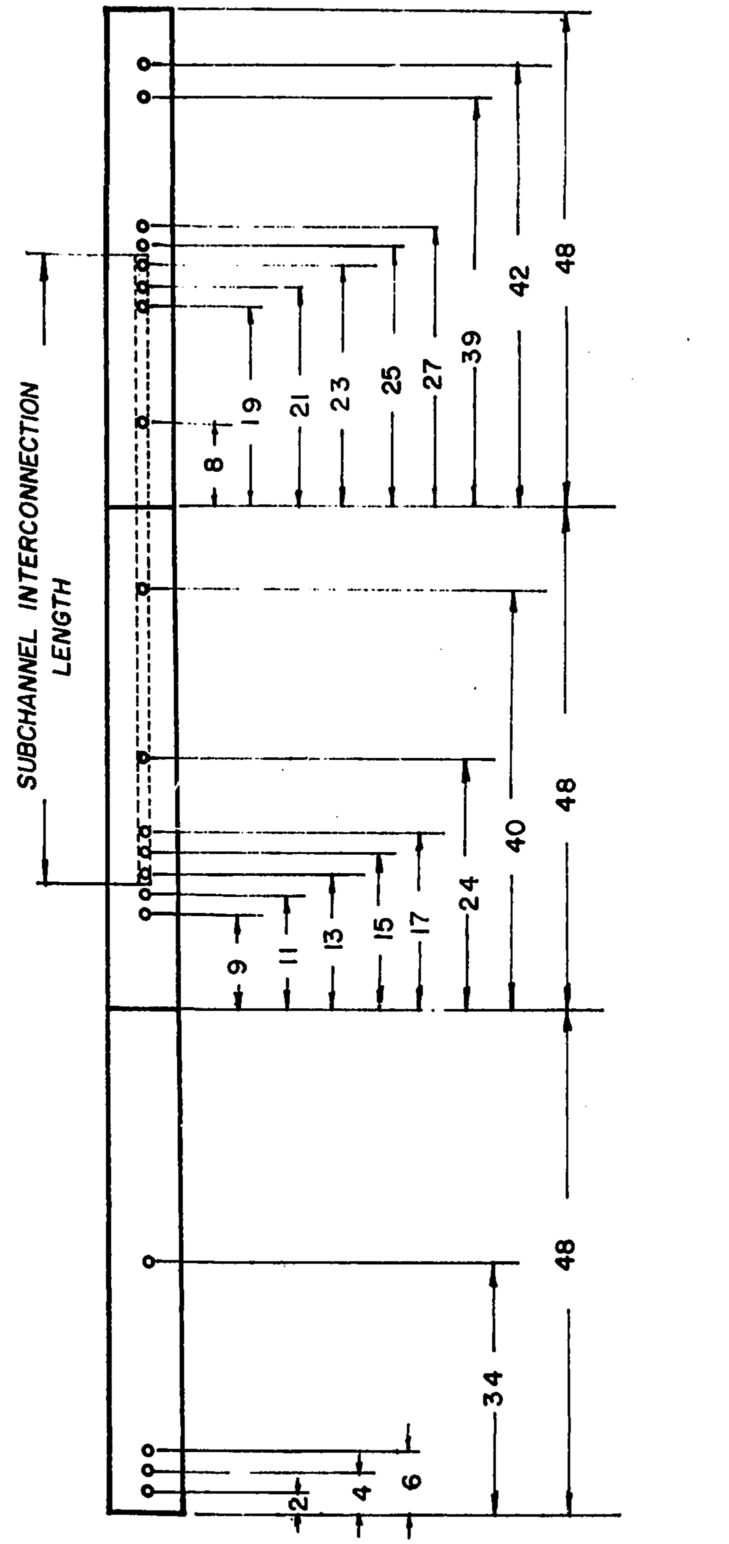

ALL DIMENSIONS IN INCHES

FIGURE 3.3 **LOCATION OF PRESSURE TAPS** effects.

Each pressure tap line, made from 1/4-in polyethylene tubing was horizontal before entering a small plexiglass accumulator of 1-in diameter by 3-in long. The polyethylene line from the top of the accumulator was connected, through a large capacitor of 4-in diameter by 6-in long, to the differential pressure measuring device. This was done in order to keep the manometer lines free of any water droplets for two-phase flow runs, to prevent accidental flooding of the manometer and to dampen the pressure oscillations. The arrangement is shown schematically in the following sketch.

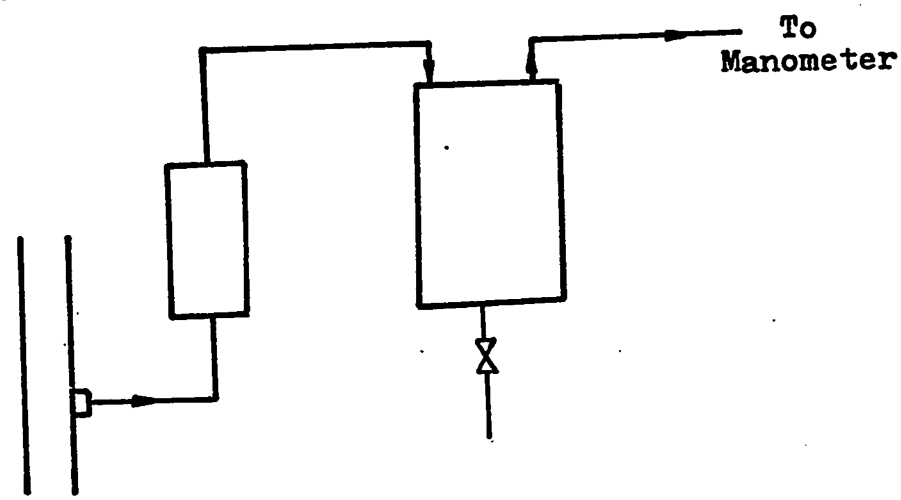

A variety of pressure measuring devices were used, depending on the range of differential pressure to be measured and the accuracy desired.

a. <u>Radial Pressure Differential</u>

The radial pressure differential for all single phase air and two-phase air-water runs was measured with Meriam inclined manometers, graduated in hundreths of an inch. All the two-phase runs with gap spacings of 35 and 15 mils were taken using damped differential pressure transducers (ITT Barton, Model 300), with a range of ± 0-10 inches of water and graduated to one-tenth of an inch. A CP51 pressure transducer with a range of ± 2.5 psid was used to measure radial pressure fluctuations at the centre of the interconnection length. Unfortunately, a mechanical failure occured in the transducer before a majority of the data were obtained.

b. Axial Pressure Differential

The axial pressure drop for the single phase air mixing runs was measured using a 60-in vertical Meriam manometer. Part of the data was taken with the differential pressure transducer mentioned previously. When the pressure drop was very low, an inclined manometer was used. For the two-phase flow runs, the pressure drop was measured by using either a 60-in vertical mercury manometer or a differential pressure transducer (ITT Barton, Model 300) with a range of 0-300 inches of water.

3. Flow Measurement

Air and water flow rates were controlled manually over the whole range using calibrated rotameters of suitable range. The air rotameters were calibrated at 50 psia and 80^0F and temperature and pressure corrections were applied when necessary. The air rotameters were factory calibrated and guaranteed to be accurate within ±1% of full scale. Calibration curves for a few of the rotameters were checked against a specially constructed gasometer in the laboratory and found to be within the accuracy limits indicated. All the water rotameters were calibrated in situ by the direct weighing technique.

4. Temperature Measurement

The temperature of air and water streams was measured by using direct reading bimetallic thermometers (range 20-120^{0}F) in the flow lines immediately before the rotameters. The exit air temperature of the two-phase mixture was measured by using mercury thermometers suspended in the air-water separators.

5. Tracer Concentration

The analysis for methane tracer concentration in the exit air streams from both subchannels was made using an on-line Varian gas chromatograph, Model 1800 with Porapak Q column and a hydrogen flame detector. The instrument was calibrated daily and analyses were reproducible to within ±1%. Potassium nitrate solutions were analyzed using a Jarrel Ash atomic absorption analyzer with a hollow cathode potassium lamp. The instrument was calibrated prior to each set of analysis with standard solutions. Analyses were reproducible to within ±2%.

6. Void Fraction

The volumetric fraction or "in situ" air hold up for the square-square geometry with a 35-mil gap spacing was measured employing the quick closing valve technique.

D. Range of Experimental Parameters

1. Square-Square Array Subchannel Arrangement

All the single phase air and two-phase air-water mixing runs were taken with a pressure of 50 psia maintained at the middle of the interconnection length. The maximum flow rates achieved were normally limited by the allowable axial pressure drop. A summary of experimental data is given in Table 3.2.

TABLE 3.2

Summary of Experimental Data

Square-Square Array Geometry

Gap Spacing mils	Number of Runs		
	Single Phase Air	Single Phase Water	Two-Phase Air-Water
80	19	23	26
35	24	18	62
15	29	23	26

For all runs, the interconnection length was 5 feet. The range of experimental parameters is shown in Table 3.3. In addition to the two-phase air-water runs shown in Table 3.3, mixing data were taken over an extended quality range at a mass flux of 0.1, 0.5 and 0.8 x 10^6 lb/(hr.sq ft). Out of all these runs, air mixing data could not be obtained at a mass

TABLE 3.3

Range of Experimental Parameters

Square-Square Array Geometry

Single Phase Air	
Air Flow Rate, lb/hr	5 - 97
Mass Flux, lb/(hr.sq ft)	4100 - 53,000
Reynolds number	2000 - 38,000
Temperature, °F	71 - 86
Single Phase Water	
Water Flow Rate, lb/hr	200 - 1,500
Mass Flux, lb/(hr.sq ft)	110,000 - 835,000
Reynolds number	1,300 - 9,900
Temperature, °F	51 - 60
Two-Phase Air-Water	
Quality	0.2 - 0.8
Mass Flux, lb/(hr.sq ft)	0.3 - 1.0 x 10^5
Air Flow Rate, lb/hr	16 - 100
Water Flow Rate, lb/hr	10 - 225
Temperature, °F	55 - 81

flux of 0.5 and 0.8 x 10^6 lb/(hr.sq ft) because either the air mixing rates were too low or the gas chromatograph was malfunctioning during this phase of the investigation.

2. Square-Triangular Array Subchannel Arrangement

All the single phase air and two-phase air-water data were taken with a pressure of 50 psia maintained at the middle of the subchannel interconnection length. The interconnection length was 5 feet and the gap spacing 35 mils. A summary of the number of experimental runs is given in Table 3.4.

TABLE 3.4.

Number of Experimental Runs

Square-Triangular Array Geometry

Single Phase Air	23
Single Phase Water	25
Two-Phase Air-Water	29

The range of experimental parameters is shown in Table 3.5.

E. Experimental Procedure

1. Method of Tracer Injection

The methane tracer used for determination of gas phase mixing was injected directly from a Research Grade methane cylinder. The tracer flow rate could be regulated to obtain concentration values within the range of the gas

TABLE 3.5

Range of Experimental Parameters

Square-Triangular Array Geometry

	Geometrical Array	
	Square	Triangular
Single Phase Air		
Air Flow Rate, lb/hr	8.4 - 75	1.25 - 11.2
Mass Flux, lb/(hr.sq ft)	5100 - 46,000	3200 - 29,000
Reynolds Number	3300. - 30,000	1000 - 8700
Single Phase Water		
Water Flow Rate, lb/hr	210 - 1500	28 - 200
Mass Flux, lb/(hr.sq ft)	128400 - 910,000	71,000 - 510,000
Reynolds Number	1370 - 8700	350 - 2250
Two-Phase Air-Water		
Quality	0.025 - 0.11	0.04 - 0.41
Mass Flux, lb/(hr.sq ft)	57,000 - 200,000	51,000 - 150,000
Air Flow Rate, lb/hr	8.0 - 37.3	2.1 - 9.7
Water Flow Rate, lb/hr	300 - 328	12 - 58
Overall Average Mass Flux, lb/(hr.sq ft)	0.18×10^6	

chromatograph. The water phase tracer (a dilute solution of potassium nitrate) was stored in a reservoir and injected into the system under pressure. To insure thorough mixing of the tracers with the flow streams, both the tracers were injected upstream of the rotameters as shown in Figure 3.1.

The effect of tracer concentration on the mixing rates was investigated by injecting various amounts of tracer (typical values were 75-400 p.p.m.) and calculating the mixing rates. It was found that the ratio of the tracer concentrations at the exit of the two subchannels was independent of the amount of tracer injected in one channel or the other.

In order to insure that diversion crossflows were negligible, since this study was concerned with determination of oscillating turbulent mixing rates, tracers were injected alternately in each channel. If the turbulent mixing rates calculated for right and left subchannel injection were within 10% of each other and there was no consistent preferential mixing direction, diversion crossflows were assumed to be negligible.

2. Square-Square Array Mixing Runs

For all single phase air, single phase water and two-phase air-water mixing runs, each subchannel carried identical flow rates of air and/or water. The flow control valves for both subchannels were adjusted to obtain the following conditions: i. identical flow rates of air and/or water in the two subchannels ii. zero radial pressure difference (time-average) along the interconnection length and iii. 50 psia pressure at the mid point of the mixing length.

For the single phase air mixing runs, subchannels were balanced to within one-hundreth of an inch of water. For the two phase runs, it was usually possible to balance the subchannels to within ±4/10-in of water. For single phase water runs, radial pressure differential measurements were not attempted. Instead, rotameters were used to measure the exit flow rates from both subchannels and the manual valves were adjusted to give equal flow rates.

3. Square-Triangular Array Mixing Runs

For all single phase air mixing runs the flow split of the fluid between the two subchannels was adjusted to get zero radial pressure difference (time-average) along the interconnection length. The pressure at the mid point of the interconnection length was maintained at 50 psia. For single phase water mixing runs, no radial pressure measurements were attempted. Instead theoretical flow split calculations were made to obtain flows in each subchannel so as to give equal axial pressure gradients. Rotameters were used to measure the exit flow rates for both subchannels. Tracers were injected alternately in each channel to insure that diversion crossflows were negligible.

For the two-phase mixing runs, the flow rates of air and water both into and out of the subchannels were adjusted to achieve the conditions of zero radial pressure difference along the interconnection length and 50 psia pressure at the mid point of the mixing length. One set of flow rates was selected for the square channel and then various combinations of mass flux and quality were introduced in the triangular channel so as to achieve the condition of equal axial pressure drop in both subchannels. Flow rates of air and water from the exit of each subchannel were measured by using rotameters and the direct weighing technique respectively.

IV. RESULTS AND DISCUSSION
SINGLE PHASE MIXING

All the turbulent mixing data illustrated here graphically are tabulated in Appendix IV.1 or in Reference (15). The mixing rates were calculated from tracer concentrations using the expression:

$$W' = - \frac{W_1 \; W_2}{W_T \; L} \quad \ln \left[\frac{(W_1/W_T) - C_{1e}}{W_1/W_T} \right] \qquad (4.1)$$

where C_{1e} is the fraction of the total tracer at the exit of the originally untraced subchannel. For the special case of the square-square geometry ($W_1 = W_2 = W$), this expression reduces to:

$$W' = - \frac{W}{2L} \quad \ln(1 - 2\, C_{1e}) \qquad (4.2)$$

These equations are derived in Appendix IV.2.

A. Square-Square Geometry Mixing Results

The variation of single phase air and water mixing rates with Reynolds number and the interconnection gap spacing was investigated.

The water and air mixing rates for all the three gap widths are plotted as a function of Reynolds number in Figure 4.1. Over the range of Reynolds number and gap spacings studied, there was no difference between air and water mixing rates within the scatter of data except for the 0.015-in

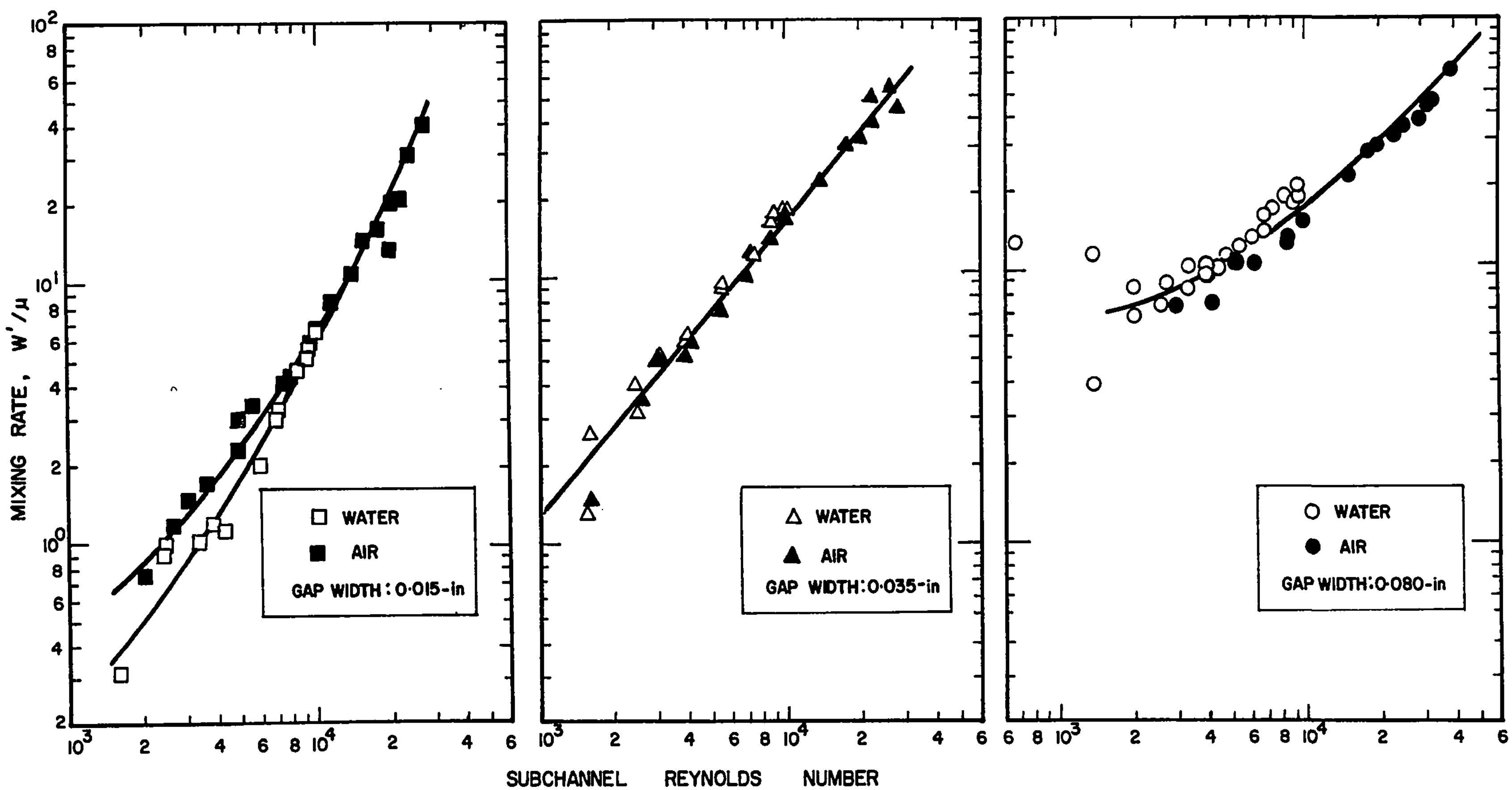

FIGURE 4.1 Variation of Single-Phase Mixing Rates with Subchannel Reynolds Number

gap at Reynolds number less than about 7000. Here water mixing rates were lower than those for air which suggested a difference in the mechanism of mixing at this small gap spacing.

The Schmidt number for methane in air is approximately unity and for potassium ions in water is approximately 1000 (14). Therefore, if diffusion is important, the mixing rates for water would be lower than those obtained for air. For this reason, molecular diffusion was negligible compared to eddy diffusion for the 0.035-in and 0.080-in gap spacings. However, for the 0.015-in gap spacing, it appears that there is an appreciable area near the gap where laminar flow exists so that mixing takes place by a combination of laminar and turbulent diffusion. For this reason, water mixing rates are expected to be less than the air mixing rates in the low Reynolds number range. Galbraith et. al. (17) discussed this phenomena in terms of a laminar sublayer which constituted a barrier to the penetration of turbulent eddies from one subchannel to the other.

The thickness of the laminar sublayer in the gap, δ, was calculated by using the relation (32):

$$y^+ = \frac{\delta}{De} \, Re \sqrt{f/2} \qquad (4.3)$$

where the laminar layer extends to a value of $y^+ = 5$. This relation yields a very approximate value of the laminar layer thickness as it applies for fully developed pipe flow.

It was found that for the 0.015-in gap geometry, the fraction of the gap spacing filled with the laminar layer varied from 0.96 to 0.33 over the Reynolds number range of 3000-10,000. This figure varied from 0.21 to 0.07 for the 0.080-in gap geometry; thus emphasizing the importance of molecular diffusion at lower gap spacings.

The Reynolds number dependency of the mixing parameter, G'/G, is shown in Figure 4.2 for both single phase air and single phase water runs. This mixing parameter is essentially a mixing Stanton number by analogy with turbulent convective heat transfer and is based upon the minimum interconnection area of the two subchannels. The variation of Stanton number with Reynolds number depended strongly on the interconnection gap spacing. Over the range of Reynolds number studied, the mixing Stanton number decreased with Reynolds number for the 0.080-in gap spacing; increased with Reynolds number up to a value of about 20,000 for the 0.035-in gap and then tended to decrease. However, the Stanton number for the 0.015-in gap spacing increased continuously over the range of Reynolds number investigated.

One hypothesis for this variation of Stanton number with Reynolds number for different gap spacings is the influence of secondary flows on turbulent mixing rates. In a non-circular duct, the generation of secondary flows is expected (33) for turbulent flow conditions. Secondary flows arise from a variation in the shear stress around the periphery of a

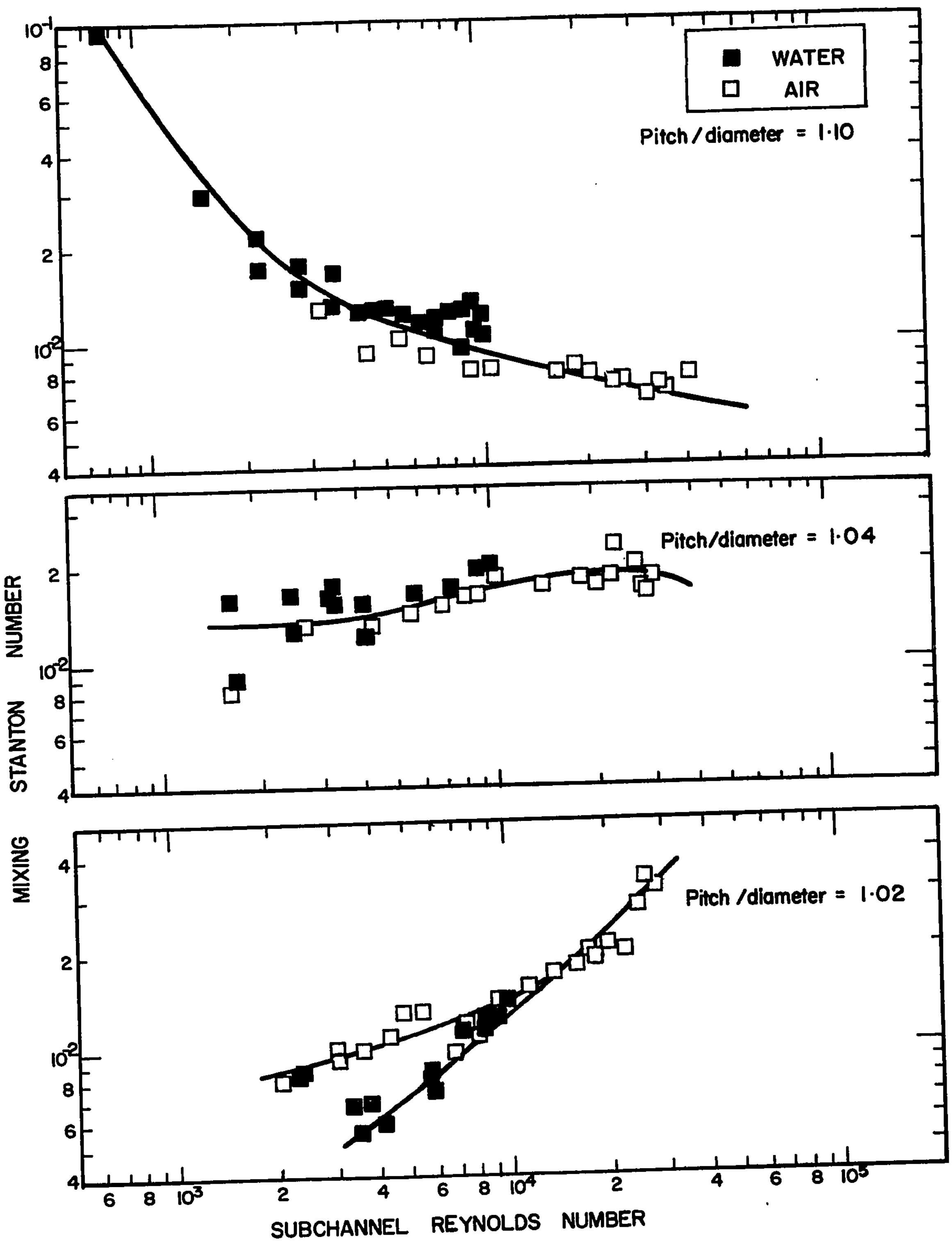

FIGURE 4.2 Variation of Single-Phase Mixing Stanton Number with Subchannel Reynolds Number

non-circular duct (34). Gessner and Jones (35) stated that secondary flow is the result of a complex interaction between the Reynolds stresses in planes normal to the axial flow direction and transverse static pressure gradients. From actual measurements, it was found that the largest turbulent stress variations along the streamline exist in the immediate vicinity of the corner where secondary flow is a maximum.

The magnitude of these secondary flows in simple rectangular or square geometries is typically in the range of 1 to 2% of the axial velocity (35). Lyall (36) measured secondary flows in two interconnected square subchannels and found their magnitude near the gap region to be as great as 3.5% of the local primary velocities. Secondary flow aids in convecting the main flow momentum and energy towards the wall in some regions and away from the wall in others. Ying (24) has shown that secondary flows have an appreciable influence on the overall Stanton number and friction coefficients; his predictions for these quantities were some 20% higher than those obtained when the secondary motions are set to zero. Skinner <u>et</u>. <u>al</u>. (16) concluded from their mixing studies on adjacent subchannels that the high rate of transfer of heat or mass through the gaps between the rods is due to secondary flow.

From measurements of Gessner and Jones (35), Lyall (36) and Hoagland (37), it is known that the magnitude of secondary flow, expressed as a percentage of the primary flow, reduces with increasing Reynolds number. This is expected as the distribution of the wall shear stress tends towards greater uniformity with increasing Reynolds mumber (35). At very high Reynolds number, the strength of secondary flows should approach zero as the shear stress distribution becomes uniform. Brundrett and Baines (38) have shown that secondary currents may penetrate further into the corners as the Reynolds number increases. The wall shear measurement of Leutheusser (39) also indicated an increasing corner penetration as the Reynolds number increased.

Deissler and Taylor (40) calculated shear stress distributions around the dividing rod surface for square and triangular arrays at various pitch to diameter ratios. The maximum variation of peripheral stress was predicted for the lowest pitch to diameter ratios, and for the square as compared to the triangular array.

From the preceeding, the generation and penetration of secondary flows into the gap region of a subchannel array are expected to be a function of Reynolds number, pitch to rod diameter ratio and subchannel type (i.e., square or triangular).

The largest variation in the shear stress over the rod periphery is experienced with the smallest pitch to diameter ratio. One would then expect to generate the strongest secondary currents under these conditions. But in order for secondary flows to enhance the mixing rate between the two subchannels, they must reach the gap region.

The damping effect of the walls on the turbulent fluctuations would be a maximum for the smallest pitch to diameter ratio. Secondary flows can not penetrate into the gap region at low Reynolds number for the 0.015- and 0.035-in gap geometries; hence the lower Stanton number compared to that for the 0.080-in gap although one would expect the strongest secondary flows with the 0.015- and 0.035-in gap spacings. For very high flows when fully developed turbulence is reached, the secondary flows penetrate the gap region completely and the smallest pitch to diameter ratio produces the highest Stanton number. For increasing Reynolds number, the magnitude of secondary flow and hence the Stanton number would decrease for all gap geometries.

B. Square-Triangular Geometry Mixing Results

For the square-triangular geometry, the variation of single-phase air and water mixing rates with Reynolds number for a fixed gap spacing of 0.035-in was investigated. The mixing rates are plotted as a function of average Reynolds number* in Figure 4.3. Over the range of Reynolds number studied, mixing rates, in general, increased with Reynolds number. The water mixing rates were lower than the air mixing rates and the difference between them decreased with increasing Reynolds number. At a Reynolds number of over 5000, the air and water mixing rates were nearly identical. This indicates

* The average Reynolds number has been defined as:

$$Re_{av} = (Re_1 + Re_2)/2$$

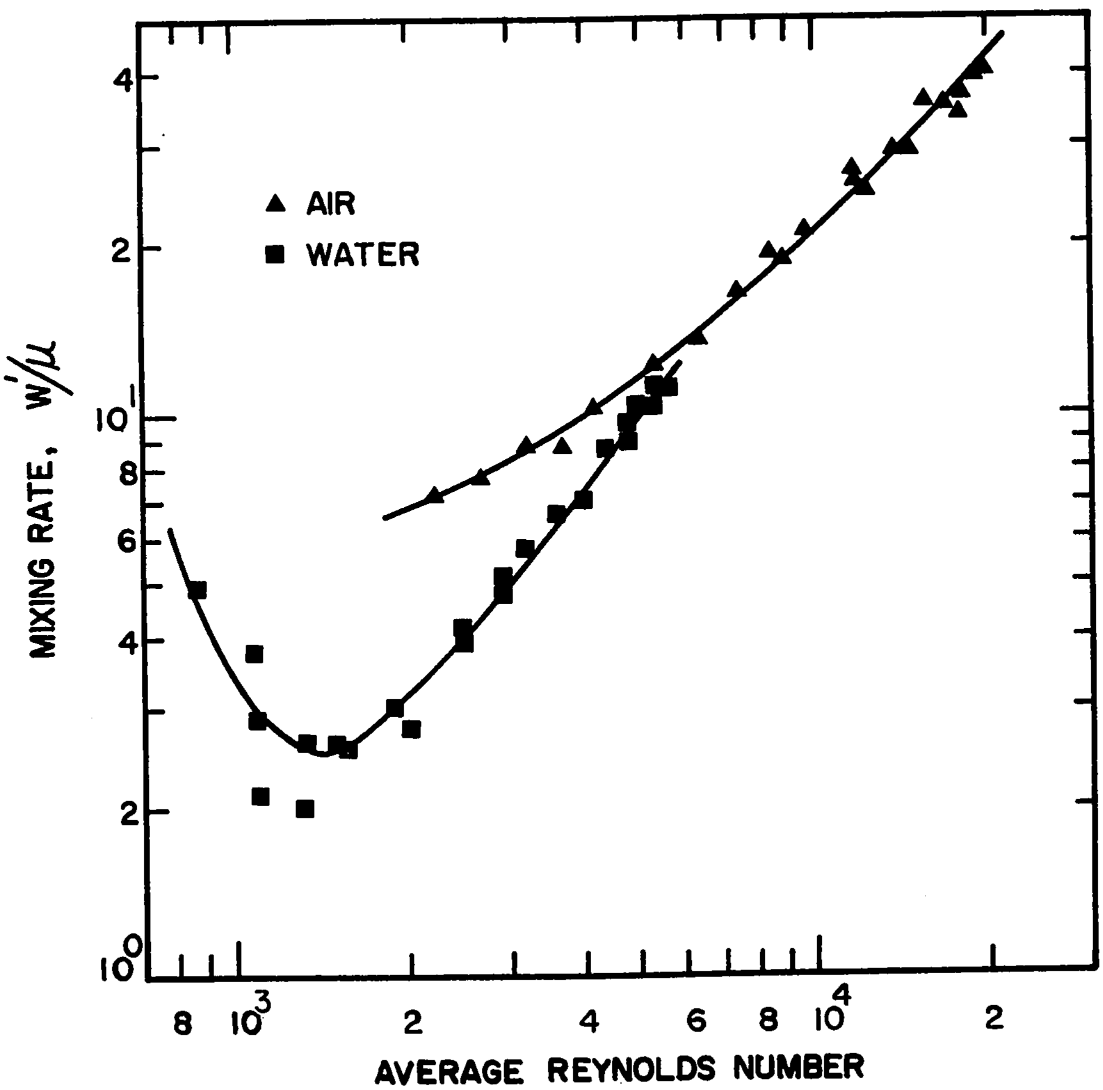

FIGURE 4.3 Variation of Single-Phase Mixing Rates with Subchannel Reynolds Number (Square-Triangular Geometry, 0.035-in gap)

that, for reasons discussed previously, molecular diffusion was important at the low Reynolds number investigated. The mixing at these Reynolds numbers apparently took place by a combination of molecular and eddy diffusion.

The fractional mixing rates for both single-phase air and water are plotted as a function of subchannel Reynolds number in Figure 4.4. On the same plot are shown Walton's (15) data for a triangular-triangular geometry with a 0.040-in gap and the square-square geometry data for a 0.035-in gap spacing. This figure demonstrated that the mixing rates are influenced by the subchannel geometry for the same nominal gap spacing and pitch to diameter ratio. The fractional mixing rates decreased in the following order: triangular-triangular, triangular-square and square-square geometries.

C. Comparison with other Investigations

Mixing rate data for rod bundle arrays are difficult to compare directly with that for two "clean" subchannels since crossflow or spacer flow scattering effects influence rod bundle mixing rates. Consequently mixing in rod bundles has been found to be appreciably higher (2 to 3 times) than mixing in "clean" two-subchannel geometries (10). There is ample evidence available now indicating that mixing is also a function of the subchannel shape; so that a comparison is made only with the geometries similar to the ones used in this work.

Results of the mixing experiments obtained with the square-square geometry are compared with Rowe and Angle's (13) data in Figure 4.5. At high Reynolds number, the Stanton number

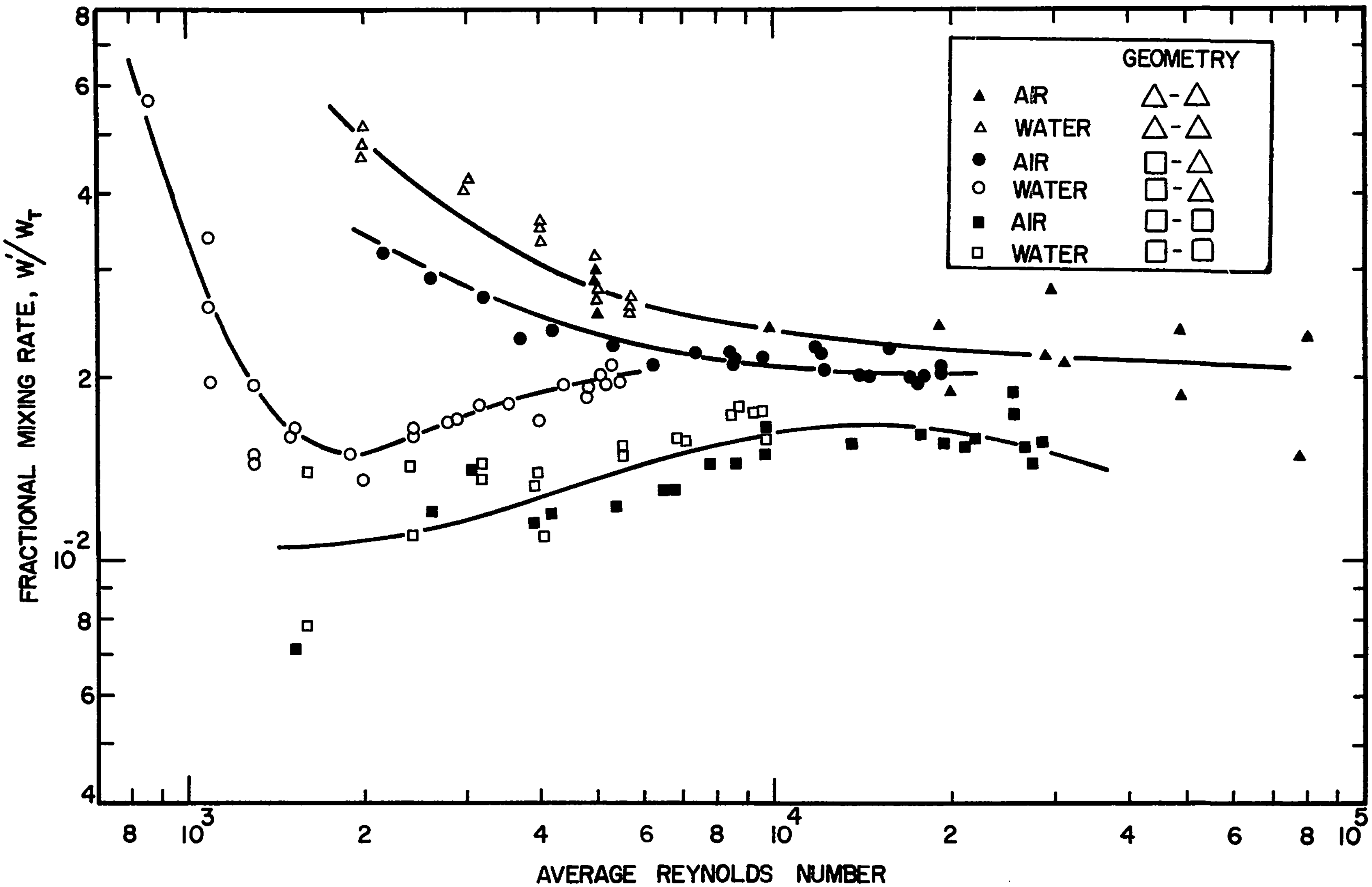

FIGURE 4.4. Variation of Single-Phase Fractional Mixing Rates with Subchannel Reynolds Number

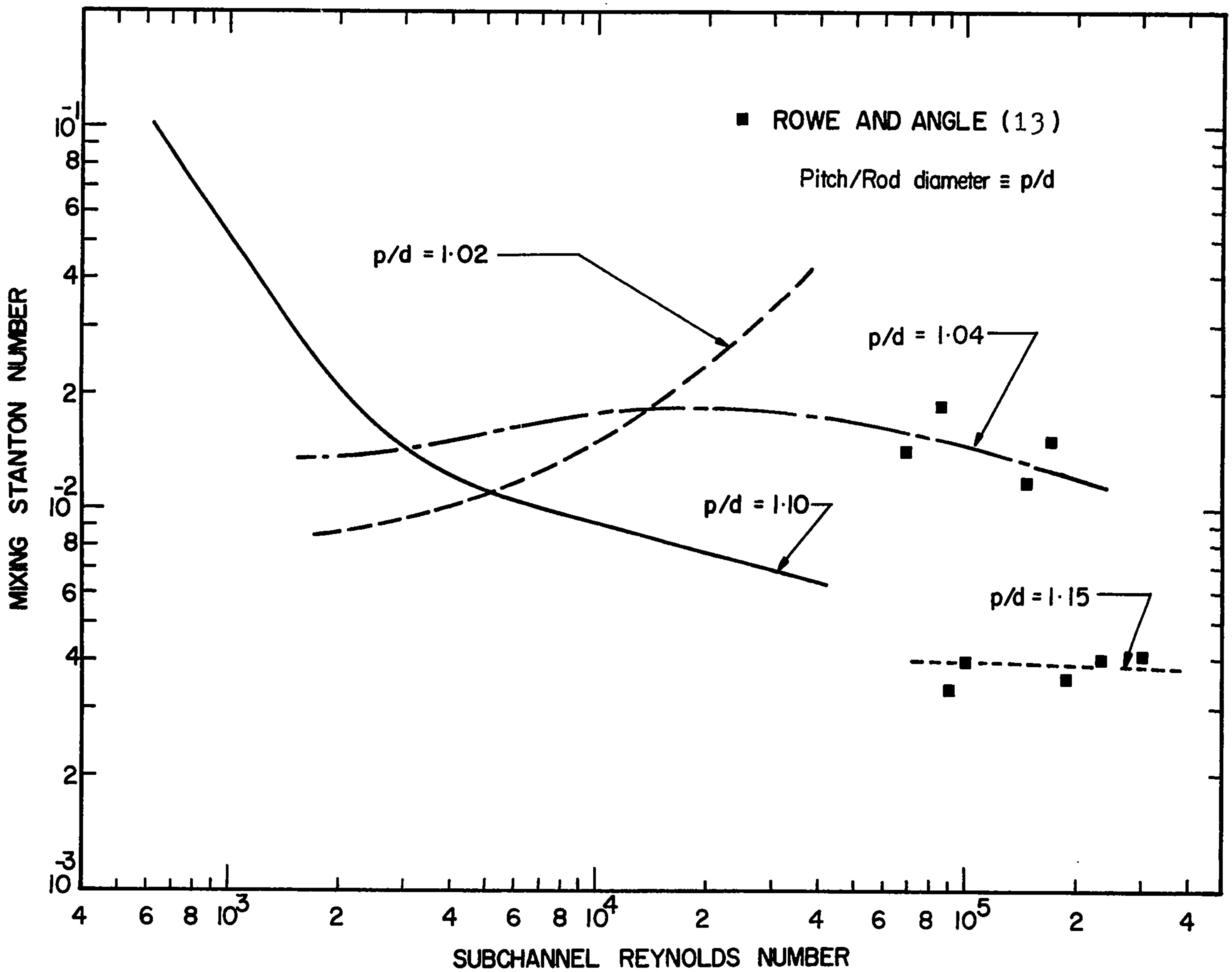

FIGURE 4.5 Variation of Mixing Stanton Number with Subchannel Reynolds Number (Square-Square Geometry)

decreased as the pitch to diameter ratio is increased. Rowe and Angle's data and results obtained here at the same pitch to diameter ratio (1.04) can be correlated with a smooth continuous curve. A consistent trend is obtained for all of the data which is promising for a mixing correlation. However, more data are required at high Reynolds number and various pitch to diameter ratios to obtain a reliable correlation.

A test section (Figure 4.6) very similar to the one used here was employed by Galbraith and Knudsen (17). Single phase

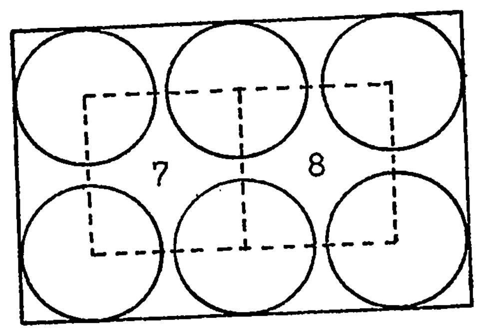

FIGURE 4.6 Cross-sectional View of Test Section used by Galbraith and Knudsen (17)

water Stanton number increased with Reynolds number for all gap spacings. However, the authors used the mean tracer concentration in one-half of the test section to calculate mixing rates between the square subchannels 7 and 8. This gave mixing rates which are believed to be lower than the actual mixing rates. An analysis of their data indicated that use of these mean concentrations for short interconnection lengths (16-in) could result in appreciable errors in mixing rates. Errors would approach a maximum magnitude of 75% at the lowest gap spacings and low Reynolds number. For this reason, Galbraith and Knudsen's mixing data are not represented on this plot.

The fractional mixing rates, $W'/(W_1 + W_2)$, are compared with Rowe and Angle's data for square-triangular (11) and square-square (13) geometries in Figure 4.7. Rowe and Angle's data show trends which are consistent with results obtained here; the mixing rates for the square-triangular geometry are higher than the ones for square-square geometry. However, no satisfactory explanation can be construed at the present moment for the difference between the results of two sets of data or for the fact that Rowe and Angle's mixing rates are apparently independent of gap spacing.

This result is also in agreement with predictions from Rosehart and Roger's (10) correlation which implied that the effective mixing distances increased in the order triangular-triangular, triangular-square and square-square. Rowe and Angle (13) postulated that tracer (or temperature) gradients within the subchannels can affect the mixing results and this can account for the different mixing results in various shaped subchannels.

D. <u>Comparision of Experimental Results with Predictions from Analytical Models</u>

Of the various models proposed for determination of turbulent mixing rates between adjacent subchannels, Bowring's (1) and Rowe and Angle's (23) were selected for comparison since they are used widely. A brief description of these models is given in Appendix IV.3.

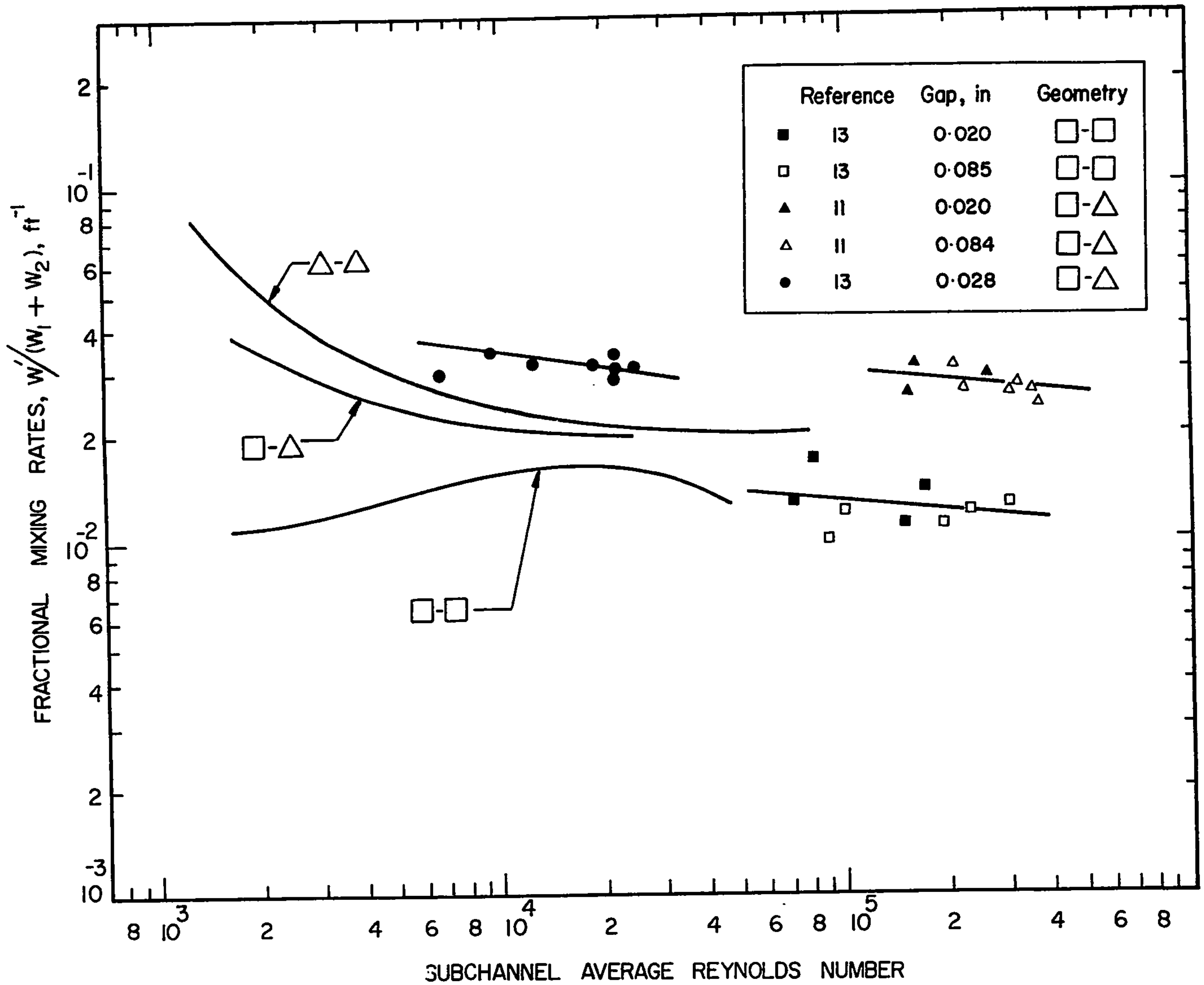

FIGURE 4.7 Variation of Fractional Mixing Rates with Subchannel Reynolds Number

The single phase air mixing results were compared with predictions from these models for both square-square geometry with a 0.080-in gap (Figure 4.8) and square-triangular geometry with a 0.035-in gap (Figure 4.9). The water mixing results for the square-triangular geometry were not included in the comparison because of an apparently strong influence of molecular diffusion on experimental mixing rates. Bowring's model accurately predicted the mixing data when F_m, a mixing factor, equalled 3 for the square-square geometry and 8 for the square-triangular geometry. These values of F_m are in approximate agreement with the values suggested by Bowring (6) for "clean" systems. Rowe's correlation predicted the mixing rates to within -25% for square-square geometry and to within +40% for the square-triangular geometry. It should be noted that neither of these models predicts the mixing trends observed for the 0.035- and 0.015-in gap square-square geometry; apparently because of the failure of these models to take into account the effect of secondary flows on mixing rates at low Reynolds number.

General correlations for the prediction of mixing rates cannot be developed until detailed information on the mechanism of mixing including the structure of turbulence in the gap (scale of turbulence, turbulence intensity, velocity profile etc.) is acquired. The effect of secondary flows on the mixing rates, especially at low Reynolds numbers, should be incorporated into these models.

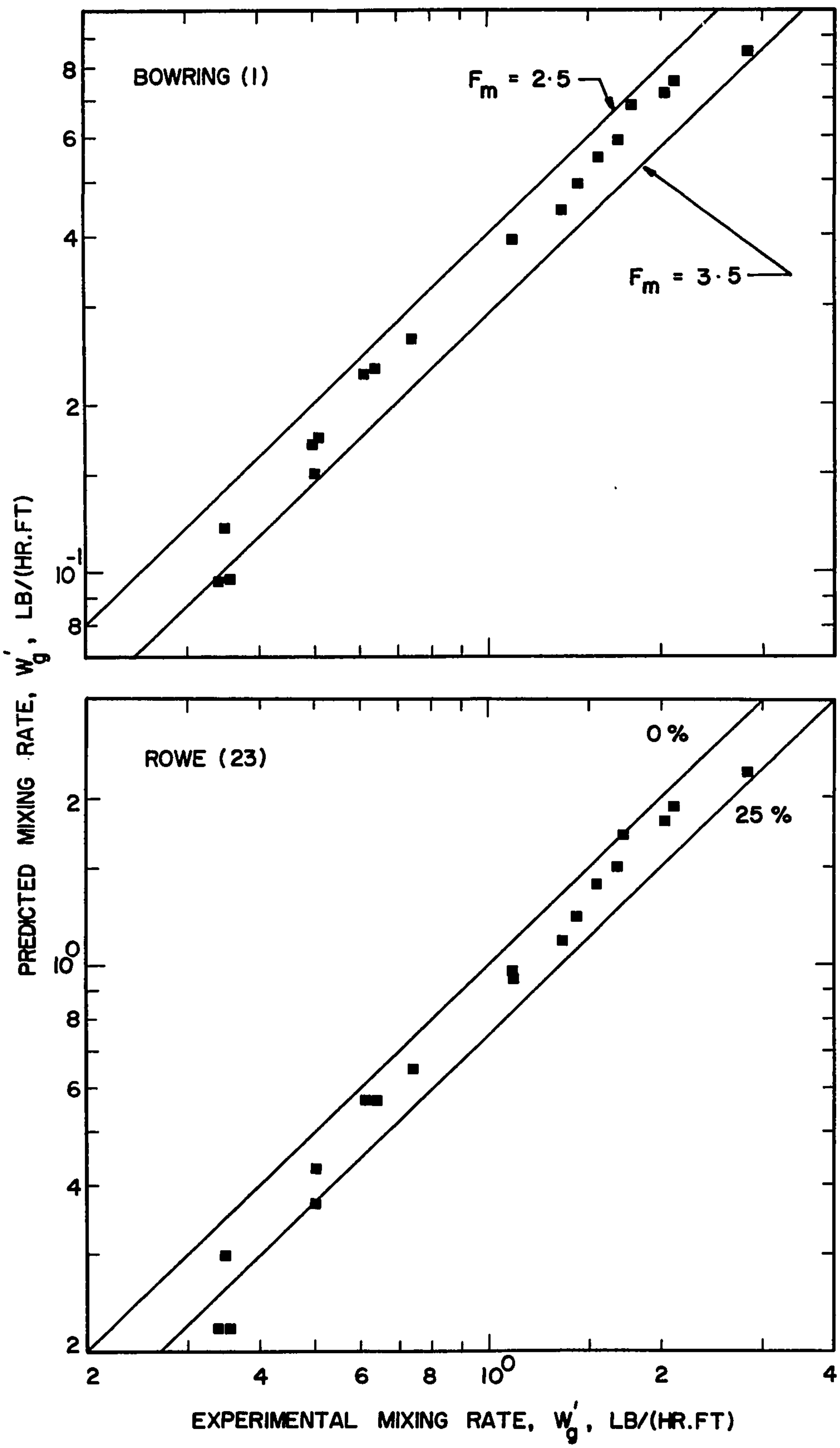

FIGURE 4.8 Comparison of Experimental and Predicted Mixing Rates (Square-Square Geometry, 0.080-in gap)

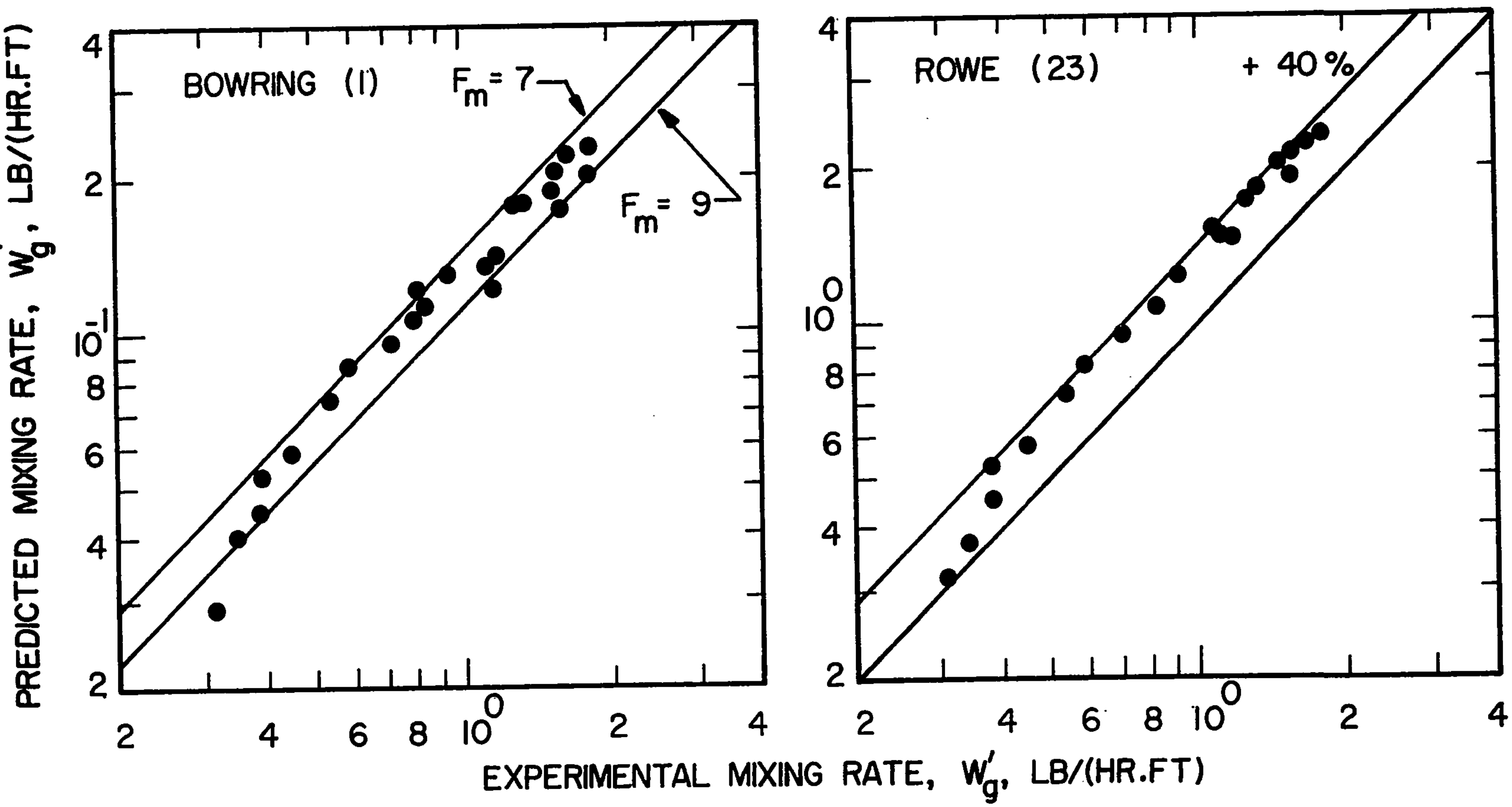

FIGURE 4.9 Comparison of Experimental and Predicted Mixing Rates (Square-Triangular Geometry, 0.035-in gap)

V. RESULTS AND DISCUSSION
TWO-PHASE MIXING

A. Square-Square Geometry Mixing Results

All the turbulent mixing data illustrated here graphically are tabulated in Appendix V.1 or in References (15,26). The mixing rates were calculated from tracer concentrations using the expression:

$$W' = -\frac{W}{2L} \ln(1 - 2 C_{1e}) \qquad (4.2)$$

where C_{1e} is the fraction of the total tracer at the exit of the originally untraced subchannel. This equation is derived in Appendix IV.2. Turbulent mixing rates were measured for a range of subchannel mass flux, quality and three interconnection gap spacings.

An error analysis of the results is given in Appendix V.2.

1. Variation of Mixing with Subchannel Mass Flux and Quality

Data over an extended quality range were acquired for the square-square geometry with a 35-mil gap spacing. The variation of air and water turbulent mixing rates with quality is illustrated in Figure 5.1 for two representative mass fluxes. Shown on the same figure are Rudzinski's (26) data which were obtained using a triangular subchannel array with a 40-mil gap spacing. Air and water mixing rate maxima, which occur at different qualities, are of major interest.

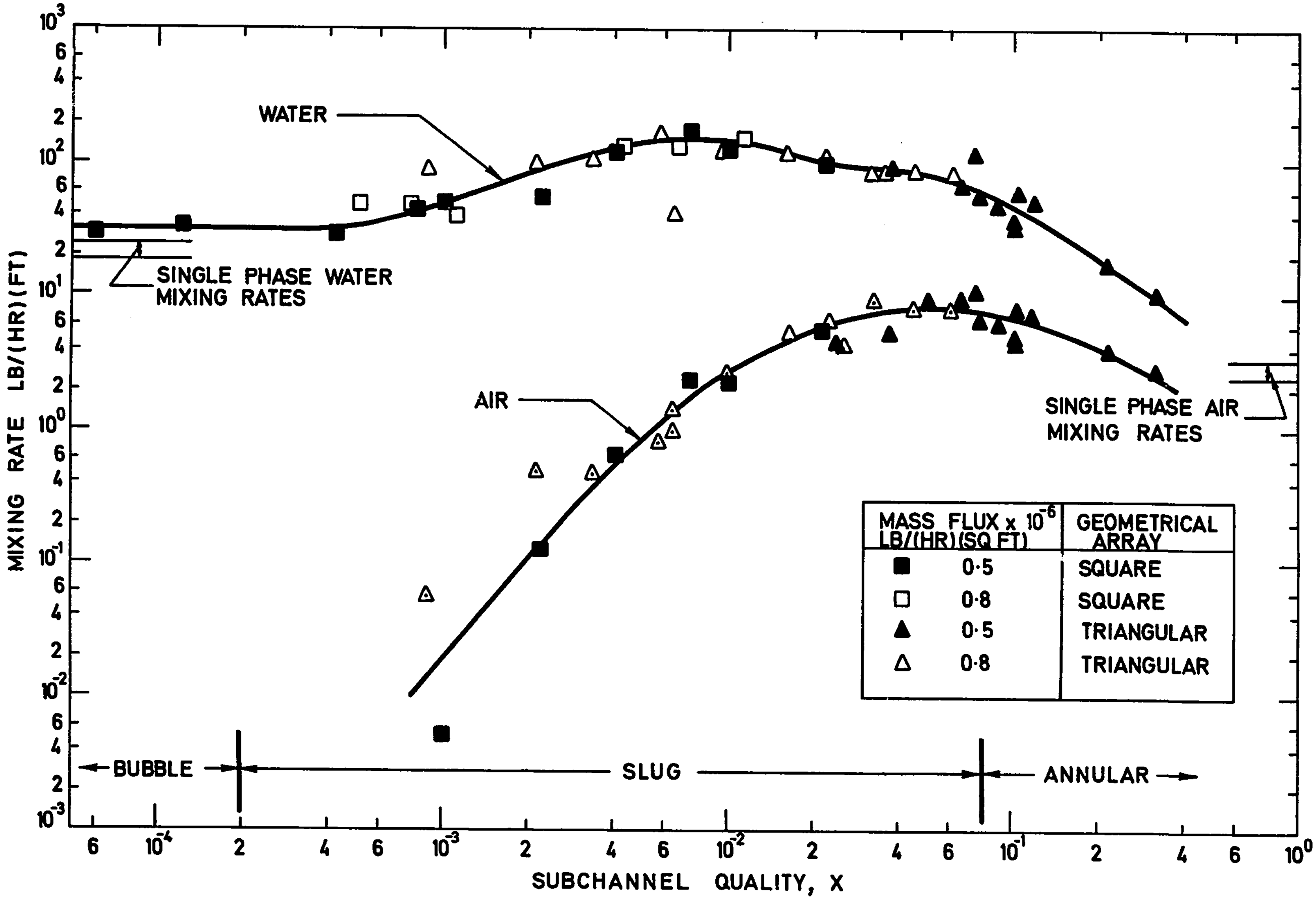

FIGURE 5.1 Variation of Mixing Rates with Subchannel Quality

The maxima occur in the slug flow regime as indicated by the approximate locations of the bubble-slug and slug-annular flow transition lines.

In the bubble flow regime and through the bubble-slug transition, which was defined arbitrarily as the quality where the air volumetric fraction equalled 10%, the water interchange rates remained essentially constant at a value greater than the single phase water mixing rates (15) measured at the same total mass flux. However, the air mixing rates decreased to such a low level that accurate tracer measurements were not possible. A marked increase in both air and water mixing rates occured when the subchannel qualities exceeded 0.04%. At a quality of 0.7%, the water mixing rates reached a maximum. The maximum air mixing rates occured at a quality of 6% at flow conditions near the slug-annular transition according to the Griffith and Haberstroh criterion (41). Similar observations were reported by Rowe and Angle (11,13) who, in a parallel study, employed a steam-water system at pressures of 400, 750 and 900 psia.

In order to investigate a possible correlation between the mixing rates and the magnitude of the radial pressure oscillations, a pressure transducer was mounted at the mid-point of the subchannel interconnection length for the 0.035-in gap spacing. Mixing rates increased with increasing pressure oscillations. The magnitude of the radial pressure difference in the annular flow regime and near the slug-annular flow regime transition was approximately 0.15-0.25 psid peak-to-peak. This is in close agreement with the values reported by Rudzinski et. al. (42) for mixing tests in a triangular array test section.

The mixing data was correlated using the parameter, G'/G, which is a mixing Stanton number by analogy with turbulent convective heat transfer; and is based upon the minimum interconnection area of the two subchannels. Figures 5.2 and 5.3 show that the mixing parameter effectively correlated the data for both square and triangular (26) array geometries as a function of mass flux and quality though admittedly over a limited parameter range. Note that the liquid mixing parameter for a mass flux of 1×10^5 lb/(hr.sq ft) in Figure 5.2 is drawn with a segmentary line between qualities of 10^{-3} and 0.06 as there was essentially complete mixing within the subchannel length for this quality range. For this reason, the shape of the G_l'/G_l curve does not give a true indication of the variation of mixing rates with quality. As before peak mixing rates were measured in the slug flow regime, where the observed slug-annular transitions for the triangular subchannel array geometry were defined by Walton (15) as $j_g^* = 4.5 + 0.6\, j_l^*$.

For increased mass flux, there was a decrease in the mixing parameters and the quality region over which higher mixing rates were observed. This is consistent with data of Rowe and Angle (13) as shown in Figure 5.4 and observations that the slug-annular flow regime transition occurs at lower qualities for increased mass flux. The liquid mixing parameter under two-phase flow conditions was greater than the

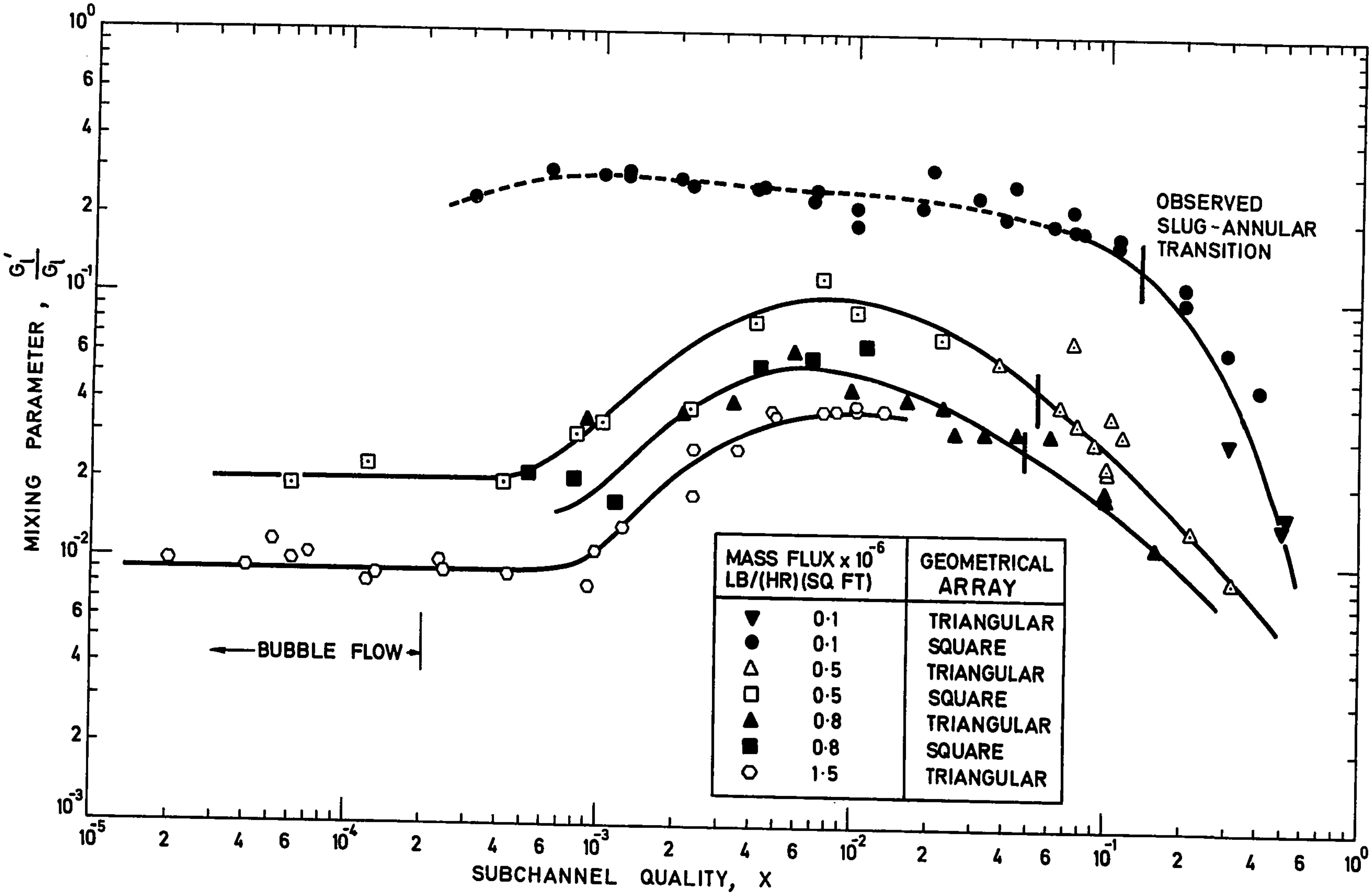

FIGURE 5.2 Variation of Water Mixing Parameter with Subchannel Quality

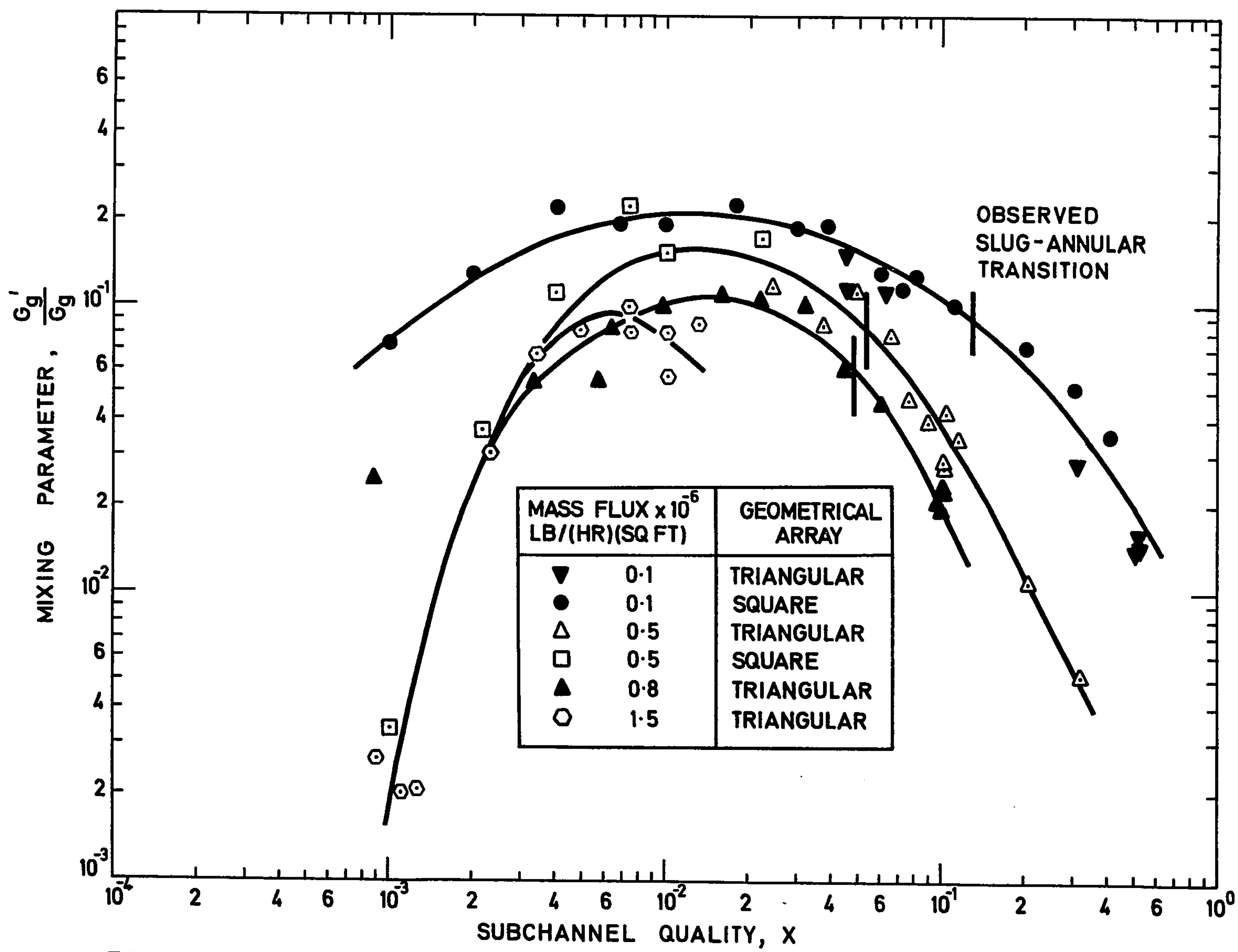

FIGURE 5.3 Variation of Air Mixing Parameter with Subchannel Quality

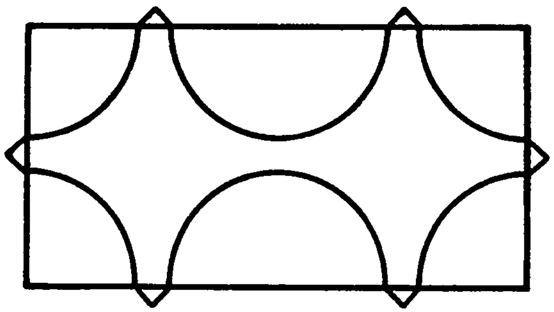

	GAP SPACING, in	
	0·020	0·085
ROD DIAMETER, in	0·564	0·564
SUBCHANNEL AREA, sq in.	0·130	0·173
INTERCONNECTION LENGTH, ft	5·0	5·0
PITCH/ROD DIAMETER	1·035	1·150

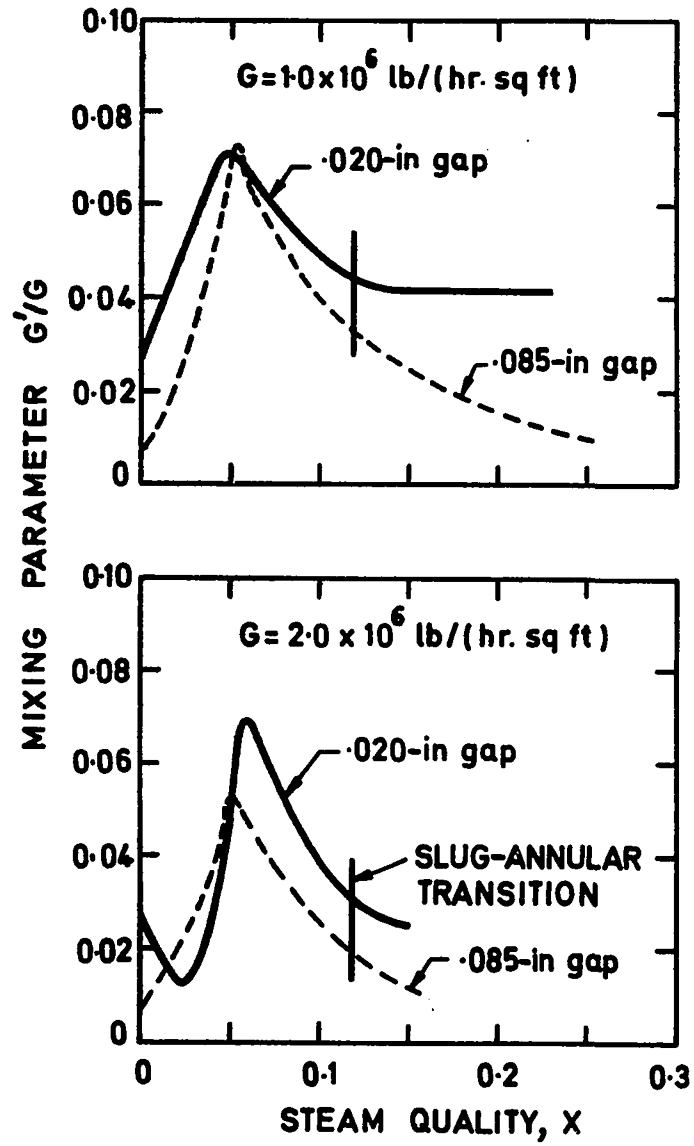

FIGURE 5.4 Estimated Variation of Mixing Parameter with Steam Quality at 400 psia (Rowe and Angle)

single phase Stanton number measured at the same total mass flux except for the high quality annular flow regime. Air mixing parameters were only greater than those for single phase flow in the slug and slug-annular flow regimes.

The air and water mixing parameters for the high quality annular flow regime range are plotted for three gap spacings as a function of subchannel quality in Figures 5.5 and 5.6 and as a function of subchannel mass flux in Figures 5.7 and 5.8. The regions of slug flow, slug-annular flow and annular flow, based on Steen-Wallis's criterion (43), are indicated on the figures. The mixing parameters over this quality range decreased exponentially with increasing quality and mass flux. The mixing increased as the slug-annular transition was approached. These trends are consistent with the data over the extended quality range reported previously.

2. Effect of Gap Spacing on Mixing Rates

One of the primary objectives of this study was the fundamental investigation of the effect of interconnection gap spacing on the two-phase turbulent mixing rates. The gap spacing was varied by more than a factor of 5 from 0.015-in to 0.080-in with only a 16% change in the subchannel flow area. The fractional mixing rates, W'/W, of air and water are shown as a function of gap spacing for two representative mass fluxes in Figures 5.9 and 5.10. Air and water fractional mixing rates increased with gap spacing for the range of subchannel mass flux and quality investigated. However, the

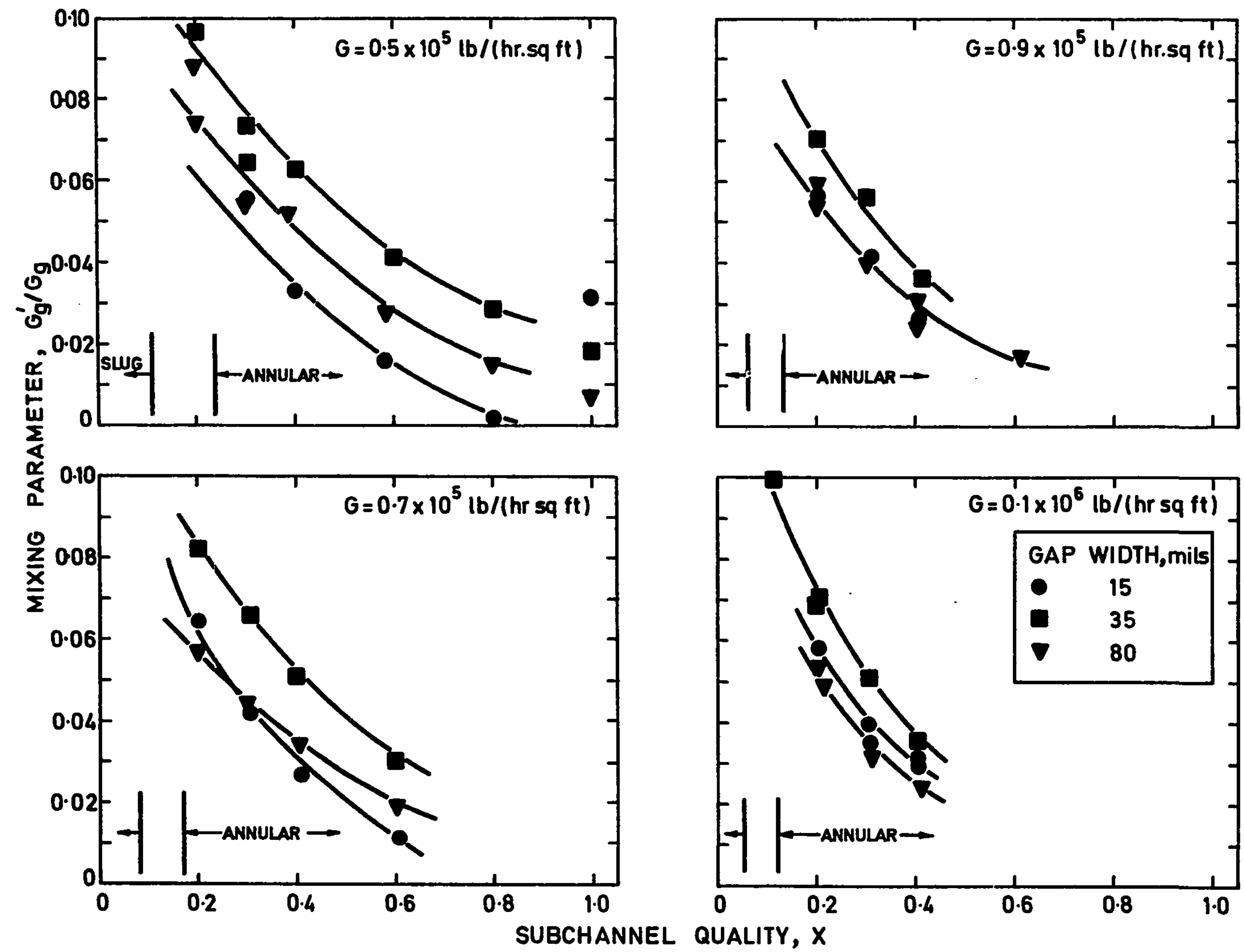

FIGURE 5.5 Variation of Air Mixing Parameter with Subchannel Quality

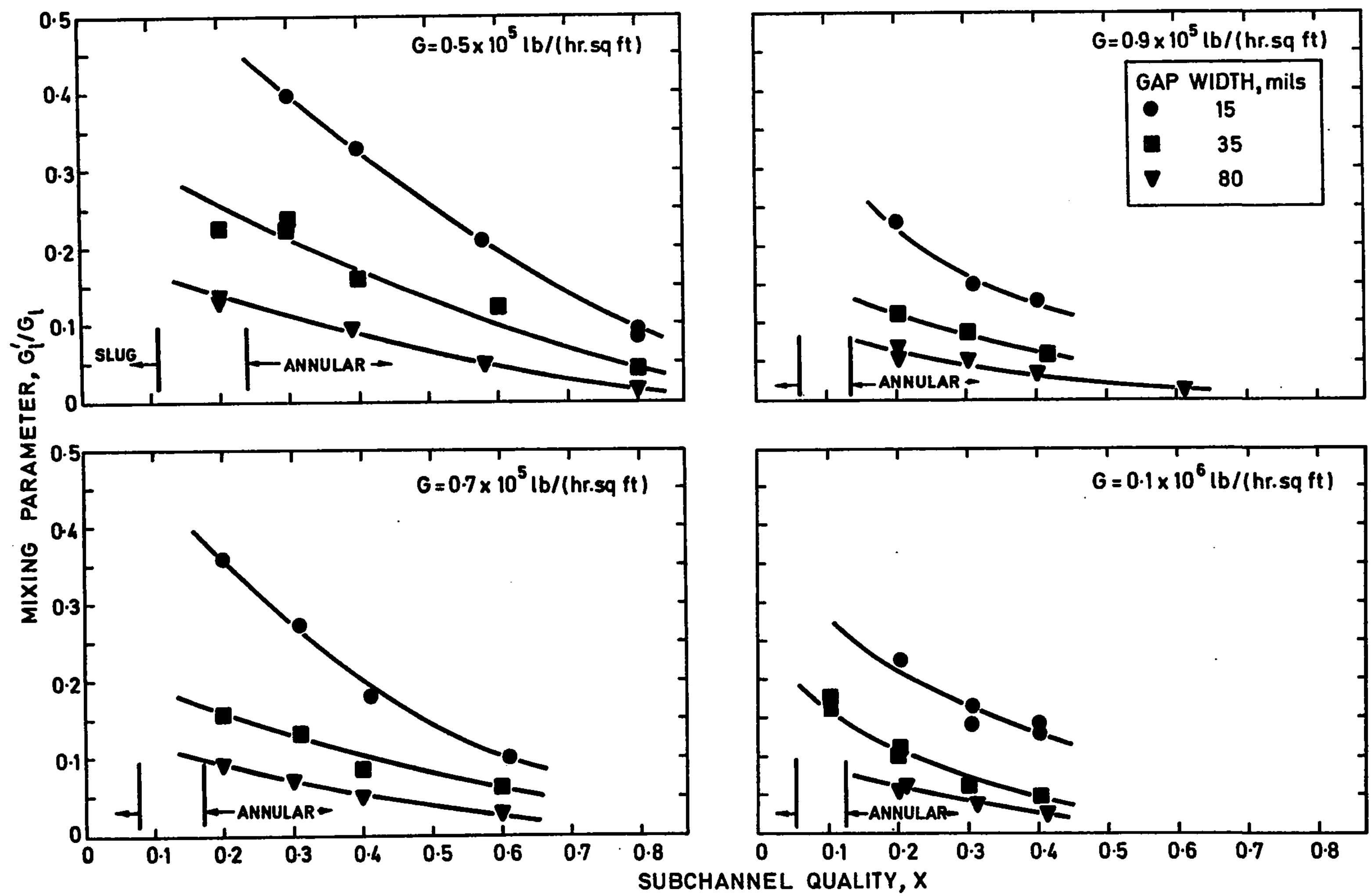

FIGURE 5.6 Variation of Water Mixing Parameter with Subchannel Quality

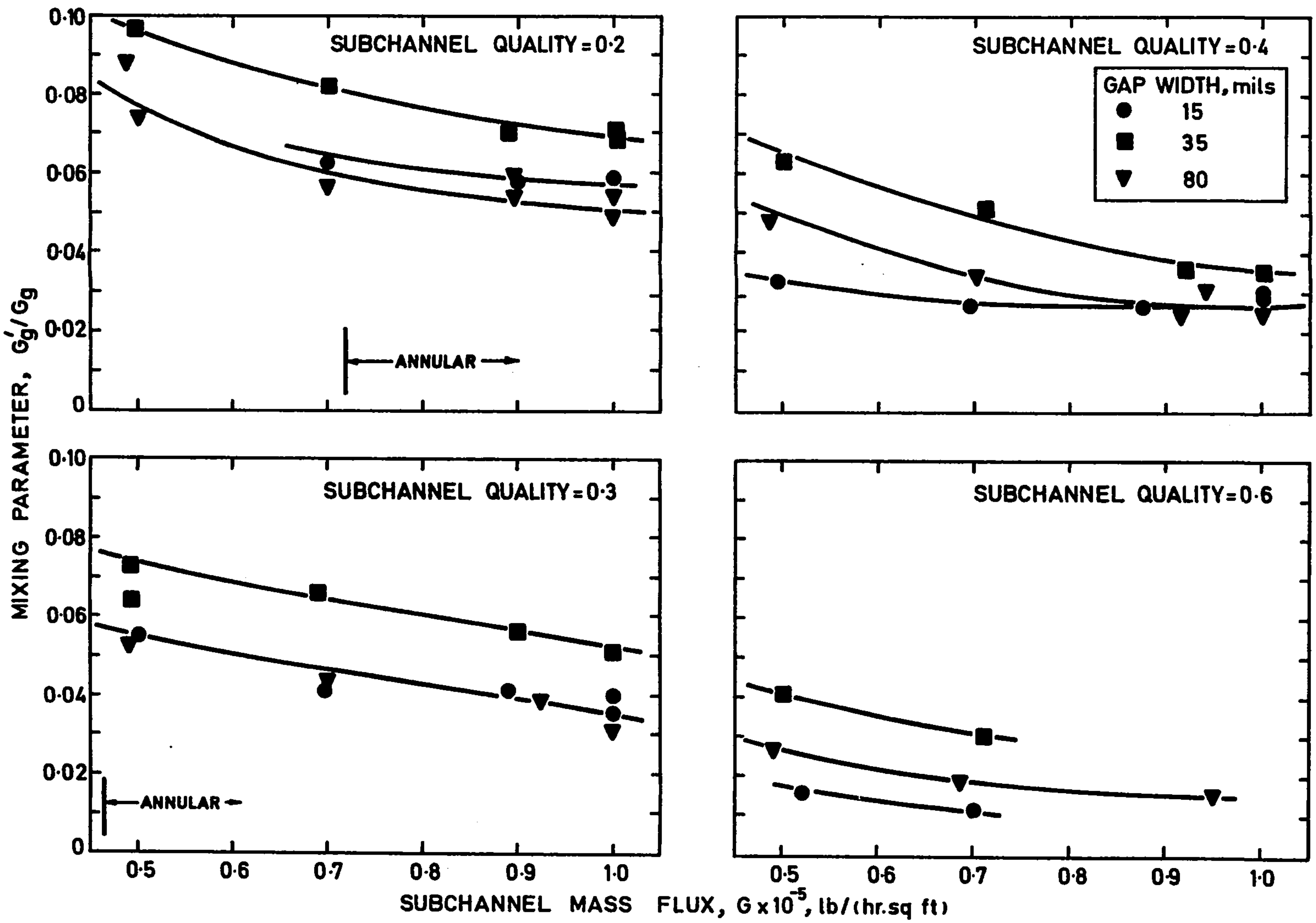

FIGURE 5.7 Variation of Air Mixing Parameter with Subchannel Mass Flux

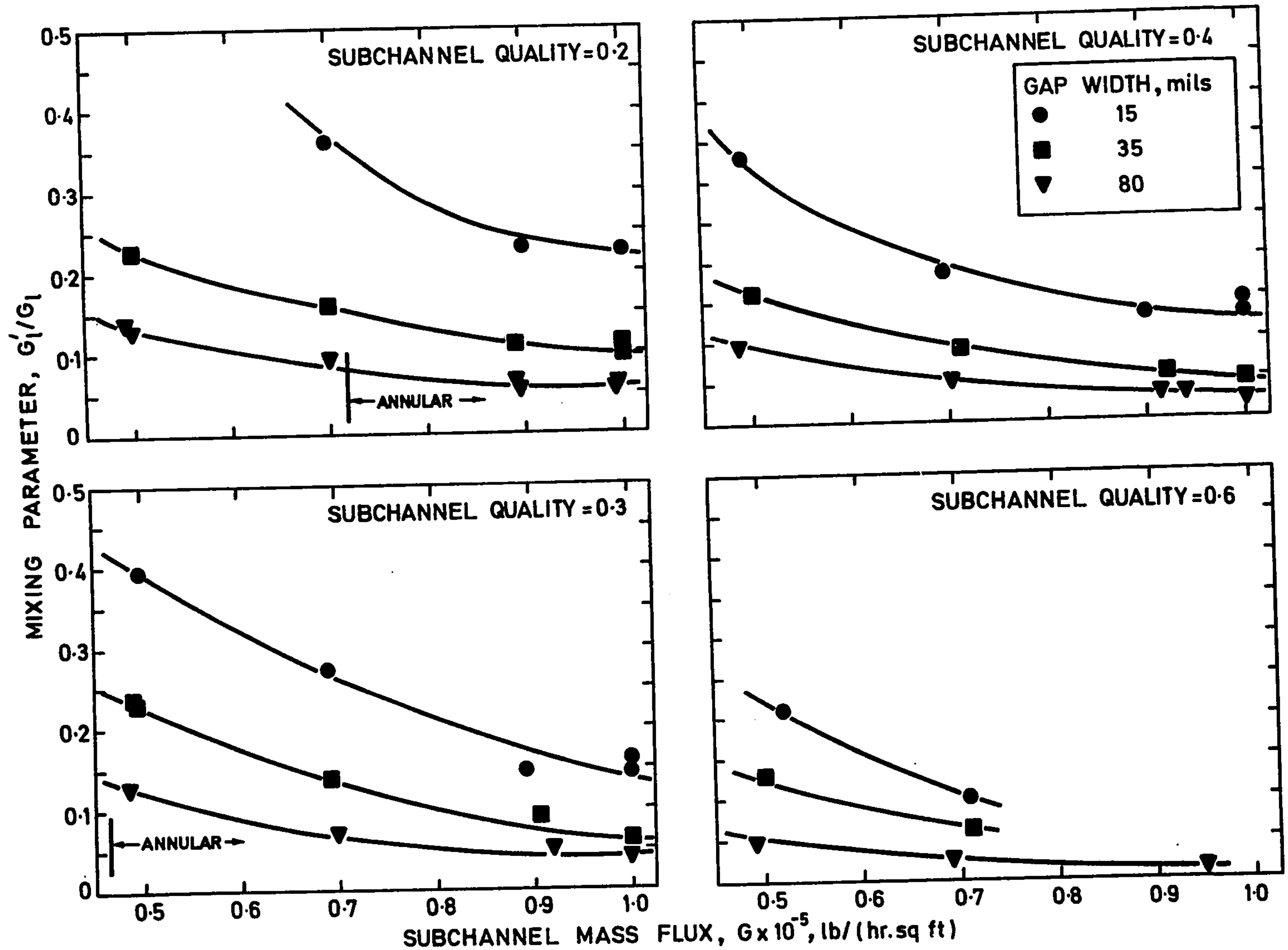

FIGURE 5.8 Variation of Water Mixing Parameter with Subchannel Mass Flux

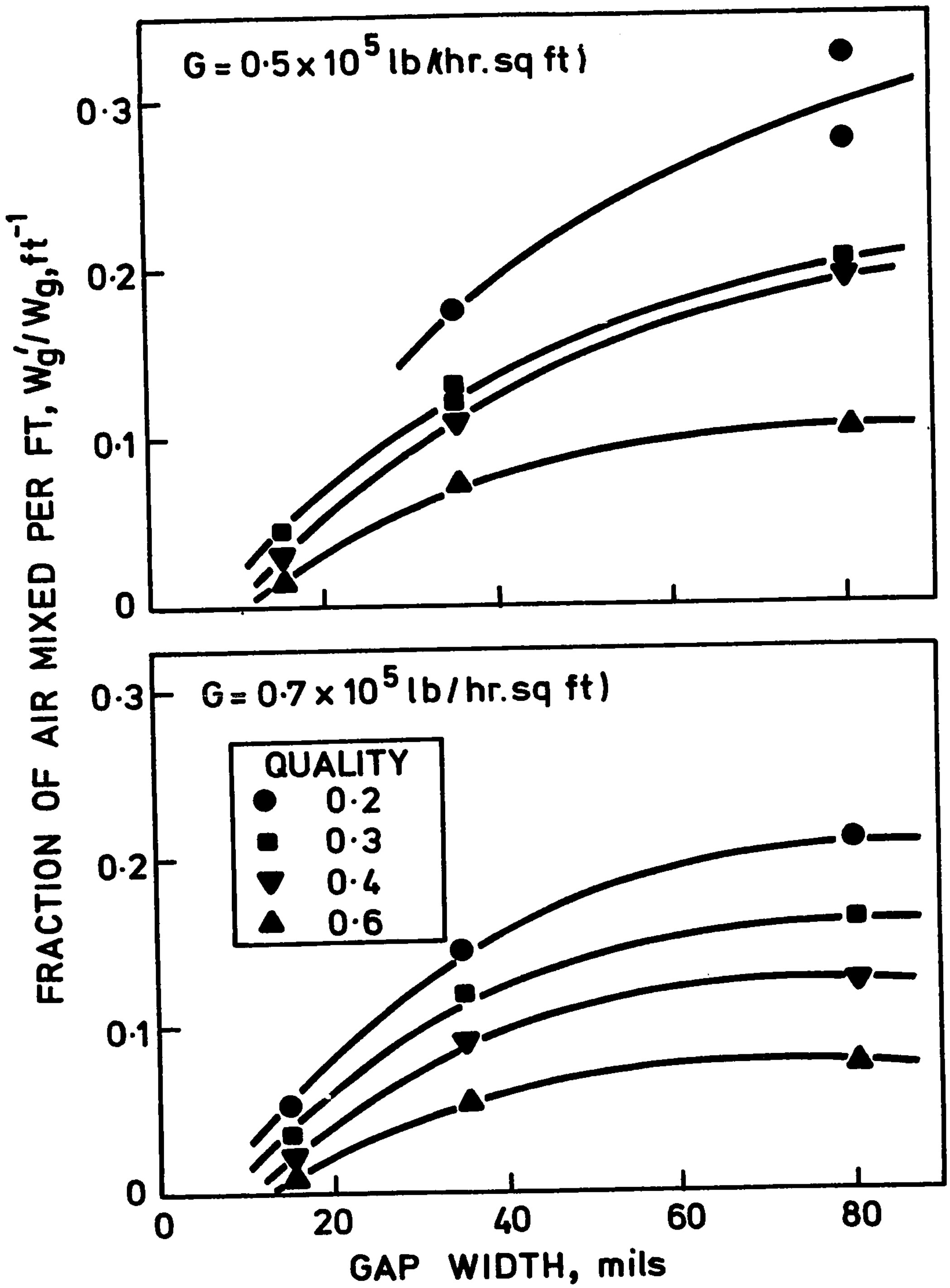

FIGURE 5.9 Effect of Gap Spacing on Air Fractional Mixing Rates

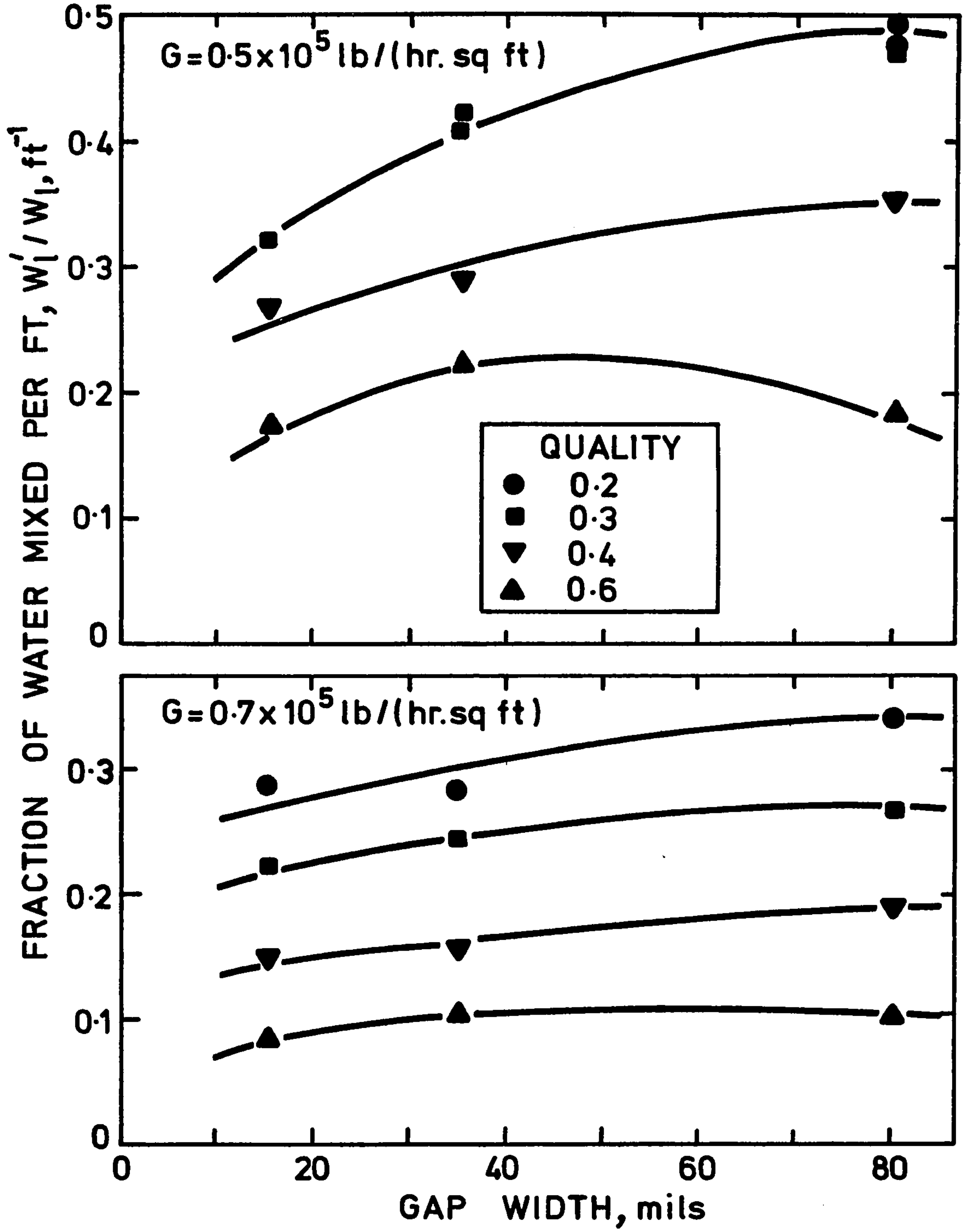

FIGURE 5.10 Effect of Gap Spacing on Water Fractional Mixing Rates

increase for water was small compared to that for air. This was not unexpected as the relative thickness of the liquid film in the gap, $\delta/(b/2)$, should be a maximum for the lowest gap spacing. Therefore, very low air mixing rates resulted for the 0.015-in gap. For the larger gap spacings, there was an appreciable increase in air mixing rates due to the greater "effective" areas available for air to mix. The increase in water mixing rates was comparatively small which indicated that the major portion of the water mixing occured in the liquid film near the gap. Another noteworthy feature of Figures 5.9 and 5.10 was that air and water fractional mixing rates were not proportional to the gap spacing.

3. Comparison of Mixing Quality with Subchannel Quality

The ratio of air to water interchange or mixing quality, $W_g'/(W_g' + W_l')$, was not always equal to the subchannel quality, $W_g/(W_g + W_l)$. This is shown in Figure 5.11 for both square-square and triangular-triangular (26) array geometries where for qualities less than 0.2%, the mixing quality fell below that in the subchannel indicating enhanced water interchange. The air mixing rates were low as the small gas volumes tended to flow as distinct bubbles or slugs in the central region of the subchannel flow area. The presence of air, however, promoted mixing of the water flowing in the gap region between subchannels. For intermediate qualities, there was enhanced air interchange. Here the air volumetric fractions ranged from ~35 to ~85% in the slug and slug-annular flow regimes where the two-phase flowing mixture

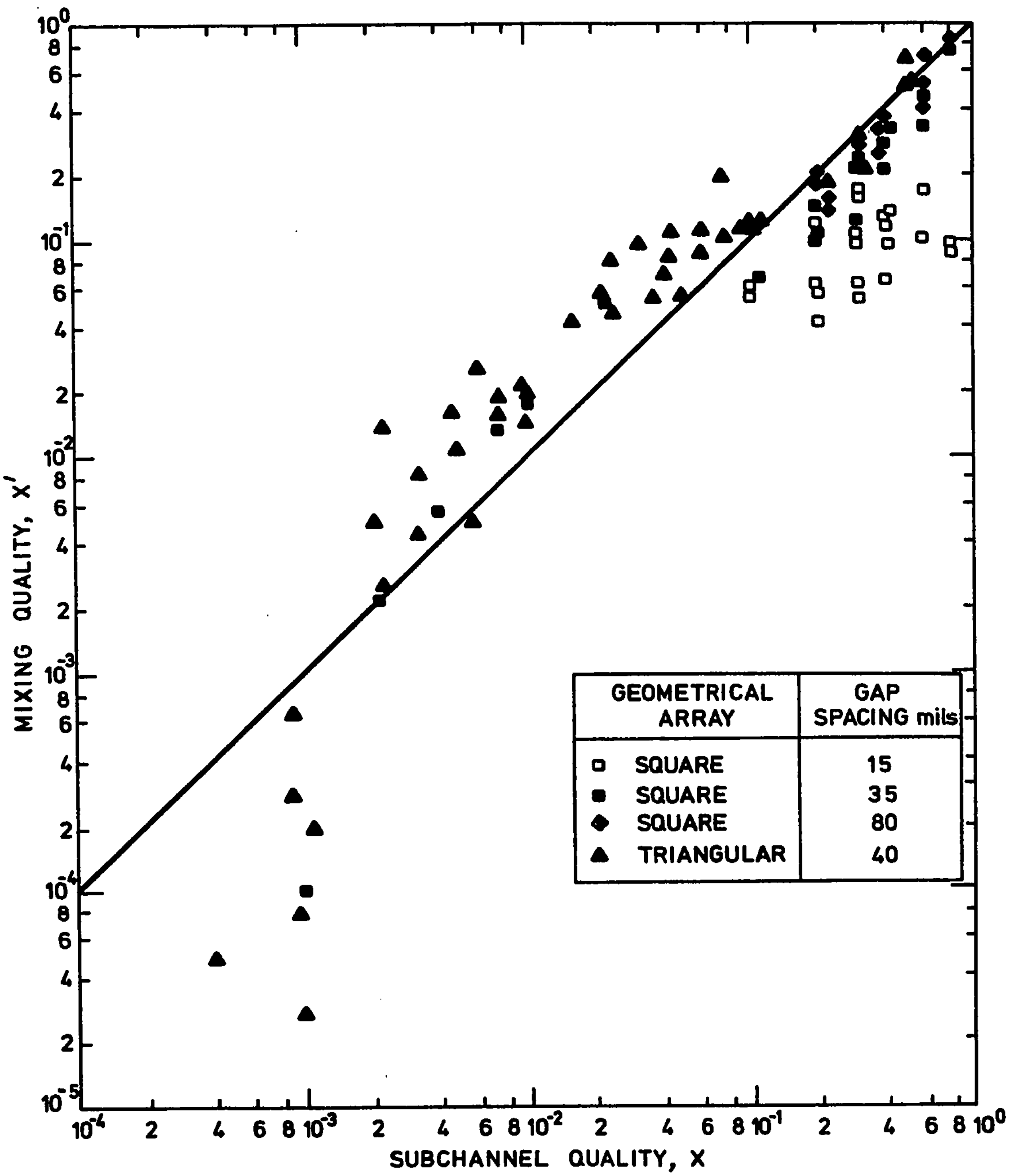

FIGURE 5.11 Comparison of Subchannel Quality with Mixing Quality

was "churned up", giving efficient mixing of both phases. Water mixing rates would be expected to be slightly lower than air as water flowing near and along the walls away from the interconnection gap is partially excluded from the turbulent mixing process.

In the high quality annular flow regime where air and water turbulent mixing rates are decreasing, enhanced liquid interchange occurs. This could be due to the liquid film effectively decreasing the gap area available for the air to mix while roll waves continue to mix the liquid. Petrunik and St. Pierre (44) also observed this enhanced water interchange in the high quality annular flow regime in their mixing tests with rectangular-rectangular subchannels (without filler rods). The degree of liquid mixing enhancement is a function of the interconnection gap spacing. The 15-mil gap geometry has the lowest mixing quality as the relatively thicker liquid film in the gap prevented significant amounts of air from mixing. As the gap spacing is increased, both air and water mixing fractions increase but not in the same proportion. The mixing quality for the 80-mil gap geometry is only fractionally lower than the subchannel quality. It was also observed that as the mass flux is increased for all gap widths, the mixing quality moves closer to the subchannel quality.

These findings do not agree with those of Rowe and Angle (13) for a boiling steam-water system where the mixing quality was essentially equal to the subchannel quality for the whole range of qualities investigated. However, this discrepancy is not conclusive as Rowe and Angle could not have accurately detected enhanced liquid interchange at low qualities. This is due to their tracers which measured either water mixing (via lithium concentrations) or total water and steam mixing (via deuterium and tritium tracers) which must necessarily approach the same value for very low steam mixing rates.

To the author's knowledge, the present work constitutes the first consistent set of turbulent mixing rate data for square-square geometries with three different gap spacings without appreciable variation in subchannel hydraulic diameter. Rowe and Angle (13) reported mixing rates at two different gap spacings but at mass fluxes an order of magnitude higher than those used here. The results reported here are in qualitative agreement with those obtained by Rowe and Angle who used a square-square array and a steam-water mixture at elevated pressures. A direct comparison with mixing rate data obtained in rod bundle arrays or two dissimilar subchannels is not presented here due to the uncertain influence of crossflow on turbulent mixing rates.

B. Square-Triangular Geometry

Two-phase, air-water turbulent mixing rates between a square subchannel and a triangular subchannel were determined at an average mass flux of 0.18×10^6 lb/(hr.sq ft). The present set of data were taken over a very narrow range of experimental parameters. Therefore, no generalized correlation is possible and the results are discussed only qualitatively in terms of the physical phenomena involved. The data are tabulated in Appendix V.3.

1. Turbulent Mass Transfer

The mixing data obtained under conditions of negligible radial pressure gradient but non-zero void gradient indicated that there was a net transfer of air from the triangular subchannel to the square subchannel while water was transferred in the opposite direction.

The subchannel exit qualities for the two subchannels are plotted as a function of overall average quality, defined as $\overline{X} = \sum G_i X_i A_i / \overline{G} A_T$, in Figure 5.12. It was observed that subchannel 1 (triangular) always had an exit quality below the average and subchannel 2 (square) had higher than average exit quality. As the average quality was increased, the exit quality in each of the subchannels increased. At average qualities between 0.03 and 0.04, the exit qualities in both subchannels equalled approximately the overall average quality, indicating very efficient mixing. An examination of these runs revealed that slug flow was present in both subchannels at the entrance as well as at the exit of the interconnection length. In all the other runs different flow regimes were present simultaneously in the adjacent subchannels. The flow regime transition boundaries were indicated by using Steen-Wallis's (43) criterion. This enhancement of mixing in the slug flow regime is in agreement with the data reported for the square-square geometry in part A of this chapter and also

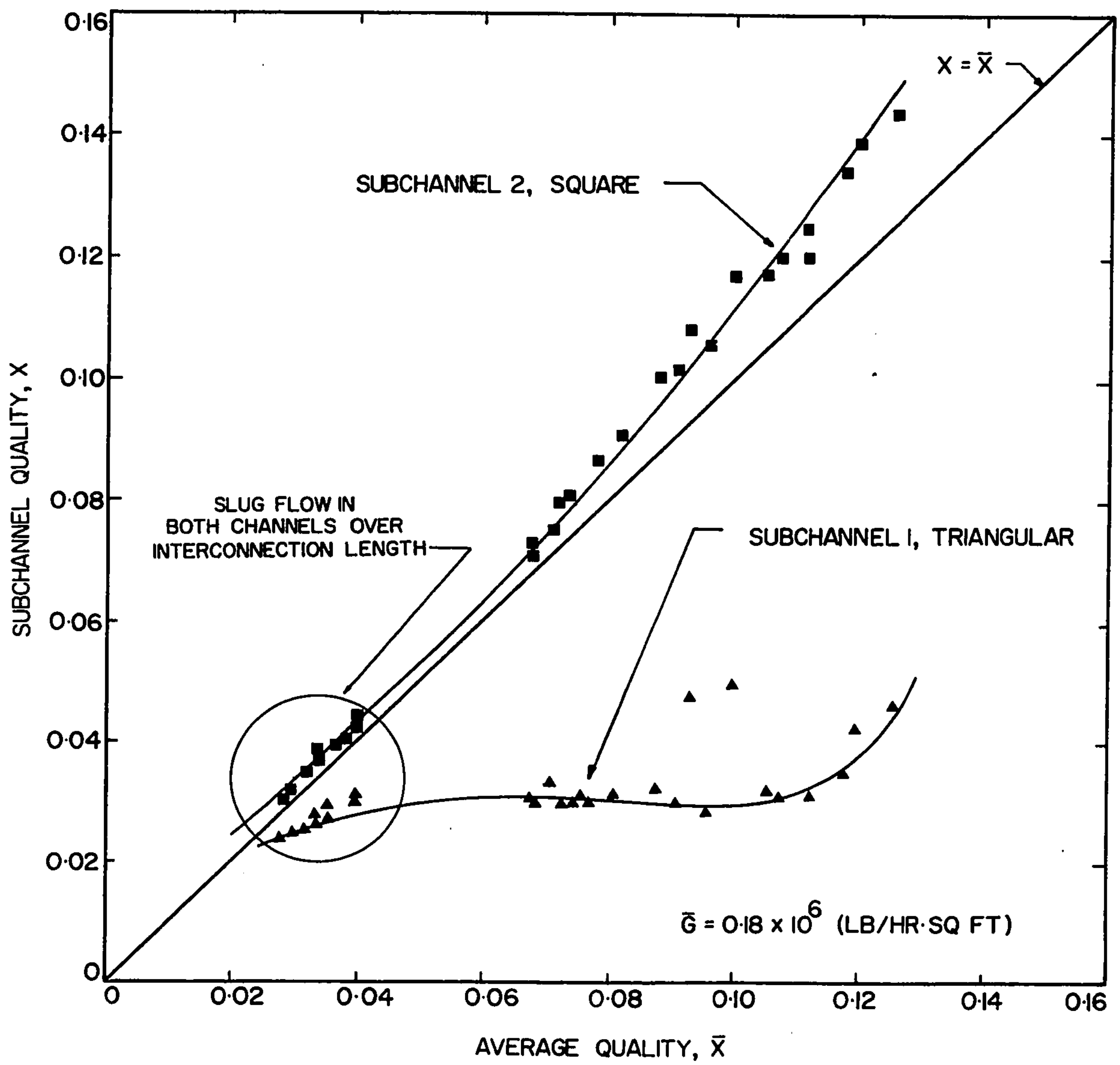

FIGURE 5.12 Variation of Subchannel Exit Quality with Overall Average Quality (Square-Triangular Geometry, 0.035-in gap spacing)

the steam-water (29) and air-water (27) data reported by other investigators.

Another noteworthy feature of Figure 5.12 is that as the average quality increased (corresponding to a higher heat flux), the difference between the exit qualities of both subchannels increased, i.e., the mixing became less efficient. This trend is in agreement with Casterline's (28) steam-water tests in which the maldistribution of enthalpy became more severe as the heat flux was increased.

2. Comparison with other Investigators

Mixing tests were performed in a 3 x 3 rod array bundle by Lahey et. al. (29) using a steam-water system. It was concluded that the corner (lower velocity) subchannel was at lower than average quality even though its power-to-flow ratio was greater than average; a trend observed in the present air-water data where the square subchannel had a higher velocity than the triangular subchannel. Steam-water mixing tests of Casterline et. al. (28) in a 16-rod geometry also indicated higher than average quality in the centre (higher velocity) subchannel. Quality contours plotted by Schraub et.al. (45) for an adiabatic 9-rod assembly showed that the air concentrations were the highest in central region while the corner subchannels had a higher water fraction than average.

Van der Ros's (5) data on the turbulent mass transfer under conditions of zero radial pressure difference also showed that the direction of air and water transfer was often opposite.

3. General Remarks on Exchange Mechanism

It is concluded from the above observations that a net transfer of mass has taken place due to turbulent mixing. For the square-square geometry, there was no net mass exchange because a zero void gradient existed but a net exchange of tracer took place because of pressure and flow fluctuations. Lahey (46) proposed that the net turbulent mass flow is composed of two parts: a mixing term and a "void drift" term. A volume-for-volume exchange of two-phases, resulting in a net mass interchange, was assumed to occur. It was postulated that the two-phase system has a tendency to approach an equilibrium void distribution which is not uniform when adjacent subchannels are dissimilar. The "void drift" term accounts for the tendency of the vapour phase to shift to a high velocity region. This mechanism is consistent with the observation that water and air are transferred in opposite directions.

The mixing mechanism observed is very important from the point of view of verifying the assumptions made in various subchannel computer codes. In all these codes, the fluid described in the mass, momentum and energy conservation equations is not considered separately in terms of liquid and vapour phases. It is rather characterized by a pseudo homogeneous fluid. An average density and an average enthalpy of the two-phase mixture is assumed to take part in the interchange processes of turbulent mixing and diversion crossflow. The various codes use turbulent mixing, W', as a turbulent energy transfer term of the form

$$q' = W' \Delta h_{ij}$$

Mass transfer due to turbulent mixing is assumed to be zero and a net mass interchange is pictured as taking place only due to radial pressure gradient. The values of the turbulent mixing coefficients are computed to suit the experimental conditions at the exit of the test section.

It is obvious from the present investigation as well as from that of Van der Ros (5) that the assumption of zero mass transfer due to turbulent mixing in bulk-boiling systems is not realistic. Mass, momentum and energy conservation equations in the various computer codes should be modified and rewritten to take into account the transfer of two phases in opposite directions and hence a net mass transfer due to turbulent mixing.

VI. CONCLUSIONS

In this study, single- and two-phase mixing experiments have been carried out in simulated square-square and square-triangular rod bundle geometries in the absence of diversion crossflow due to radial pressure gradients and any forced mixing effects. Turbulent mixing rates between adjacent sub-channels were determined for single-phase air, single-phase water and two-phase air-water mixtures at 50 psia, simulating steam-water system at elevated pressures. The effect of gap spacing on the turbulent mixing rates was investigated for the square-square geometry over the gap spacing range of 15-80 mils. Two-phase mixing data were acquired for the 0.035-in gap square-square geometry over an extended quality range.

The following conclusions can be drawn from this investigation:

A. Single-Phase Mixing

1. Square-Square Geometry

a. The mixing rates, expressed as W'/μ, increased with subchannel Reynolds number for all gap spacings (Figure 4.1). There was no difference between air and water mixing rates except for the 0.015-in gap where the water mixing rates were lower than the air mixing rates for Reynolds number less than about 7000. It is believed that at these lower Reynolds numbers, molecular diffusion plays an important role in the mixing mechanism for the smallest gap spacing.

b. Over the range of Reynolds number studied, the following variation in the mixing Stanton number, G'/G, was observed as the Reynolds number was increased: i. for the 0.080-in gap, a continuous decrease; ii. for the 0.035-in gap, an increase followed by a decrease; and iii. for the 0.015-in gap, a continuous increase (Figure 4.2). To explain this behaviour, it is hypothesized that secondary flows have considerable influence on the turbulent mixing rates. The generation and penetration of secondary flows into the gap region of a subchannel array is a function of Reynolds number and pitch to diameter ratio; hence the different behaviour of Stanton number-Reynolds number plot for various gap spacings.

c. At high Reynolds number, the mixing Stanton number decreased as the pitch to diameter ratio decreased (Figure 4.5).

2. <u>Square-Triangular Geometry</u>

a. The mixing rates, expressed as W'/μ, increased with Reynolds number (Figure 4.3). As in the square-square geometry, mixing apparently occurred by a combination of molecular and eddy diffusion at low Reynolds number.

b. The fractional mixing rates, W'/W, decreased in the following order (for the same gap spacing): triangular-triangular, triangular-square and square-square geometries (Figure 4.4).

B. Two-Phase Mixing

1. Square-Square Geometry

a. The curves of the turbulent mixing rates, W', for both air and water as a function of subchannel quality exhibited a maximum in the slug-flow regime (Figure 5.1). It was observed that mixing rates increased with increasing radial pressure oscillations.

b. The mixing data for both square and triangular array geometries were correlated over a limited parameter range using a new Stanton number type parameter, G'/G (Figures 5.2 and 5.3). This mixing parameter decreased with increasing mass flux. Both water and air mixing parameters were greater than the single phase Stanton number measured at the same total mass flux except for the high quality annular flow regime.

c. Over the range of gap spacing studied (0.015- to 0.080-in), the fractional mixing rates, W'/W, of both air and water increased with gap spacing (Figures 5.9 and 5.10). The increase for water was small compared to that for air. Moreover, air and water fractional mixing rates were <u>not</u> proportional to the gap spacing.

d. The mixing quality, $W'_g/(W'_g + W'_l)$, in general, was not equal to the subchannel quality, $W_g/(W_g + W_l)$, (Figure 5.11). Enhanced liquid interchange occurred in the bubble and annular flow regimes. The enhanced liquid interchange in the annular flow regime was observed to be a function of gap spacing and the subchannel mass flux. Enhanced gas interchange occurred in the intermediate quality range in the slug and slug-annular flow regimes.

2. Square-Triangular Geometry

a. In every case studied here, there was a net transfer of air from the smaller triangular subchannel to the larger square subchannel while water was transferred in the opposite direction due to turbulent mixing.

b. In every case, the larger square subchannel exit quality was greater than the overall average quality while the converse was true for the triangular subchannel.

c. Efficient mixing occurred in the slug-flow regime as evidenced by both subchannels having approximately the same exit qualities.

C. Summary and Recommendations

The mixing experiments in this investigation have demonstrated the effect of important parameters governing mixing rates between adjacent subchannels for single- and two-phase flows in simulated rod bundle geometries. The data showed that some fundamental changes need to be made in various subchannel computer codes to predict the local subchannel flows and enthalpies accurately. The single-phase turbulent mixing rates calculated from the tracer transfer data can be applied directly to determine energy exchange between adjacent subchannels in single phase systems. The two-phase mixing results obtained here with air-water mixtures are in qualitative agreement with high pressure steam-water mixing results. There is some evidence available (47) suggesting that mixing results obtained from the tracer data can be used to calculate enthalpy transport between adjacent sub-channels but more work needs to be done in order to justify the quantitative use of tracer data in bulk boiling systems and to study other problems associated with modelling the mixing phenomenon with air-water. Attention should also be focused on how mixing data obtained with two-subchannel geometries can be applied realistically to rod bundles.

NOMENCLATURE

A	subchannel flow area	sq ft
b	gap spacing	ft
C	fraction of total tracer	
d	rod diameter	ft
D_e	equivalent diameter	ft
f	Fanning friction factor	
F_m	empirical mixing factor defined by Bowring, equation IV.3.1	
G	subchannel mass flux, W/A	lb/(hr.sq ft)
G'	turbulent mixing mass flux, W'/b	lb/(hr.sq ft)
H	enthalpy	Btu/lb
j^*	dimensionless velocity	
K, K_g	empirical coefficients defined by Rosehart and Rogers, Table 2.1	
L	subchannel interconnection length	ft
m	empirical Reynolds number exponent, Table 2.1	
P	subchannel heated perimeter	ft
q	heat flux	Btu/(hr.sq ft)
Re	Reynolds number	
S_m	subchannel shape factor defined by Bowring, equation IV.3.1	
St	mixing Stanton number, G/G	
W	mass flow rate	lb/hr
W'	turbulent mixing rate per foot	lb/(hr.ft)

NOMENCLATURE (Contd.)

X	subchannel quality, $W_g/(W_g + W_l)$	
X'	turbulent mixing quality, $W_g'/(W_g' + W_l')$	
y	rectangular coordinate in the direction transverse to main flow direction	ft
y^+	dimensionless thickness of laminar sublayer, equation 4.3	
Y	Inter-subchannel mixing distance	ft
z	rectangular coordinate in axial direction	ft

Greek Symbols

ρ	fluid density	lb/cu ft
α	non-dimensional factor in Roger's correlation, Table 2.1	
β	mixing parameter defined by Rowe as $W' = b\,\beta\,\bar{G}$	
δ	thickness of laminar sublayer	ft
μ	dynamic viscosity	lb/(ft.hr)
ν	kinematic viscosity	sq ft/hr
ϵ	eddy diffusivity of heat	sq ft/hr
γ	relative centroidal distance between subchannels normalized to a square pitch array	

Superscripts

$\overline{}$	overbar denotes an average value

Subscripts

av	denotes "average"
e	denotes "exit"
g	denotes gas phase

NOMENCLATURE (Contd.)

i	denotes subchannel "i"
j	denotes subchannel "j"
l	denotes liquid phase
T	denotes total
1	denotes subchannel "1"
2	denotes subchannel "2"

REFERENCES

1. Bowring, R.W., HAMBO, A Computer Program for the Subchannel Analysis of the Hydraulic and Burnout Characteristics of Rod Clusters- Part 2, The Equations, AEEW-R-582, Atomic Energy Est., Winfrith, Dorset, England, (1968).

2. St. Pierre, C.C., SASS Code 1, Subchannel Analysis for the Steady-State, APPE-41, Atomic Energy of Canada Ltd., Chalk River, Ontario, (1966).

3. Rowe, D.S., COBRA-II: A Digital Computer Program for Thermo-hydraulic Subchannel Analysis of Rod Bundle Nuclear Fuel Elements, BNWL-1229, Pacific Northwest Laboratory, Richland, Washington, (February, 1970).

4. Zernick, W., Currin, H.B., Elyash, E. and Previti, G., THINC, A Thermal Hydrodynamic Interaction Code for a Semi-open or Closed Channel Core, WCAP-3704, (1962).

5. Van der Ros, T., On Two-Phase Flow Exchange between Interacting Hydraulic Channels, Doctor of Engineering Science Thesis, Eindhoven University of Technology, Netherlands, (1970).

6. Rogers, J.T. and Todreas, N.E., Coolant Interchannel Mixing in Reactor Fuel Rod Bundles, Single-Phase Coolants, Symposium on Heat Transfer in Rod Bundles, A.S.M.E. Winter Annual Meeting, New York, (1968).

7. Moyer, C.B., Coolant Mixing in Multi-rod Fuel Bundles, Riso Report No. 125, (July, 1964; Issued 1966).

8. Ingesson, L. and Hedberg, S., Heat Transfer between Subchannels in a Rod Bundle, Paper No. FC 7.11, Fourth International Heat Transfer Conference, Paris-Versailles, 1970.

9. Rapier, A.C., Turbulent Mixing in a Fluid Flowing in a Passage of Constant Cross-section, TRG Report 1417(W), U.K.A.E.A., (February, 1967).

10. Rosehart, R.G. and Rogers, J.T., Turbulent Interchange Mixing between Subchannels in Close-packed Nuclear Reactor

Fuel Bundles, Report No. R69PP1, Atomic Energy of Canada Ltd., Chalk River, Ontario, (February, 1969).

11. Rowe, D.S. and Angle, C.W., Crossflow Mixing between Parallel Flow Channels During Boiling, Part II, Measurement of Flow and Enthalpy in Two Parallel Channels, BNWL-371, Pt. 2, Pacific Northwest Laboratory, Richland, Washington, (1967).

12. Hetsroni, G., Leon, J. and Hakim, M., Crossflow and Mixing of Water between Semi-open Channels, Nucl. Sci. Eng., 34, pp. 189-193, (1968).

13. Rowe, D.S. and Angle, C.W., Crossflow Mixing between Parallel Flow Channels During Boiling, Part III, Effect of Spacers on Mixing between Two Channels, BNWL-371, Pt. 3, Pacific Northwest Laboratory, Richland, Washington, (1969).

14. Petrunik, K.J., Turbulent Mixing Measurements for Single-Phase Air, Single-Phase Water and Two-Phase Air-Water Flows in Adjacent Rectangular Subchannels, M.A.Sc. Thesis, Chemical Engineering, University of Windsor, Windsor, Ontario, (1968).

15. Walton, F.B., Turbulent Mixing Measurements for Single-Phase Air, Single-Phase Water and Two-Phase Air-Water Flows in Adjacent Triangular Subchannels, M.A.Sc. Thesis, Chemical Engineering, University of Windsor, Windsor, Ontario, (1969).

16. Skinner, V.R., Freeman, A.R. and Lyall, H.G., Gas Mixing in Rod Clusters, Int. J. Heat Mass Transfer, 12, pp. 265-278, (1969).

17. Galbraith, K.P. and Knudsen, J.G., Turbulent Mixing between Adjacent Channels for Single Phase Flow in a Simulated Rod Bundle, Presented at 12th National Heat Transfer Conference, Tulsa, Oklahoma, (August 12-15, 1971).

18. Van der Ros, T. and Bogaardt, M., Mass and Heat Exchange between Adjacent Channels in Liquid-Cooled Rod Bundles, Nucl. Eng. Design, 12, No. 2, pp. 259-268, (May, 1970).

19. Singleton, N.R., Mixing Due to Eddy Diffusion between Parallel Open Flow Channels, M.Sc. Thesis, Mechanical Engineering Department, University of Pittsburgh, (1963).

20. Elder, J.W., The Dispersion of Marked Fluid in Turbulent Shear Flow, J. Fluid Mech., 5, pp. 544-560, (1959).

21. Nijsing, R., Gargantini, I. and Eifler, W., Fundamental Studies of Fluid Flow and Heat Transfer in Fuel Element Geometries, EUR. 2193. e-I, Joint Nuclear Research Center, Ispra, Italy, (1964).

22. Rowe, D.S., Crossflow Mixing between Parallel Flow Channels During Boiling, Part I, COBRA- Computer Program for Coolant Boiling in Rod Arrays, BNWL-371, Pt. I, Pacific Northwest Laboratory, Richland, Washington, (1967).

23. Rowe, D.S., A Mechanism for Turbulent Mixing between Rod Bundle Subchannels, American Nuclear Society Trans., 12, No. 2, (November, 1969).

24. Launder, B.E. and Spalding, D.B., Turbulence Models and their Application to the Prediction of Internal Flows, Paper No. 1, Presented at Symposium on Internal Flows, Salford, England, (May, 1971).

25. Lahey, R.T. and Schraub, F.A., Mixing, Flow Regimes and Void Fraction for Two-Phase Flow in Rod Bundles, A.S.M.E. Winter Annual Meeting, Los Angeles, Calif., (1969).

26. Rudzinski, K.F., Two-Phase Turbulent Mixing for Air-Water Flows in Adjacent Triangular Array Subchannels, M.A.Sc. Thesis, Chemical Engineering, University of Windsor, Windsor, Ontario, (1970).

27. Spigt, C.L., et. al., Final Report on the Research Program on the Heat Transfer and Fluid Flow Characteristics of a Pressurized Water Reactor, WW-015-R128, Eindhoven University of Technology, Netherlands, (December, 1967).

28. Casterline, J.E. and Castellana, F.S., Flow and Enthalpy Redistribution in a Simulated Nuclear Fuel Assembly, Topical Report No. 11, UC-80 Reactor Technology, Department of Chemical Engineering, Columbia University, New York, (1969).

29. Lahey, R.T., Shiralkar, B.S. and Radcliffe, D.W., Mass Flux and Enthalpy Distribution in a Rod Bundle for Single- and Two-Phase Flow Conditions, Trans. A.S.M.E., J. Heat Transfer, Paper No. 70-WA/HT-8, pp. 197-209, (May, 1971).

30. Bowring, R.W. and Levy, J., Freon 7-Rod Cluster Subchannel Mixing Experiments, AEEW-R663, Atomic Energy Est., Winfrith, Dorset, England, (December, 1969).

31. Bhattacharyya, A., Sallay, S. and Haga, I., Analytical and Experimental Studies of the Hydraulic Behaviour of Rod Clusters, Eindhoven University of Technology, Netherlands, (1967)

32. Knudsen, J.G. and Katz, D.L., Fluid Dynamics and Heat Transfer, McGraw-Hill Book Co., Inc., New York, pp. 166-167, (1958).

33. Nikuradse, J., Investigation of Turbulent Flow in Tubes of Non-circular Cross-section, Ingen.-Arch., 1, pp. 306-332, (1930).

34. Launder, B.E. and Singham, J.R., The Prediction of Fully-Developed Flow in Non-circular Ducts, Paper No. 12, Presented at Symposium on Internal Flows, Salford, England, (May, 1971).

35. Gessner, F.B. and Jones, J.B., On some Aspects of Fully-Developed Turbulent Flow in Rectangular Channels, J. Fluid Mech., 23, pp. 689-713, (1965).

36. Lyall, H.G., Measurement of Flow Distribution and Secondary Flow in Ducts composed of Two Square Interconnected Sub-channels, Paper No. 33, Presented at Symposium on Internal Flows, Salford, England, (May, 1971).

37. Hoagland, L.C., Fully Developed Turbulent Flow in Straight Rectangular Ducts... Secondary Flow, its Cause and Effect on the Primary Flow, Doctor of Science Thesis, Department of Mechanical Engineering, Massachusetts Institute of Technology, (1960).

38. Brundrett, E. and Baines, W.D., The Production and Diffusion of Vorticity in Duct Flow, J. Fluid Mech., 19, No. 3, pp. 375-394, (1964).

39. Leutheusser, H.J., Turbulent Flow in Rectangular Ducts, J. Hydraulics Division, 89, No. HY3, pp. 1-19, (May, 1963).

40. Deissler, R.G. and Taylor, M.F., Analysis of Axial Turbulent Flow and Heat Transfer Through Banks of Rods or Tubes, TID 7529, Reactor Heat Transfer Conference (Pt. 1), Book 2, pp. 416-461, (1957).

41. Griffith, P. and Haberstrah, R.D., The Transition from the Annular to the Slug Flow Regime in Two-Phase Flow, Report No. 5003-28, Mechanical Engineering Department, Mass Inst. Tech., (1964).

42. Rudzinski, K.F., Singh, Kuldip and St. Pierre, C.C., Turbulent Mixing for Air-Water Flows in Simulated Rod Bundle Geometries, To be published in C.J.Ch.E., 50, (1972).

43. Wallis, G.B. and Collier, J.G., Two-Phase Flow and Heat Transfer, 2, Stanford University Press, (August, 1967).

44. Petrunik, K.J. and St. Pierre, C.C., Turbulent Mixing Rates for Air-Water Two-Phase Flows in Adjacent Rectangular Channels, C.J.Ch.E., 48, No. 1, (1970).

45. Schraub, F.A., Simpson, R.L. and Janssen, E., Two-Phase Flow and Heat Transfer in Multirod Geometries: Air-Water Flow Structure Data for a Round Tube, Concentric and Eccentric Annulus, and Nine-Rod Bundle, AEC Research and Development Report, GEAP-5739, (1969).

46. Lahey, R.T., Jr., Shiralkar, B.S., Radcliffe, D.W. and Polomik, E.E., Out-of-Pile Subchannel Measurements in a Nine-Rod Bundle for Water at 1000 PSIA, Paper 3-1, International Symposium on Two-Phase Systems, Technion City, Haifa, Israel, Aug 29-Sept 2, (1971).

47. Rowe, D.S., A Thermal Hydraulic Subchannel Analysis for Rod Bundle Nuclear Fuel Elements, Paper No. 7.13, Fourth International Heat Heat Transfer Conference, Paris-Versailles, 1970.

48. Kline, S.J. and McClintock, F.A., Describing Uncertainties in Single-sample Experiments, Mechanical Engineering, 75, pp. 3-8, (January, 1953).

APPENDIX IV.1
Single-Phase Mixing Data

The run number was recorded in a five digit code. The first two numerical digits on the left represent the run number. The third digit is alphabetic and gives the tracer injection side i.e., right (R) or left (L). The two right digits represent the interconnection gap spacing in mils.

<u>Example</u>

Run Number: 10 R 35

Run 10 → 10

Tracer injection right → R

Gap Spacing → 35

TABLE IV.1.1

Single-Phase Air Mixing
Square-Square Geometry

SERIAL NUMBER	RUN NUMBER	MASS FLOW (LB/HR)	MASS FLUX (LB/HR.FT2)	REYNOLDS NUMBER	STANTON NUMBER	MIXING RATE (LB/HR.FT)	RELATIVE MIXING(%/FT)	TEMP (F)	FRICTION FACTOR
1	1L15	7.70	4957	3018	0.0143	0.09	1.15	83	0.0178
2	1R15	7.70	4957	3018	0.0066	0.04	0.53	83	0.0178
3	18L15	7.90	5086	3139	0.0116	0.07	0.93	73	0.0096
4	18R15	7.90	5086	3139	0.0073	0.05	0.59	73	0.0096
5	2L15	12.28	7909	4815	0.0133	0.13	1.07	83	0.0108
6	2R15	12.28	7909	4815	0.0137	0.14	1.10	83	0.0108
7	3L15	20.42	13150	8006	0.0129	0.21	1.04	83	0.0081
8	3R15	20.42	13150	8006	0.0108	0.18	0.87	83	0.0081
9	4L15	24.22	15599	9498	0.0124	0.24	1.00	83	0.0075
10	4R15	24.22	15599	9498	0.0141	0.27	1.13	83	0.0075
11	25L15	24.78	15961	9823	0.0092	0.18	0.74	75	0.0065
12	25R15	24.78	15961	9823	0.0202	0.40	1.63	75	0.0065
13	5L15	19.70	12684	7733	0.0081	0.13	0.66	82	0.0087
14	5R15	19.70	12684	7733	0.0170	0.27	1.37	82	0.0087
15	6L15	29.64	19086	11636	0.0146	0.35	1.18	82	0.0069
16	6R15	29.64	19086	11636	0.0171	0.41	1.37	82	0.0069
17	15L15	29.61	19072	11786	0.0120	0.29	0.96	72	0.0064
18	15R15	29.61	19072	11786	0.0179	0.43	1.44	72	0.0064
19	7L15	39.75	25598	15627	0.0176	0.56	1.42	81	0.0058
20	7R15	39.75	25598	15627	0.0228	0.73	1.84	81	0.0058
21	13L15	40.08	25813	15952	0.0152	0.49	1.22	72	0.0058
22	13R15	40.08	25813	15952	0.0205	0.66	1.65	72	0.0058
23	20L15	40.00	25764	15900	0.0142	0.46	1.15	73	0.0057
24	20R15	40.00	25764	15900	0.0220	0.71	1.77	73	0.0057
25	8L15	44.80	28854	17616	0.0151	0.54	1.22	81	0.0056
26	8R15	44.80	28854	17616	0.0242	0.87	1.95	81	0.0056
27	14L15	45.18	29097	17982	0.0141	0.51	1.13	72	0.0057
28	14R15	45.18	29097	17982	0.0251	0.91	2.02	72	0.0057
29	9L15	56.00	36065	22107	0.0142	0.64	1.14	78	0.0050
30	9R15	56.00	36065	22107	0.0264	1.19	2.13	78	0.0050
31	10L15	60.68	39081	23956	0.0318	1.56	2.56	78	0.0051
32	10R15	60.68	39081	23956	0.0260	1.27	2.09	78	0.0051
33	21L15	60.97	39264	24232	0.0259	1.27	2.09	73	0.0051
34	21R15	60.97	39264	24232	0.0268	1.32	2.16	73	0.0051
35	11L15	65.82	42388	25983	0.0402	2.13	3.23	78	0.0049
36	11R15	65.82	42388	25983	0.0277	1.47	2.23	78	0.0049
37	12L15	71.03	45744	28040	0.0302	1.73	2.43	78	0.0048
38	12R15	71.03	45744	28040	0.0312	1.78	2.51	78	0.0048
39	16L15	50.32	32405	20026	0.0191	0.77	1.54	72	0.0053
40	16R15	50.32	32405	20026	0.0239	0.97	1.92	72	0.0053
41	17L15	20.89	13453	8314	0.0145	0.24	1.17	72	0.0066
42	17R15	20.89	13453	8314	0.0093	0.16	0.75	72	0.0066
43	19L15	11.02	7097	4391	0.0163	0.14	1.31	71	0.0116
44	19R15	11.02	7097	4391	0.0059	0.05	0.48	71	0.0116
45	22L15	9.17	5903	3638	0.0092	0.07	0.74	74	0.0029
46	22R15	9.17	5903	3638	0.0108	0.08	0.87	74	0.0029
47	23L15	13.97	8994	5543	0.0090	0.10	0.72	74	0.0079
48	23R15	13.97	8994	5543	0.0176	0.20	1.42	74	0.0079
49	24L15	18.43	11871	7316	0.0118	0.18	0.95	74	0.0070
50	24R15	18.43	11871	7316	0.0127	0.19	1.02	74	0.0070

TABLE IV.1.1 (Contd.)

SERIAL NUMBER	RUN NUMBER	MASS FLOW (LB/HR)	MASS FLUX (LB/HR.FT2)	REYNOLDS NUMBER	STANTON NUMBER	MIXING RATE (LB/HR.FT)	RELATIVE MIXING(%/FT)	TEMP (F)	FRICTION FACTOR
51	26L15	34.90	22476	13833	0.0134	0.38	1.08	75	0.0058
52	26R15	34.90	22476	13833	0.0207	0.58	1.67	75	0.0058
53	27L15	45.14	29072	17893	0.0129	0.47	1.04	75	0.0055
54	27R15	45.14	29072	17893	0.0250	0.91	2.01	75	0.0055
55	28L15	5.19	3345	2056	0.0065	0.03	0.53	76	0.0120
56	28R15	5.19	3345	2056	0.0093	0.04	0.75	76	0.0120
57	29L15	6.60	4251	2609	0.0083	0.04	0.66	77	0.0093
58	29R15	6.60	4251	2609	0.0110	0.06	0.88	77	0.0093
59	1L35	17.43	10607	6795	0.0179	0.55	3.18	85	0.0065
60	1R35	17.43	10607	6795	0.0120	0.37	2.12	85	0.0065
61	17L35	17.18	10457	6726	0.0177	0.54	3.15	82	0.0066
62	17R35	17.18	10457	6726	0.0122	0.37	2.16	82	0.0066
63	2L35	22.01	13392	8568	0.0189	0.74	3.35	86	0.0066
64	2R35	22.01	13392	8568	0.0140	0.55	2.48	86	0.0066
65	18L35	21.95	13356	8591	0.0186	0.72	3.30	82	0.0065
66	18R35	21.95	13356	8591	0.0142	0.55	2.51	82	0.0065
67	4L35	24.60	14967	9653	0.0216	0.94	3.83	80	0.0065
68	4R35	24.60	14967	9653	0.0161	0.70	2.86	80	0.0065
69	9L35	24.67	15013	9669	0.0181	0.79	3.22	81	0.0065
70	9R35	24.67	15013	9669	0.0161	0.70	2.85	81	0.0065
71	5L35	34.50	20994	13540	0.0171	1.05	3.04	80	0.0059
72	5R35	34.50	20994	13540	0.0179	1.09	3.17	80	0.0059
73	6L35	44.71	27210	17549	0.0179	1.42	3.18	80	0.0055
74	6R35	44.71	27210	17549	0.0189	1.50	3.36	80	0.0055
75	7L35	55.25	33623	21685	0.0191	1.87	3.39	80	0.0051
76	7R35	55.25	33623	21685	0.0175	1.72	3.10	80	0.0051
77	8L35	7.79	4737	3051	0.0231	0.32	4.11	81	0.0112
78	8R35	7.79	4737	3051	0.0087	0.12	1.55	81	0.0112
79	10L35	54.98	33460	21551	0.0267	2.61	4.75	81	0.0051
80	10R35	54.98	33460	21551	0.0197	1.92	3.49	81	0.0051
81	11L35	49.85	30336	19512	0.0164	1.45	2.91	82	0.0053
82	11R35	49.85	30336	19512	0.0187	1.66	3.32	82	0.0053
83	12L35	65.35	39768	25579	0.0237	2.75	4.21	82	0.0047
84	12R35	65.35	39768	25579	0.0192	2.23	3.41	82	0.0047
85	14L35	65.23	39695	25464	0.0199	2.30	3.53	84	0.0049
86	14R35	65.23	39695	25464	0.0193	2.23	3.42	84	0.0049
87	13L35	71.04	43231	27732	0.0137	1.73	2.44	84	0.0047
88	13R35	71.04	43231	27732	0.0189	2.38	3.35	84	0.0047
89	16L35	10.63	6471	4162	0.0171	0.32	3.04	82	0.0073
90	16R35	10.63	6471	4162	0.0098	0.18	1.74	82	0.0073
91	19L35	13.76	8371	5384	0.0170	0.42	3.02	82	0.0068
92	19R35	13.76	8371	5384	0.0108	0.26	1.92	82	0.0068
93	20L35	1.46	886	577	0.0014	0.00	0.25	73	0.0228
94	20R35	1.46	886	577	0.0422	0.11	7.49	73	0.0228
95	21L35	3.87	2354	1537	0.0086	0.06	1.52	71	0.0158
96	21R35	3.87	2354	1537	0.0077	0.05	1.37	71	0.0158
97	22L35	6.52	3966	2589	0.0117	0.14	2.07	71	0.0118
98	22R35	6.52	3966	2589	0.0153	0.18	2.72	71	0.0118
99	23L35	9.78	5949	3884	0.0155	0.27	2.74	71	0.0112
100	23R35	9.78	5949	3884	0.0103	0.18	1.83	71	0.0112

TABLE IV.1.1 (Contd.)

SERIAL NUMBER	RUN NUMBER	MASS FLOW (LB/HR)	MASS FLUX (LB/HR.FT2)	REYNOLDS NUMBER	STANTON NUMBER	MIXING RATE (LB/HR.FT)	RELATIVE MIXING(%/FT)	TEMP (F)	FRICTION FACTOR
101	24L35	19.73	12006	7838	0.0174	0.61	3.09	71	0.0086
102	24R35	19.73	12006	7838	0.0157	0.55	2.78	71	0.0086
103	25L35	66.54	40494	26294	0.0158	1.86	2.80	75	0.0050
104	25R35	66.54	40494	26294	0.0191	2.26	3.40	75	0.0050
105	26L35	72.37	44039	28596	0.0161	2.07	2.86	75	0.0048
106	26R35	72.37	44039	28596	0.0193	2.48	3.43	75	0.0048
107	1L80	7.47	4108	2939	0.0150	0.41	5.52	72	C.0103
108	1R80	7.47	4108	2939	0.0098	0.27	3.58	72	C.0103
109	11L80	7.46	4104	2936	0.0115	0.31	4.21	72	C.0103
110	11R80	7.46	4104	2936	0.0145	0.40	5.32	72	C.0103
111	2L80	10.43	5736	4103	0.0093	0.35	3.40	72	0.0084
112	2R80	10.43	5736	4103	0.0092	0.35	3.36	72	0.0084
113	3L80	13.17	7245	5184	0.0104	0.50	3.80	72	0.0076
114	3R80	13.17	7245	5184	0.0104	0.50	3.80	72	0.0076
115	4L80	15.70	8638	6180	0.0094	0.54	3.45	72	0.0072
116	4R80	15.70	8638	6180	0.0082	0.47	3.00	72	0.0072
117	12L80	15.70	8638	6180	0.0099	0.57	3.65	72	0.0075
118	12R80	15.70	8638	6180	0.0080	0.46	2.94	72	0.0075
119	5L80	21.38	11759	8413	0.0084	0.66	3.10	72	0.0068
120	5R80	21.38	11759	8413	0.0071	0.56	2.62	72	0.0068
121	13L80	21.28	11704	8374	0.0080	0.62	2.93	72	0.0072
122	13R80	21.28	11704	8374	0.0084	0.66	3.09	72	0.0072
123	6L80	24.65	13559	9700	0.0093	0.84	3.42	72	0.0067
124	6R80	24.65	13559	9700	0.0071	0.64	2.61	72	0.0067
125	7L80	38.27	21054	15063	0.0073	1.02	2.66	72	0.0064
126	7R80	38.27	21054	15063	0.0084	1.18	3.10	72	0.0064
127	14L80	38.57	21220	15182	0.0079	1.11	2.88	72	0.0064
128	14R80	38.57	21220	15182	0.0077	1.09	2.83	72	0.0064
129	8L80	44.20	24314	17396	0.0073	1.19	2.69	72	0.0062
130	8R80	44.20	24314	17396	0.0093	1.50	3.40	72	0.0062
131	9L80	57.64	31708	22686	0.0070	1.47	2.56	72	0.0056
132	9R8C	57.64	31708	22686	0.0077	1.62	2.82	72	0.0056
133	10L80	72.60	39938	28574	0.0063	1.67	2.31	72	0.0054
134	10R8C	72.60	39938	28574	0.0070	1.87	2.58	72	0.0054
135	15L80	49.80	27393	19598	0.0072	1.31	2.62	72	0.0059
136	15R80	49.80	27393	19598	0.0085	1.56	3.13	72	0.0059
137	16L80	62.51	34388	24603	0.0059	1.35	2.16	72	0.0055
138	16R8C	62.51	34388	24603	0.0088	2.02	3.23	72	0.0055
139	17L80	77.35	42553	30445	0.0053	1.50	1.94	72	0.0052
140	17R80	77.35	42553	30445	0.0091	2.58	3.34	72	0.0052
141	18L80	82.55	45414	32492	0.0053	1.62	1.96	72	0.0051
142	18R80	82.55	45414	32492	0.0085	2.59	3.13	72	0.0051
143	19L8C	97.04	53385	38194	0.0068	2.43	2.50	72	0.0047
144	19R8C	97.04	53385	38194	0.0091	3.24	3.34	72	0.0048

TABLE IV.1.2

Single-Phase Water Mixing
Square-Square Geometry

RUN NUMBER	MASS FLOW (LB/HR)	MASS FLUX (LB/HR.FT2)	REYNOLDS NUMBER	STANTON NUMBER	MIXING RATE (LB/HR.FT)	RELATIVE MIXING(%/FT)	TEMP (F)	FRICTION FACTOR
1L15	200.19	128926	1583	0.0043	0.70	0.35	75	0.0106
1R15	200.19	128926	1583	0.0257	4.14	2.07	75	0.0106
2L15	300.38	193450	2460	0.0087	2.10	0.70	78	0.0097
2R15	300.38	193450	2460	0.0165	4.00	1.33	78	0.0097
3L15	398.00	256323	3338	0.0066	2.11	0.53	80	0.0095
3R15	398.00	256323	3338	0.0185	5.91	1.49	80	0.0095
4L15	494.00	318150	4194	0.0058	2.31	0.47	81	0.0090
4R15	488.00	314286	4144	0.0145	5.68	1.16	81	0.0092
5L15	698.00	449532	5927	0.0073	4.08	0.58	81	0.0083
5R15	698.00	449532	5927	0.0161	9.05	1.30	81	0.0083
6L15	896.00	577050	7009	0.0100	7.25	0.81	74	0.0082
6R15	896.00	577050	7009	0.0153	11.01	1.23	74	0.0082
7L15	1097.00	706500	8486	0.0116	10.29	0.94	73	0.0076
7R15	1097.00	706500	8486	0.0168	14.82	1.35	73	0.0076
8L15	1199.00	772191	9275	0.0127	12.30	1.03	73	0.0073
8R15	1199.00	772191	9275	0.0158	15.27	1.27	73	0.0073
9L15	1298.00	835949	9930	0.0141	14.76	1.14	72	0.0071
9R15	1298.00	835949	9930	0.0174	18.18	1.40	72	0.0071
10L15	1097.00	706500	8392	0.0115	10.12	0.92	72	0.0076
10R15	1097.00	706500	8392	0.0157	13.82	1.26	72	0.0076
11L15	300.38	193450	2376	0.0082	1.98	0.66	75	0.0099
11R15	300.38	193450	2376	0.0110	2.65	0.88	75	0.0099
12L15	494.00	318150	3779	0.0068	2.70	0.55	72	0.0100
12R15	494.00	318150	3779	0.0143	5.70	1.15	72	0.0100
13L15	896.00	577050	6780	0.0095	6.82	0.76	71	0.0083
13R15	896.00	577050	6780	0.0156	11.29	1.26	71	0.0083
14L15	1199.00	772191	9073	0.0125	12.03	1.00	71	0.0075
14R15	1199.00	772191	9073	0.0172	16.59	1.38	71	0.0075
1L35	198.67	120899	1603	0.0088	3.11	1.56	77	
1R35	198.67	120899	1603	0.0230	8.10	4.08	77	
2L35	301.89	183715	2436	0.0123	6.60	2.19	77	
2R35	301.89	183715	2436	0.0165	8.83	2.92	77	
3L35	398.00	242200	3212	0.0153	10.84	2.72	77	
3R35	398.00	242200	3212	0.0153	10.82	2.72	77	
4L35	494.00	300621	3941	0.0122	10.72	2.17	76	
4R35	494.00	300621	3941	0.0210	18.42	3.73	76	
5L35	698.00	424764	5568	0.0166	20.57	2.95	76	
5R35	692.00	421113	5520	0.0194	23.77	3.44	76	
6L35	890.00	541605	7100	0.0177	27.91	3.14	76	
6R35	890.00	541605	7100	0.0226	35.69	4.01	76	
7L35	1094.00	665748	8727	0.0204	39.61	3.62	76	
7R35	1094.00	665748	8727	0.0242	46.92	4.29	76	
8L35	1199.00	729645	9565	0.0196	41.67	3.48	76	
8R35	1199.00	729645	9565	0.0261	55.53	4.63	76	
9L35	1199.00	729645	9565	0.0190	40.34	3.36	76	
9R35	1199.00	729645	9565	0.0239	50.90	4.24	76	
10L35	494.00	300621	3941	0.0158	13.82	2.80	76	
10R35	494.00	300621	3941	0.0315	27.65	5.60	76	
11L35	200.19	121823	1578	0.0158	5.63	2.81	75	0.0150
11R35	200.19	121823	1578	0.0162	5.75	2.87	75	0.0150

TABLE IV.1.2 (Contd.)

RUN NUMBER	MASS FLOW (LB/HR)	MASS FLUX (LB/HR.FT2)	REYNOLDS NUMBER	STANTON NUMBER	MIXING RATE (LB/HR.FT)	RELATIVE MIXING(%/FT)	TEMP (F)	FRICTION FACTOR
12L35	301.89	183715	2381	0.0165	8.82	2.92	75	0.0127
12R35	301.89	183715	2381	0.0304	16.29	5.40	75	0.0127
13L35	398.00	242200	3139	0.0165	11.63	2.92	75	0.0112
13R35	398.00	242200	3139	0.0174	12.31	3.09	75	0.0112
14L35	494.00	300621	3896	0.0150	13.17	2.67	75	0.0105
14R35	494.00	300621	3896	0.0208	18.25	3.69	75	0.0105
15L35	698.00	424764	5505	0.0174	21.54	3.09	75	0.0090
15R35	698.00	424764	5505	0.0233	28.89	4.14	75	0.0090
16L35	890.00	541605	6940	0.0182	28.68	3.22	74	0.0082
16R35	890.00	541605	6940	0.0206	32.57	3.66	74	0.0082
17L35	1094.00	665748	8531	0.0197	38.28	3.50	74	0.0075
17R35	1094.00	665748	8531	0.0221	42.82	3.91	74	0.0075
18L35	1199.00	729645	9350	0.0200	42.46	3.54	74	0.0072
18R35	1199.00	729645	9350	0.0226	48.05	4.01	74	0.0072
1L80	200.19	110126	1337	0.0140	10.25	5.12	60	
1R80	200.19	110126	1337	0.0041	3.02	1.51	60	
2L80	301.89	166076	2017	0.0217	24.01	7.95	60	
2R80	300.38	165241	2007	0.0140	15.45	5.14	60	
3L80	398.00	218946	2659	0.0175	25.48	6.40	60	
3R80	398.00	218946	2659	0.0150	21.85	5.49	60	
4L80	500.00	275058	3341	0.0164	30.16	6.03	60	
4R80	494.00	271757	3301	0.0164	29.79	6.03	60	
5L80	602.00	331170	4023	0.0119	26.27	4.36	60	
5L80	602.00	331170	4023	0.0121	26.61	4.42	60	
5R80	602.00	331170	4023	0.0125	27.63	4.59	60	
5R80	602.00	331170	4023	0.0142	31.40	5.22	60	
6L80	698.00	383981	4664	0.0127	32.55	4.66	60	
6R80	698.00	383981	4664	0.0118	30.31	4.34	60	
6L80	698.00	383981	4664	0.0127	32.43	4.65	60	
6R80	698.00	383981	4664	0.0095	24.31	3.48	60	
7L80	800.00	440093	5346	0.0119	34.83	4.35	60	
7R80	800.00	440093	5346	0.0121	35.53	4.44	60	
7L80	800.00	440093	5346	0.0121	35.46	4.43	60	
7R80	800.00	440093	5346	0.0138	40.52	5.07	60	
8L80	896.00	492904	5988	0.0114	37.59	4.19	60	
8R80	896.00	492904	5988	0.0106	34.90	3.89	60	
8L80	896.00	492904	5988	0.0117	38.30	4.27	60	
8R80	896.00	492904	5988	0.0099	32.69	3.65	60	
9L80	998.00	549016	6669	0.0117	42.79	4.29	60	
9R80	998.00	549016	6669	0.0123	44.88	4.50	60	
9L80	998.00	549016	6669	0.0108	39.38	3.95	60	
9R80	998.00	549016	6669	0.0116	42.64	4.27	60	
10L80	1094.00	601827	7311	0.0129	51.93	4.75	60	
10R80	1094.00	601827	7311	0.0116	46.43	4.24	60	
10L80	1094.00	601827	7311	0.0121	48.44	4.43	60	
10R80	1094.00	601827	7311	0.0117	46.99	4.30	60	
11L80	1196.00	657939	7992	0.0125	54.77	4.58	60	
11R80	1196.00	657939	7992	0.0126	55.28	4.62	60	
11L80	1196.00	657939	7992	0.0093	40.70	3.40	60	
11R80	1196.00	657939	7992	0.0079	34.79	2.91	60	

TABLE IV.1.2 (Contd.)

RUN NUMBER	MASS FLOW (LB/HR)	MASS FLUX (LB/HR.FT2)	REYNOLDS NUMBER	STANTON NUMBER	MIXING RATE (LB/HR.FT)	RELATIVE MIXING(%/FT)	TEMP (F)
12L80	1298.00	714051	8674	0.0140	66.82	5.15	60
12R80	1298.00	714051	8674	0.0152	72.22	5.56	60
12L80	1298.00	714051	8674	0.0108	51.37	3.96	60
12R80	1298.00	714051	8674	0.0115	54.56	4.20	60
13L80	1394.00	766862	9316	0.0129	66.00	4.73	60
13R80	1394.00	766862	9316	0.0137	70.19	5.04	60
13L80	1394.00	766862	9316	0.0105	53.66	3.85	60
13R80	1394.00	766862	9316	0.0120	61.25	4.39	60
14L80	100.00	55011	661	0.0997	36.56	36.56	59
14R80	100.00	55011	661	0.0997	36.56	36.56	59
15L80	200.19	110126	1324	0.0442	32.44	16.20	59
15R80	200.19	110126	1324	0.0510	37.47	18.72	59
16L80	300.38	165241	1988	0.0170	18.73	6.23	59
16R80	300.38	165241	1988	0.0195	21.47	7.15	59
17L80	398.00	218946	2634	0.0144	21.04	5.29	59
17R80	392.00	215645	2594	0.0207	29.77	7.60	59
18L80	497.00	273407	3289	0.0132	24.10	4.85	59
18R80	494.00	271757	3269	0.0201	36.41	7.37	59
19L80	698.00	383981	4289	0.0126	32.20	4.61	51
19R80	698.00	383981	4289	0.0169	43.21	6.19	51
20L80	896.00	492904	5506	0.0123	40.50	4.52	51
20R80	896.00	492904	5506	0.0176	57.73	6.44	51
21L80	1094.00	601827	6723	0.0122	48.94	4.47	51
21R80	1094.00	601827	6723	0.0152	61.12	5.59	51
22L80	1298.00	714051	7976	0.0125	59.29	4.57	51
22R80	1298.00	714051	7976	0.0123	58.67	4.52	51
23L80	1496.00	822974	9193	0.0118	64.91	4.34	51
23R80	1496.00	822974	9193	0.0116	63.40	4.24	51

TABLE IV.1.3

Single-Phase Air Mixing
Square-Triangular Geometry

RUN NUMBER	SUBCHANNEL MASS FLOW (LB/HR) CH.1	CH.2	SUBCHANNEL MASS FLUX (LB/HR.FT2) CH.1	CH.2	AVERAGE MASS FLUX (LB/HR.FT2)	SUBCHANNEL REYNOLDS NUMBER CH.1	CH.2	AVERAGE REYNOLDS NUMBER	MIXING RATE (LB/HR.FT)	SUBHANNEL STANTON NUMBER CH.1	CH.2	AVERAGE STANTON NUMBER
1L	1.27	8.44	3259	5136	4198	988	3349	2169	0.36	0.0376	0.0238	0.0307
1R	1.27	8.44	3259	5136	4198	988	3349	2169	0.27	0.0286	0.0182	0.0234
2L	1.45	10.43	3718	6345	5031	1127	4137	2632	0.40	0.0365	0.0214	0.0289
2R	1.45	10.43	3718	6345	5031	1127	4137	2632	0.30	0.0273	0.0160	0.0216
3L	1.78	12.62	4559	7681	6120	1382	5009	3196	0.43	0.0321	0.0190	0.0256
3R	1.78	12.62	4559	7681	6120	1382	5009	3196	0.35	0.0264	0.0157	0.0210
4L	2.02	14.66	5187	8923	7055	1573	5819	3696	0.42	0.0275	0.0160	0.0217
4R	2.02	14.66	5187	8923	7055	1573	5819	3696	0.36	0.0241	0.0140	0.0190
5L	2.32	16.58	5954	10091	8023	1805	6581	4193	0.49	0.0284	0.0168	0.0226
5R	2.32	16.58	5954	10091	8023	1805	6581	4193	0.42	0.0240	0.0142	0.0191
6L	2.92	21.18	7481	12886	10183	2268	8403	5336	0.61	0.0277	0.0161	0.0219
6R	2.92	21.18	7481	12886	10183	2268	8403	5336	0.49	0.0225	0.0131	0.0178
7L	3.51	24.75	8985	15063	12024	2725	9823	6274	0.61	0.0231	0.0138	0.0185
7R	3.51	24.75	8985	15063	12024	2725	9823	6274	0.59	0.0227	0.0135	0.0181
8L	4.19	29.02	10739	17661	14200	3257	11517	7387	0.78	0.0250	0.0152	0.0201
8R	4.19	29.02	10739	17661	14200	3257	11517	7387	0.69	0.0219	0.0133	0.0176
9L	4.63	33.52	11854	20395	16125	3590	13282	8436	0.90	0.0261	0.0152	0.0207
9R	4.63	33.52	11854	20395	16125	3590	13282	8436	0.80	0.0233	0.0135	0.0184
10L	5.17	38.36	13249	23343	18296	4012	15202	9607	0.95	0.0245	0.0139	0.0192
10R	5.17	38.36	13249	23343	18296	4012	15202	9607	0.92	0.0238	0.0135	0.0187
11L	6.78	46.34	17360	28197	22779	5258	18363	11810	1.17	0.0231	0.0142	0.0187
11R	6.78	46.34	17360	28197	22779	5258	18363	11810	1.23	0.0242	0.0149	0.0196
12L	7.41	55.87	18993	33999	26496	5752	22142	13947	1.28	0.0231	0.0129	0.0180
12R	7.41	55.87	18993	33999	26496	5752	22142	13947	1.28	0.0231	0.0129	0.0180
13L	7.97	58.21	20411	35424	27917	6165	23007	14586	1.25	0.0209	0.0121	0.0165
13R	7.97	58.21	20411	35424	27917	6165	23007	14586	1.39	0.0234	0.0135	0.0184
14L	9.36	67.69	23995	41193	32594	7248	26754	17001	1.55	0.0221	0.0129	0.0175
14R	9.36	67.69	23995	41193	32594	7248	26754	17001	1.58	0.0226	0.0132	0.0179
15L	9.60	71.88	24596	43740	34168	7429	28408	17918	1.55	0.0216	0.0121	0.0169
15R	9.60	71.88	24596	43740	34168	7429	28408	17918	1.77	0.0247	0.0139	0.0193
16L	10.35	76.88	26513	46785	36649	8019	30427	19223	1.71	0.0221	0.0125	0.0173
16R	10.35	76.88	26513	46785	36649	8019	30427	19223	1.94	0.0251	0.0142	0.0197
17L	4.64	33.71	11899	20515	16207	3599	13342	8470	0.85	0.0245	0.0142	0.0194
17R	4.64	33.71	11899	20515	16207	3599	13342	8470	0.79	0.0227	0.0132	0.0179
18L	7.02	46.29	17991	28168	23079	5441	18319	11880	1.19	0.0227	0.0145	0.0186
18R	7.02	46.29	17991	28168	23079	5441	18319	11880	1.16	0.0221	0.0141	0.0181
20L	7.13	47.68	18258	29013	23636	5530	18895	12212	1.10	0.0207	0.0130	0.0169
20R	7.13	47.68	18258	29013	23636	5530	18895	12212	1.15	0.0215	0.0135	0.0175
22L	9.04	61.41	23161	37367	30264	7015	24335	15675	1.67	0.0247	0.0153	0.0200
22R	9.04	61.41	23161	37367	30264	7015	24335	15675	1.50	0.0223	0.0138	0.0180
23L	10.08	67.94	25819	41345	33582	7819	26926	17373	1.36	0.0180	0.0112	0.0146
23R	10.08	67.94	25819	41345	33582	7819	26926	17373	1.69	0.0225	0.0140	0.0183
24L	11.19	75.03	28668	45661	37165	8671	29696	19183	1.61	0.0193	0.0121	0.0157
24R	11.19	75.03	28668	45661	37165	8671	29696	19183	1.95	0.0233	0.0146	0.0190
32L	4.99	33.71	12796	20515	16655	3870	13342	8606	0.87	0.0232	0.0145	0.0188
32R	4.99	33.71	12796	20515	16655	3870	13342	8606	0.80	0.0214	0.0134	0.0174

Channel 1 Triangular
Channel 2 Square

TABLE IV.1.4

Single-Phase Water Mixing
Square-Triangular Geometry

RUN NUMBER	SUBCHANNEL MASS FLOW (LB/HR) CH.1	CH.2	SUBCHANNEL MASS FLUX (LB/HR.FT2) CH.1	CH.2	AVERAGE MASS FLUX (LB/HR.FT2)	SUBCHANNEL REYNOLDS NUMBER CH.1	CH.2	AVERAGE REYNOLDS NUMBER	MIXING RATE (LB/HR.FT)	SUBHANNEL STANTON NUMBER CH.1	CH.2	AVERAGE STANTON NUMBER
27L	180.46	1332.00	462431	810581	636506	2043	7702	4873	29.03	0.0215	0.0123	0.0169
27R	180.46	1332.00	462431	810581	636506	2043	7702	4873	28.55	0.0212	0.0121	0.0166
28L	187.54	1398.00	480570	850745	665658	2123	8084	5104	33.01	0.0236	0.0133	0.0184
28R	187.54	1398.00	480570	850745	665658	2123	8084	5104	30.55	0.0218	0.0123	0.0171
29L	193.83	1446.00	496693	879956	688324	2195	8361	5278	36.35	0.0251	0.0142	0.0196
29R	193.83	1446.00	496693	879956	688324	2195	8361	5278	32.74	0.0226	0.0128	0.0177
30L	199.34	1500.00	510801	912817	711809	2257	8674	5465	34.62	0.0232	0.0130	0.0181
30P	199.34	1500.00	510801	912817	711809	2257	8674	5465	33.95	0.0228	0.0128	0.0178
3L	35.01	262.04	89703	159466	124584	453	1732	1092	12.69	0.0485	0.0273	0.0379
3F	35.01	262.04	89703	159466	124584	453	1732	1092	7.62	0.0291	0.0164	0.0228
4L	42.04	314.73	107734	191528	149631	544	2080	1312	8.96	0.0285	0.0160	0.0223
4R	42.04	314.73	107734	191528	149631	544	2080	1312	5.04	0.0160	0.0090	0.0125
5L	49.16	366.11	125971	222796	174383	636	2420	1528	6.26	0.0170	0.0096	0.0133
5F	49.16	366.11	125971	222796	174383	636	2420	1528	7.41	0.0202	0.0114	0.0158
6L	62.88	472.21	161139	287360	224250	791	3034	1912	7.97	0.0170	0.0095	0.0132
6R	62.88	472.21	161139	287360	224250	791	3034	1912	8.29	0.0176	0.0099	0.0138
8L	91.70	685.14	234970	416940	325955	1153	4402	2778	13.32	0.0194	0.0110	0.0152
8R	91.70	685.14	234970	416940	325955	1153	4402	2778	13.24	0.0193	0.0109	0.0151
9L	104.22	790.07	267072	480791	373932	1287	4984	3136	16.57	0.0213	0.0118	0.0165
9P	104.22	790.07	267072	480791	373932	1287	4984	3136	15.65	0.0201	0.0112	0.0156
10L	119.48	854.99	306176	544642	425409	1476	5646	3561	18.95	0.0212	0.0119	0.0166
10P	119.48	854.99	306176	544642	425409	1476	5646	3561	18.22	0.0204	0.0115	0.0159
11L	133.22	999.92	341369	608493	474931	1645	6308	3977	20.05	0.0201	0.0113	0.0157
11R	133.22	999.92	341369	608493	474931	1645	6308	3977	19.15	0.0192	0.0108	0.0150
12L	146.95	1104.84	376562	672344	524453	1815	6970	4393	25.28	0.0230	0.0129	0.0180
12R	146.95	1104.84	376562	672344	524453	1815	6970	4393	23.91	0.0218	0.0122	0.0170
13L	160.69	1203.59	411755	732439	572097	1985	7593	4789	25.26	0.0210	0.0118	0.0164
13R	160.69	1203.59	411755	732439	572097	1985	7593	4789	25.27	0.0210	0.0118	0.0164
14L	174.42	1311.60	446949	798168	622558	2155	8275	5215	30.01	0.0230	0.0129	0.0180
14R	174.42	1311.60	446949	798168	622558	2155	8275	5215	28.26	0.0217	0.0121	0.0169
16L	28.00	211.00	71751	128403	100077	355	1368	862	16.67	0.0797	0.0445	0.0621
16P	28.00	211.00	71751	128403	100077	355	1368	862	10.60	0.0506	0.0283	0.0395
17L	35.01	262.04	89703	159466	124584	444	1699	1072	11.03	0.0422	0.0237	0.0329
17P	35.01	262.04	89703	159466	124584	444	1699	1072	4.39	0.0168	0.0094	0.0131
18L	42.04	316.40	107734	192545	150140	529	2033	1281	4.17	0.0133	0.0074	0.0103
18R	42.04	316.40	107734	192545	150140	529	2033	1281	6.28	0.0200	0.0112	0.0156
19L	48.88	366.11	125250	222796	174023	615	2352	1483	7.10	0.0194	0.0109	0.0152
19R	48.88	366.11	125250	222796	174023	615	2352	1483	6.80	0.0186	0.0105	0.0145
20L	63.15	475.30	161824	289238	225531	825	3171	1998	6.93	0.0147	0.0082	0.0115
20R	63.15	475.30	161824	289238	225531	825	3171	1998	7.80	0.0165	0.0092	0.0129
21L	76.76	580.22	196686	353089	274888	1003	3872	2437	10.32	0.0180	0.0100	0.0140
21P	76.76	580.22	196686	353089	274888	1003	3872	2437	11.02	0.0192	0.0107	0.0149
22L	91.25	685.14	233834	416940	325387	1192	4572	2882	13.31	0.0195	0.0109	0.0152
22R	91.25	685.14	233834	416940	325387	1192	4572	2882	13.38	0.0196	0.0110	0.0153
23L	76.76	580.22	196686	353089	274888	1003	3872	2437	10.37	0.0181	0.0101	0.0141
23R	76.76	580.22	196686	353089	274888	1003	3872	2437	11.31	0.0197	0.0110	0.0153
25L	35.01	262.04	89703	159466	124584	448	1715	1082	6.16	0.0235	0.0132	0.0184
25R	35.01	262.04	89703	159466	124584	448	1715	1082	5.58	0.0213	0.0120	0.0167
26L	42.04	316.40	107734	192545	150140	539	2071	1305	4.21	0.0134	0.0075	0.0104
26R	42.04	316.40	107734	192545	150140	539	2071	1305	6.49	0.0206	0.0115	0.0161

Channel 1 Triangular
Channel 2 Square

APPENDIX IV.2

Derivation of Mixing Equation

The air and water turbulent mixing rates reported in this work have been determined using the following tracer mass balance.

Consider two subchannels connected by a region of width "b" and length "L" through which an interchange of fluid takes place. In one subchannel, a tracer is injected upstream of the interconnection length.

The following assumptions are made in this analysis:

i. Axial pressure gradients in each channel are identical, thus eliminating radial pressure gradients and a net transfer of fluid from one channel to the other.

ii. Tracer concentrations are low and have a negligible effect on physical properties of the fluids.

iii. The fluid leaving one channel has the average tracer concentration of that subchannel.

iv. After the fluid has left the donor channel, it mixes immediately in the receiving channel.

v. There is a negligible relative velocity of the tracer with respect to the fluid.

Let C_1 and C_2 be the fraction of the total tracer flowing in the two subchannels.

A tracer mass balance for channel 1 over a differential length dz (in the interchange region) gives:

$$W_1\ C_1 - W'\ C_1\ dz + W'\ C_2\ dz = W_1\ C_1 + W_1\ dC_1$$

or

$$\frac{dC_1}{dz} + \frac{W'}{W_1}(C_1 - C_2) = 0 \qquad \text{(IV.1)}$$

Similarly

$$\frac{dC_2}{dz} + \frac{W'}{W_2}(C_2 - C_1) = 0 \qquad \text{(IV.2)}$$

From an overall tracer mass balance,

$$W_1\ \frac{dC_1}{dz} + W_2\ \frac{dC_2}{dz} = 0 \qquad \text{(IV.3)}$$

From equation (IV.1),

$$\frac{d^2C_1}{dz^2} + \frac{W'}{W_1}\left(\frac{dC_1}{dz} - \frac{dC_2}{dz}\right) = 0$$

Substituting for $\frac{dC_2}{dz}$ from equation (IV.3), we get

$$\frac{d^2C_1}{dz^2} + \frac{W'}{W_1}\ \frac{W_1 + W_2}{W_2}\ \frac{dC_1}{dz} = 0 \qquad \text{(IV.4)}$$

The solution to equation (IV.4) is

$$C_1 = A + B\ e^{-\int \frac{W'}{W_1} \frac{W_T}{W_2}\ dz} \qquad \text{(IV.5)}$$

where

$$W_T = W_1 + W_2$$

Incorporating the appropriate boundary conditions:

$$W' = -\frac{W_1\ W_2}{W_T\ L}\ \ln\left[\frac{W_1/W_T - C_{1e}}{W_1/W_T}\right] \qquad \text{(IV.6)}$$

where C_{1e} is the fraction of the total tracer flowing at the exit of the originally untraced channel.

For the special case of the square-square geometry ($W_1 = W_2 = W$), equation (IV.6) reduces to:

$$W' = -\frac{W}{2L} \ln \left[1 - 2\, C_{1e} \right] \qquad \text{(IV.7)}$$

APPENDIX IV.3

Turbulent Mixing Predictive Models

Of the various models proposed for calculation of turbulent mixing rates between adjacent subchannels, the ones proposed by Bowring (1) and Rowe and Angle (13,23) are used widely.

Bowring considered the heat transfer between adjacent subchannels "i" and "j" as the product of a diffusion coefficient, defined as the product of density and eddy diffusivity, ϵ_{Hij}, and the enthalpy gradient through the gap. Expressing the mixing distance Y_{ij} in terms of a gap shape factor, S_m, and using the assumptions listed in Table 2.1, Bowring arrived at the following mixing equation:

$$W'_{ij} = F_m \frac{\sqrt{f_i + f_j}}{80\ S_m} \left(\frac{b}{d}\right) \left(D_{ei}\, G_i + D_{ej}\, G_j \right) \qquad \text{(IV.3.1)}$$

Here Fm is an empirical mixing factor which theoretically equals 1 for "clean" systems. Bowring suggested that for a square-triangular geometry, F_m should be set a value somewhat greater than 1.

From his experimental data on mixing between square-square and square-triangular geometries, Rowe suggested a possible correlation for the prediction of mixing rates, W'_{ij} :

$$W'_{ij} = 0.0038 \, Re_j^{-0.1} \, G_j \, D_{ej} / \gamma_{ij} \qquad \text{(IV.3.2)}$$

where γ_{ij} is the relative centroidal distance between subchannels normalized to a square pitch array (=1 for square-square array, 0.79 for square-triangular array). Channel "j" is the larger subchannel.

APPENDIX V.1
Two-Phase Mixing Data

TABLE V.1.1

Two-Phase Turbulent Mixing
Square-Square Geometry

SERIAL NUMBER	RUN NUMBER	TOTAL MASS FLUX (LB/HR.FT2)	QUALITY OF STREAM	AVERAGE MIXING RATE(LB/HR.FT) AIR	WATER	DIMENSIONLESS VELOCITIES JG*	JL*	PRESSURE DROP (PSI/FT) OBSERVED	OWENS	MARTINELLI
1	18L&18R15	153982	0.09881	1.657	25.405	1.19	0.66	0.22	0.10	0.14
2	19L&19R15	152046	0.20474	2.379	16.237	2.44	0.58	0.25	0.15	0.17
3	20L&20R15	151567	0.30906	2.320	11.769	3.67	0.50	0.29	0.19	0.22
4	25L&25R15	153274	0.31676	2.538	13.527	3.80	0.50	0.28	0.20	0.23
5	1L& 1R15	101377	0.19926	1.496	22.878	1.59	0.39	0.17	0.08	0.12
6	2L& 2R15	100624	0.30625	1.393	12.575	2.42	0.33	0.18	0.10	0.14
7	21L&21R15	100822	0.30761	1.559	14.030	2.43	0.33	0.18	0.10	0.14
8	3L& 3R15	102537	0.40634	1.626	11.007	3.27	0.29	0.20	0.12	0.17
9	22L&22R15	103368	0.40236	1.512	10.133	3.26	0.30	0.21	0.12	0.17
10	24L&24R15	89861	0.20354	1.334	20.798	1.43	0.34	0.16	0.06	0.12
11	16L&16R15	89292	0.30815	1.424	11.610	2.16	0.30	0.17	0.08	0.13
12	17L&17R15	90180	0.40648	1.271	8.686	2.88	0.26	0.17	0.10	0.15
13	4L& 4R15	70422	0.20047	1.107	25.177	1.11	0.27	0.15	0.04	0.10
14	5L& 5R15	69173	0.30821	1.099	16.334	1.67	0.23	0.15	0.05	0.11
15	6L& 6R15	69478	0.40967	0.983	9.506	2.23	0.20	0.14	0.06	0.12
16	7L& 7R15	70719	0.60925	0.687	3.509	3.38	0.13	0.15	0.08	0.15
17	8L& 8R15	49776	0.29903	1.030	17.218	1.17	0.17	0.13	0.03	0.09
18	28L&28R15	49267	0.40173	0.834	12.113	1.56	0.14	0.13	0.04	0.09
19	10L&10R15	52309	0.58005	0.653	5.843	2.38	0.10	0.12	0.05	0.10
20	11L&11R15	50263	0.80051	0.113	1.104	3.17	0.05	0.09	0.06	0.11
21	11L&11R15	50263	0.80051	0.113	1.185	3.17	0.05	0.09	0.06	0.11
22	27L&27R15	32261	0.37948	0.775	9.841	0.97	0.10	0.12	0.02	0.07
23	29L&29R15	29278	0.41854	0.702	9.738	0.96	0.08	0.12	0.02	0.07
24	12L&12R15	29410	0.61411	1.274	6.906	1.42	0.05	0.10	0.02	0.06
25	13L&13R15	30037	0.79593	2.060	3.854	1.88	0.03	0.09	0.03	0.06
26	26L&26R15	30106	0.79639	0.404	3.461	1.89	0.03	0.09	0.03	0.06
27	67L&67R35	797599	0.00051		49.281	0.03	3.71		0.47	0.46
28	66L&66R35	797816	0.00078		47.294	0.05	3.71	0.50	0.45	0.46
29	65L&65R35	798085	0.00112		38.953	0.07	3.71		0.43	0.46
30	61L&61R35	798727	0.01106		144.670	0.68	3.67	0.60	0.39	0.57
31	62L&62R35	800600	0.00426		126.559	0.26	3.71	0.48	0.36	0.50
32	63L&63R35	798862	0.00666		137.486	0.41	3.69	0.56	0.36	0.52
33	69L&69R35	497819	0.00006		27.852	0.00	2.32		0.46	0.43
34	68L&68R35	497851	0.00012		33.240	0.00	2.32		0.45	0.41
35	60L&60R35	498000	0.00042		28.921	0.02	2.32		0.43	0.38
36	59L&59R35	498188	0.00080		43.694	0.03	2.32	0.46	0.40	0.37
37	58L&58R35	498289	0.00100	0.005	48.328	0.04	2.32	0.46	0.39	0.36
38	57L&57R35	495244	0.00223	0.120	53.960	0.08	2.30	0.40	0.33	0.35
39	56L&56R35	492437	0.00396	0.635	114.792	0.15	2.28	0.40	0.28	0.34
40	55L&55R35	494116	0.00734	2.278	164.625	0.28	2.28	0.37	0.24	0.35

TABLE V.1.1 (Contd.)

SERIAL NUMBER	RUN NUMBER	TOTAL MASS FLUX (LB/HR.FT2)	QUALITY OF STREAM	AVERAGE MIXING RATE(LB/HR.FT) AIR	AVERAGE MIXING RATE(LB/HR.FT) WATER	DIMENSIONLESS VELOCITIES JG*	DIMENSIONLESS VELOCITIES JL*	PRESSURE DROP (PSI/FT) OBSERVED	PRESSURE DROP (PSI/FT) OWENS	PRESSURE DROP (PSI/FT) MARTINELLI
41	53L&53R35	495578	0.01027	2.249	125.247	0.39	2.28	0.37	0.23	0.36
42	54L&54R35	501723	0.02240	5.475	101.293	0.86	2.28	0.43	0.26	0.40
43	43L&43R35	100601	0.00031		67.815	0.00	0.47		0.40	0.30
44	42R&42L35	100632	0.00062		86.300	0.00	0.47		0.37	0.27
45	39L&39R35	99743	0.00102	0.022	82.145	0.01	0.46	0.0	0.34	0.26
46	52L&52R35	101624	0.00124		84.444	0.01	0.47	0.46	0.33	0.25
47	52L&52R35	101624	0.00124		85.374	0.01	0.47	0.46	0.33	0.25
48	38L&38R35	101699	0.00197	0.075	80.384	0.02	0.47	0.25	0.29	0.24
49	51L&51R35	101721	0.00219		76.473	0.02	0.47	0.45	0.28	0.23
50	50L&50R35	100991	0.00417		74.928	0.03	0.47	0.35	0.21	0.21
51	49L&49R35	101239	0.00661		67.679	0.05	0.47	0.32	0.16	0.20
52	36L&36R35	96593	0.00689	0.362	69.591	0.05	0.45	0.32	0.16	0.20
53	35L&35R35	102552	0.01027	0.574	55.978	0.08	0.47	0.25	0.12	0.19
54	48L&48R35	101636	0.01049		63.719	0.08	0.47	0.24	0.12	0.19
55	47L&47R35	102558	0.01938		90.011	0.15	0.47	0.20	0.08	0.17
56	34L&34R35	106251	0.01851	1.269	67.466	0.15	0.49	0.20	0.08	0.17
57	33L&33R35	111382	0.03871	2.329	63.385	0.33	0.50	0.19	0.06	0.14
58	29L&29R35	102753	0.03028	1.650	70.239	0.24	0.46	0.18	0.06	0.15
59	37L&37R35	100053	0.00412	0.256	73.453	0.03	0.46	0.41	0.21	0.21
60	44L&44R35	100121	0.04189		74.338	0.32	0.45	0.19	0.06	0.14
61	27L&27R35	98174	0.06073	2.237	51.186	0.46	0.43	0.14	0.05	0.13
62	28L&28R35	103359	0.08089	2.980	49.986	0.64	0.44	0.18	0.05	0.12
63	20L&20R35	100819	0.19852	4.159	23.630	1.54	0.38	0.18	0.07	0.12
64	45L&45R35	100344	0.07179		50.403	0.55	0.43	0.20	0.05	0.12
65	32L&32R35	97427	0.07258	2.309	56.809	0.54	0.42	0.19	0.05	0.12
66	46L&46R35	101408	0.10900		42.080	0.85	0.42	0.19	0.06	0.12
67	31L&31R35	100421	0.10948	3.195	44.776	0.84	0.42	0.19	0.05	0.12
68	1L& 1R35	99962	0.19985	4.116	25.986	1.54	0.37	0.17	0.07	0.11
69	2L& 2R35	100190	0.30018	4.486	12.897	2.32	0.33	0.18	0.09	0.13
70	3L& 3R35	100672	0.40326	4.131	8.239	3.11	0.28	0.19	0.11	0.16
71	17L&17R35	89059	0.20343	3.419	22.888	1.39	0.33	0.17	0.06	0.11
72	18L&18R35	90635	0.29993	4.462	16.407	2.09	0.30	0.18	0.08	0.12
73	19L&19R35	92046	0.41255	3.993	8.638	2.91	0.25	0.18	0.10	0.14
74	4L& 4R35	70491	0.19619	3.300	26.130	1.06	0.26	0.14	0.04	0.10
75	5L& 5R35	69221	0.30782	4.103	19.018	1.64	0.22	0.14	0.05	0.10
76	6L& 6R35	71116	0.40268	4.273	10.887	2.20	0.20	0.14	0.06	0.11
77	12L&12R35	71549	0.59868	3.726	4.878	3.28	0.13	0.16	0.08	0.14
78	22L&22R35	49771	0.20512	2.911	26.361	0.78	0.18	0.15	0.03	0.09
79	10L&10R35	49380	0.29844	2.745	23.258	1.13	0.16	0.12	0.03	0.08
80	7L& 7R35	50498	0.39744	3.712	14.366	1.54	0.14	0.12	0.04	0.09

TABLE V.1.1(Contd.)

SERIAL NUMBER	RUN NUMBER	TOTAL MASS FLUX (LB/HR.FT2)	QUALITY OF STREAM	AVERAGE MIXING RATE(LB/HR.FT) AIR	WATER	DIMENSIONLESS VELOCITIES JG*	JL*	PRESSURE DROP (PSI/FT) OBSERVED	OWENS	MARTINELLI
81	8L& 8R35	49952	0.59912	3.544	7.242	2.30	0.09	0.12	0.04	0.09
82	9L& 9R35	50238	0.80307	3.431	1.186	3.10	0.05	0.10	0.05	C.10
83	21L&21R35	49208	0.29598	3.128	23.902	1.12	0.16	0.13	0.03	0.08
84	16L&16R35	29813	0.30378	2.558	14.913	0.70	0.10	0.13	0.02	0.07
85	15L&15R35	29880	0.39818	2.875	11.749	0.91	0.08	0.12	0.02	0.07
86	13L&13R35	29076	0.60297	2.949	6.220	1.35	0.05	0.09	0.02	0.06
87	23L&23R35	30281	0.79403	2.480	3.791	1.85	0.03	0.10	0.02	0.06
88	24L&24R80	201407	0.10382	8.680	44.970	1.51	0.80	0.26	0.13	0.22
89	9L& 9R80	99287	0.21202	6.907	33.704	1.51	0.35	0.19	0.06	0.11
90	11L&11R80	101371	0.41178	6.963	9.817	2.99	0.26	0.20	0.10	0.15
91	16L&16R80	100026	0.20298	7.406	33.900	1.48	0.35	0.18	0.06	0.11
92	23L&23R80	101156	0.31453	6.749	18.137	2.30	0.31	0.17	0.08	0.13
93	8L& 8R80	89658	0.20180	6.576	26.114	1.30	0.32	0.15	0.05	0.11
94	10L&10R80	93755	0.40444	7.908	12.377	2.72	0.25	0.18	0.08	0.14
95	15L&15R80	89017	0.20439	7.123	31.994	1.33	0.31	0.15	0.05	0.10
96	17L&17R80	91499	0.40648	6.154	12.352	2.72	0.24	0.17	0.08	0.13
97	19L&19R80	92664	0.29987	7.318	21.406	2.01	0.29	0.15	0.07	0.12
98	30L&30R80	94688	0.61616	6.548	2.896	4.22	0.16	0.19	0.11	0.18
99	7L& 7R80	68084	0.60734	5.228	4.814	2.98	0.12	0.13	0.06	C.12
100	20L&20R80	70390	0.40771	6.550	14.466	2.07	0.18	0.13	0.05	0.10
101	21L&21R80	70344	0.30513	6.262	23.706	1.55	0.22	0.14	0.05	0.10
102	26L&26R80	69952	0.20179	5.398	34.734	1.02	0.25	0.18	0.04	0.10
103	1L& 1R80	49399	0.20586	5.961	34.020	0.73	0.17	0.13	0.02	0.09
104	2L& 2R80	48656	0.38747	6.590	19.145	1.36	0.13	0.13	0.03	0.08
105	3L& 3R80	49032	0.58394	5.330	6.694	2.06	0.09	0.11	0.04	0.08
106	18L&18R80	49242	0.30347	5.434	33.049	1.09	0.15	0.09	0.03	0.08
107	4L& 4R80	49859	0.79811	3.938	0.763	2.87	0.04	0.07	0.05	0.09
108	25L&25R80	47783	0.31324	2.227	28.961	1.08	0.15	0.13	0.03	0.08
109	27L&27R80	49155	0.20193	4.917	36.231	0.72	0.17	0.13	0.02	0.09
110	12L&12R80	30359	0.80769	4.846	2.274	1.77	0.03	0.08	0.02	0.06
111	13L&13R80	29811	0.60106	6.380	9.267	1.30	0.05	0.11	0.02	0.06
112	14L&14R80	30046	0.39753	5.285	12.516	0.86	0.08	0.09	0.02	0.07
113	28L&28R80	30060	0.40334	6.292	14.815	0.88	0.08	0.11	0.02	0.07
114	29L&29R80	29893	0.29592	3.882	14.914	0.64	0.09	0.09	0.01	0.07

APPENDIX V.2

Error Analysis

The turbulent mixing rates were calculated by using the expression:

$$W' = -\frac{W}{2\,L} \quad \ln\left[1 - \frac{2\,C_1}{C_1 + C_2}\right] \qquad (4.2)$$

The air and water flow rates, W, could be measured with an accuracy of ±1% of full scale reading. The methane and potassium nitrate concentrations could be measured within ±1% and ±2% respectively.

In order to provide some measure of the reliability of the experimental results, an error analysis, based on the method of Kline and McClintock (48) was carried out. The method is based on a specification of the uncertainties in the various experimental measurements. Let W'_R be the uncertainty in the measured turbulent mixing rates and W_U, C_{1U}, C_{2U} be the uncertainties in the independent variables. Then the uncertainty in the result is given as:

$$W'_R = \left[\left(\frac{\partial W'}{\partial W} \; W_U\right)^2 + \left(\frac{\partial W'}{\partial C_1} \; C_{1U}\right)^2 + \left(\frac{\partial W'}{\partial C_2} \; C_{2U}\right)^2\right]^{1/2} \qquad (V.2.1)$$

By making use of equation (V.2.1) and the limits of uncertainties mentioned previously, the uncertainty in the turbulent mixing rates, W′, was calculated. It was found that the average error propagated into W′ is ±5.5% for the air mixing rates and ±6.2% for the water mixing rates. The reproducibility of the runs repeated at random is given in Table V.2.1.

Table V.2.1

Reproducibility of the Experimental Runs

	Single-Phase		Two-Phase	
	Air	Water	Air	Water
Total Number of Runs	72	64	114	
Runs Repeated	16	19	17	17
Average Reproducibility	3.1%	4.7%	5.4%	3.8%
Theoretical Uncertainty	5.5%	6.2%	5.5%	7.5%

The percentage error in the air mixing rates for two-phase flow runs at low qualities (less than 0.01) was significantly higher than the above limits.

APPENDIX V.3

Two Phase Turbulent Mixing
Square-Triangular Geometry

RUN NUMBER	QUALITY OF STREAM INLET CH.1	INLET CH.2	EXIT CH.1	EXIT CH.2	AVERAGE	TOTAL MASS FLUX (LB/HR.FT2) INLET CH.1	INLET CH.2	EXIT CH.1	EXIT CH.2	AVERAGE
1L	0.2040	0.0269	0.0308	0.0428	0.0399	68547.	205211.	209974.	172341.	178984.
1R	0.2040	0.0269	0.0308	0.0428	0.0399	68547.	205211.	209974.	172341.	178984.
2L	0.1313	0.0262	0.0300	0.0387	0.0367	95287.	202985.	168095.	181226.	182316.
2R	0.1313	0.0262	0.0300	0.0387	0.0367	95287.	202985.	168095.	181226.	182316.
3L	0.0964	0.0265	0.0278	0.0360	0.0345	107681.	199917.	142407.	189349.	182215.
3R	0.0964	0.0265	0.0278	0.0360	0.0345	107681.	199917.	142407.	189349.	182215.
13L	0.1240	0.0887	0.0476	0.1083	0.0924	97152.	200188.	231261.	166674.	180414.
13R	0.1240	0.0887	0.0476	0.1083	0.0924	97152.	200188.	231261.	166674.	180414.
14L	0.1678	0.0888	0.0493	0.1170	0.0959	84303.	202421.	209188.	163439.	179753.
14R	0.1678	0.0888	0.0493	0.1170	0.0959	84303.	202421.	209188.	163439.	179753.
15L	0.2176	0.0890	0.0308	0.1213	0.0996	76132.	201363.	131356.	176687.	177329.
15R	0.2176	0.0890	0.0308	0.1213	0.0996	76132.	201363.	131356.	176687.	177329.
16L	0.2553	0.0881	0.0319	0.1167	0.1007	69862.	203384.	124696.	190187.	177759.
16R	0.2553	0.0881	0.0319	0.1167	0.1007	69862.	203384.	124696.	190187.	177759.
17L	0.1296	0.0828	0.0321	0.1001	0.0873	93319.	205516.	174006.	187105.	183983.
17R	0.1296	0.0828	0.0321	0.1001	0.0873	93319.	205516.	174006.	187105.	183983.
18L	0.1623	0.0824	0.0286	0.1021	0.0896	85664.	205435.	148026.	192976.	182449.
18R	0.1623	0.0824	0.0286	0.1021	0.0896	85664.	205435.	148026.	192976.	182449.
19L	0.2206	0.0829	0.0275	0.1063	0.0939	74299.	204452.	119515.	194333.	179473.
19R	0.2206	0.0829	0.0275	0.1063	0.0939	74299.	204452.	119515.	194333.	179473.
19L	0.2206	0.0829	0.0284	0.1063	0.0939	74299.	204452.	115692.	194333.	179473.
19R	0.2206	0.0829	0.0284	0.1063	0.0939	74299.	204452.	115692.	194333.	179473.
20L	0.3928	0.0622	0.0310	0.0896	0.0814	52386.	201005.	130405.	181294.	172483.
20R	0.3928	0.0622	0.0310	0.0896	0.0814	52386.	201005.	130405.	181294.	172483.
21L	0.2415	0.0622	0.0287	0.0810	0.0753	67476.	202088.	125143.	188798.	176254.
21R	0.2415	0.0622	0.0287	0.0810	0.0753	67476.	202088.	125143.	188798.	176254.
22L	0.2038	0.0636	0.0294	0.0800	0.0749	73775.	199144.	99815.	192231.	175084.
22R	0.2038	0.0636	0.0294	0.0800	0.0749	73775.	199144.	99815.	192231.	175084.
23L	0.1644	0.0631	0.0329	0.0734	0.0719	79134.	198499.	58208.	204045.	175591.
23R	0.1644	0.0631	0.0329	0.0734	0.0719	79134.	198499.	58208.	204045.	175591.
24L	0.1161	0.0633	0.0294	0.0707	0.0682	85675.	199077.	57316.	206157.	177314.
24R	0.1161	0.0633	0.0294	0.0707	0.0682	85675.	199077.	57316.	206157.	177314.
25L	0.3953	0.0619	0.0309	0.0858	0.0811	51846.	201480.	145997.	186883.	172763.
25R	0.3953	0.0619	0.0309	0.0858	0.0811	51846.	201480.	145997.	186883.	172763.
26L	0.2065	0.0626	0.0291	0.0797	0.0742	74030.	200552.	123626.	190859.	176271.
26R	0.2065	0.0626	0.0291	0.0797	0.0742	74030.	200552.	123626.	190859.	176271.
26L	0.2065	0.0626	0.0290	0.0797	0.0742	74030.	200552.	123878.	190859.	176271.
26R	0.2065	0.0626	0.0290	0.0797	0.0742	74030.	200552.	123878.	190859.	176271.

Subchannel 1 Triangular
Subchannel 2 Square

APPENDIX V.3 (Cont'd)

RUN NUMBER	QUALITY OF STREAM INLET CH.1	QUALITY OF STREAM INLET CH.2	QUALITY OF STREAM EXIT CH.1	QUALITY OF STREAM EXIT CH.2	QUALITY OF STREAM AVERAGE	TOTAL MASS FLUX (LB/HR.FT2) INLET CH.1	TOTAL MASS FLUX (LB/HR.FT2) INLET CH.2	TOTAL MASS FLUX (LB/HR.FT2) EXIT CH.1	TOTAL MASS FLUX (LB/HR.FT2) EXIT CH.2	TOTAL MASS FLUX (LB/HR.FT2) AVERAGE
27L	0.1186	0.0638	0.0306	0.0719	0.0689	85028.	199191.	88799.	199038.	177281.
27R	0.1186	0.0638	0.0306	0.0719	0.0689	85028.	199191.	88799.	199038.	177281.
27L	0.1186	0.0638	0.0313	0.0719	0.0689	85028.	199191.	86629.	199038.	177281.
27R	0.1186	0.0638	0.0313	0.0719	0.0689	85028.	199191.	86629.	199038.	177281.
28L	0.1621	0.0271	0.0298	0.0427	0.0381	75999.	202118.	212126.	168467.	177914.
28R	0.1621	0.0271	0.0298	0.0427	0.0381	75999.	202118.	212126.	168467.	177914.
29L	0.1236	0.0270	0.0269	0.0386	0.0359	86411.	202108.	159277.	182484.	179904.
29R	0.1236	0.0270	0.0269	0.0386	0.0359	86411.	202108.	159277.	182484.	179904.
30L	0.0407	0.0270	0.0245	0.0309	0.0291	152086.	202108.	191883.	192364.	192508.
30R	0.0407	0.0270	0.0245	0.0309	0.0291	152086.	202108.	191883.	192364.	192508.
31L	0.0352	0.0270	0.0244	0.0301	0.0283	153397.	204201.	184800.	195072.	194451.
31R	0.0352	0.0270	0.0244	0.0301	0.0283	153397.	204201.	184800.	195072.	194451.
32L	0.3841	0.1064	0.0466	0.1448	0.1258	64783.	204138.	175235.	177501.	177393.
32R	0.3841	0.1064	0.0466	0.1448	0.1258	64783.	204138.	175235.	177501.	177393.
32L	0.3841	0.1064	0.0469	0.1442	0.1258	64783.	204138.	174052.	178250.	177393.
32R	0.3841	0.1064	0.0469	0.1442	0.1258	64783.	204138.	174052.	1782 0.	177393.
33L	0.2207	0.1070	0.0419	0.1385	0.1174	85892.	204290.	176743.	181465.	181568.
33R	0.2207	0.1070	0.0419	0.1385	0.1174	85892.	204290.	176743.	181465.	181568.
33L	0.2207	0.1070	0.0415	0.1355	0.1174	85892.	204290.	178381.	185487.	181568.
33R	0.2207	0.1070	0.0415	0.1355	0.1174	85892.	204290.	178381.	185487.	181568.
34L	0.1661	0.1108	0.0365	0.1345	0.1163	95535.	205161.	164507.	190631.	184122.
34R	0.1661	0.1108	0.0365	0.1345	0.1163	95535.	205161.	164507.	190631.	184122.
34L	0.1661	0.1108	0.0363	0.1356	0.1163	95535.	205161.	165582.	189045.	184122.
34R	0.1661	0.1108	0.0363	0.1356	0.1163	95535.	205161.	165582.	189045.	184122.
35L	0.1410	0.1084	0.0312	0.1248	0.1118	101761.	203461.	127867.	196134.	183943.
35R	0.1410	0.1084	0.0312	0.1248	0.1118	101761.	203461.	127867.	196134.	183943.
35L	0.1410	0.1084	0.0314	0.1248	0.1118	101761.	203461.	127104.	196036.	183943.
35R	0.1410	0.1084	0.0314	0.1248	0.1118	101761.	203461.	127104.	196036.	183943.
36L	0.1083	0.1091	0.0306	0.1212	0.1090	101462.	202492.	95969.	201798.	183102.
36R	0.1083	0.1091	0.0306	0.1212	0.1090	101462.	202492.	95969.	201798.	183102.
36L	0.1083	0.1091	0.0304	0.1206	0.1090	101462.	202492.	96714.	202839.	183102.
36R	0.1083	0.1091	0.0304	0.1206	0.1090	101462.	202492.	96714.	202839.	183102.
37L	0.0706	0.0269	0.0244	0.0346	0.0313	95709.	201039.	171606.	180728.	180825.
37R	0.0706	0.0269	0.0244	0.0346	0.0313	95709.	201039.	171606.	180728.	180825.
38L	0.0970	0.0267	0.0259	0.0372	0.0334	88223.	201000.	174470.	178272.	179356.
38R	0.0970	0.0267	0.0259	0.0372	0.0334	88223.	201000.	174470.	178272.	179356.

Subchannel 1 Triangular
Subchannel 2 Square

VITA AUCTORIS

1940	Born in Gujranwala, India.
1960	Received the B.Sc. (Hons) degree from Punjab University, Chandigarh, India.
1964	Received the B.Sc. (Chemical Engineering) degree from Punjab University, Chandigarh, India.
1967	Received the M.A.Sc. (Chemical Engineering) degree from University of Windsor, Windsor Ontario.
1972	Presently, a candidate for the degree of Ph.D. in Chemical Engineering.